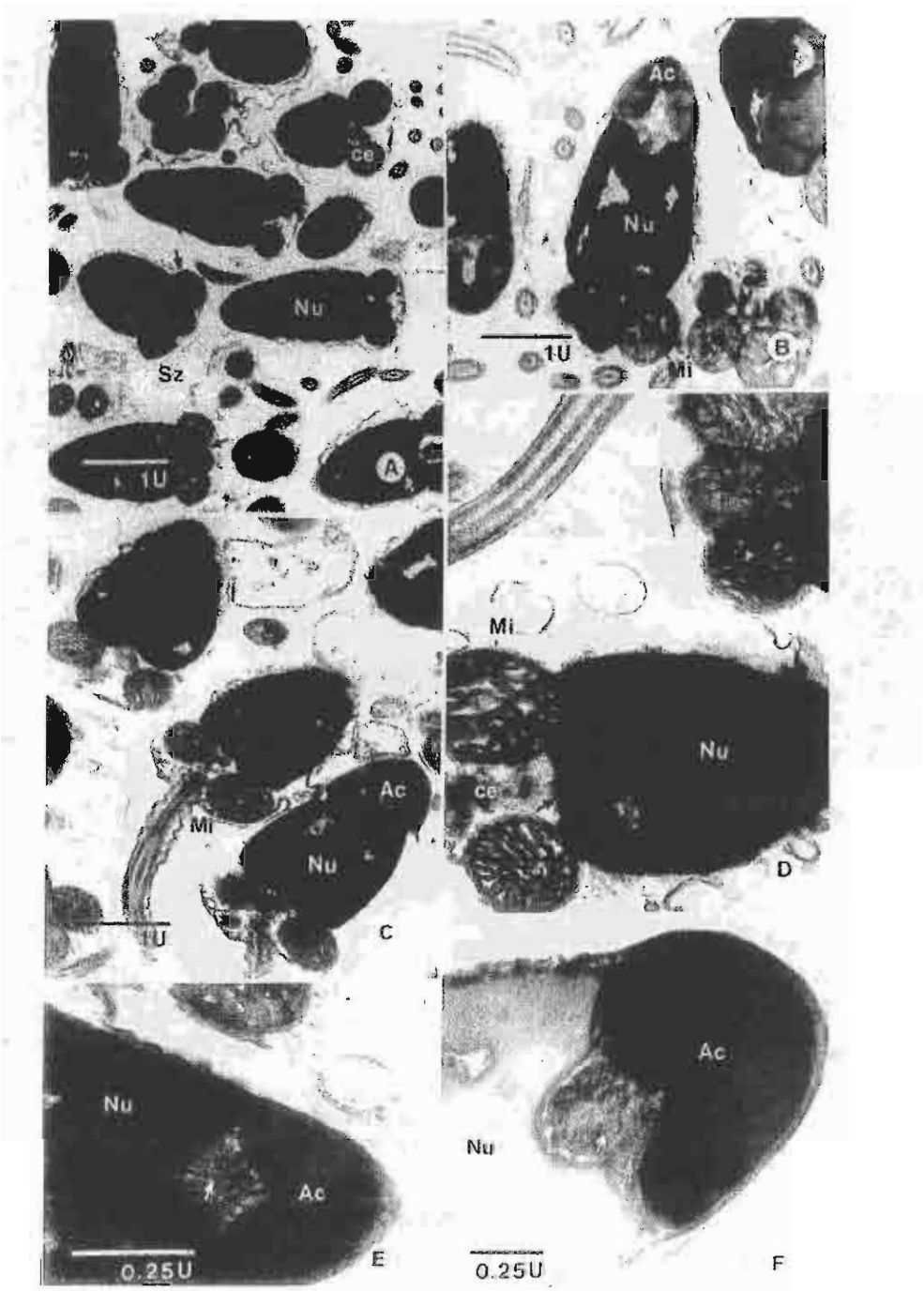

FIG. 2. Transmission electron micrographs of mature spermatozoa (Sz) showing nucleus (Nu), acrosome (Ac), plasma membrane, mitochondria (Mi), and vacuoles (va) in the nucleus. Five globular mitochondria (arrows in A, B) surround a pair of centriole (ce), which is tightly attached to the nucleus by thickened double plates (arrow in D) at the neck region. An acrosomal core with crystalline structure filling the concavity of the subacrosomal space at the anterior tip of the nucleus (arrows in E, F).

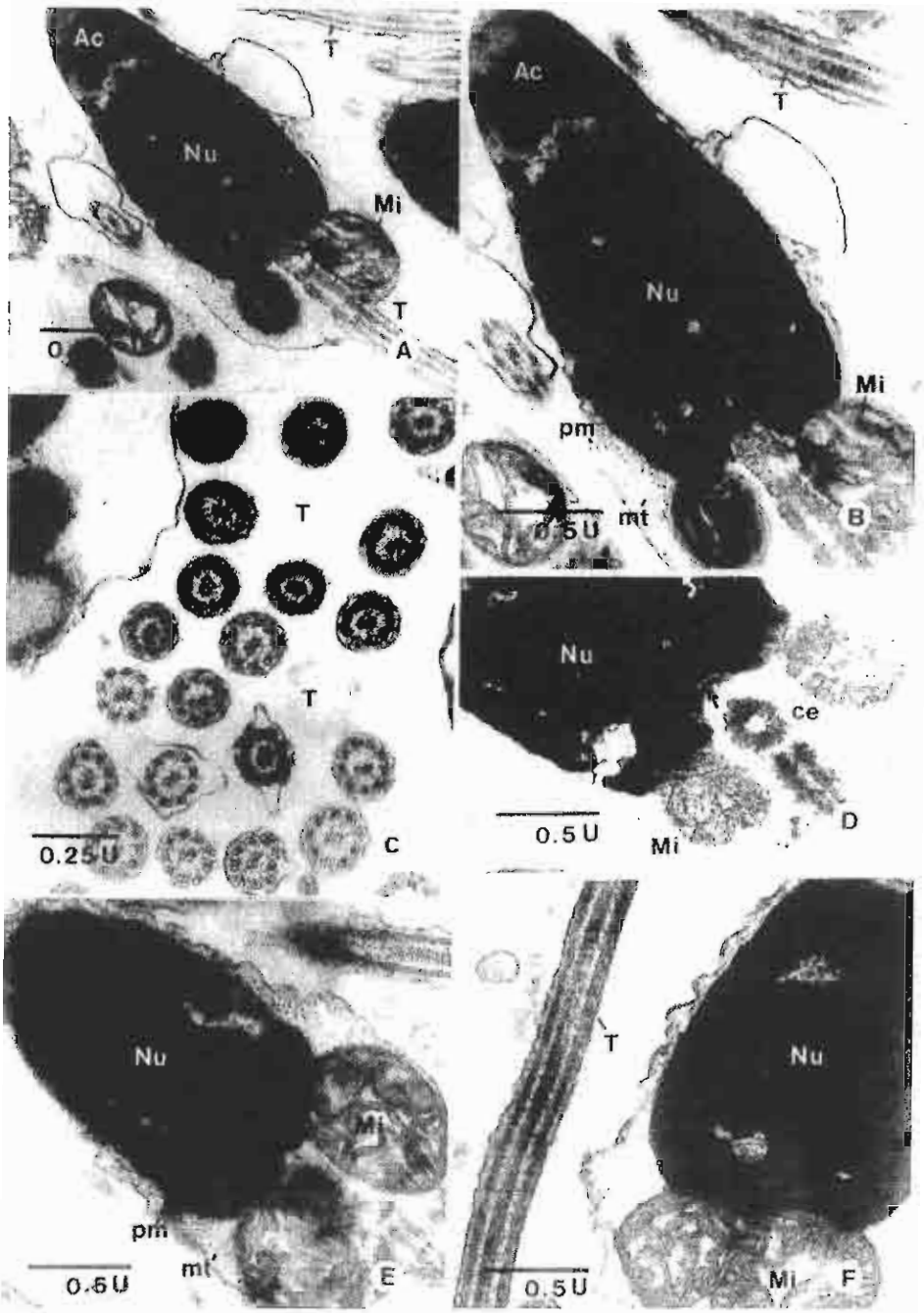

FIG. 3. Transmission electron micrographs showing the nuclei (Nu), and tails (T) of spermatozoa consisting of centrioles (ce), the proximal one attached to the nucleus by the thickened plates (arrows in A, B, D). The zig-zag filaments (mt) in the cytoplasm link the nucleus and mitochondria to the posterior sperm membrane (pm) (B, E). The tail consists of an axoneme of 9+2 doublets of microtubules surrounded by a plasma membrane (cross-section in C, long-section in F). Chromatin in the nuclei of cells in B and D still show incomplete condensation, wherein individual chromatin granules with 60 nm diameter are closely packed together, yet the outline of each granules is still visible.

location the nuclear membrane appears thickened (Fig. 3B, E, F). Mitochondria contain shelf-like cristae, with some stretching from one side to the opposite side (Fig. 3B, E, F).

In the posterior corner of cytoplasm between the nucleus and mitochondria (Fig.3A, B, E, F), there are bundle of thin zig-zag filaments, whose width is about 15-20 nm. These filaments link mitochondria to the adjacent cell membrane, and some filaments appear attached to the latter at a specific location (Fig. 3B, E, F). These filaments also surround the entire lower half of the nucleus.

The tail piece commences from a pair of centrioles whose proximal member is embedded in the socket at the middle region of the slightly indented posterior border of the nucleus (Fig. 3A, B, D). The nuclear membrane at this region is also visibly thickened (Fig. 3B, D). A long axoneme stretches backwards from the distal centriole that is surrounded by mitochondria (Figs. 2C, 3A). In cross-sections (Fig. 3C) the axoneme appears as 9+2 doublets of microtubules, and this pattern appears to exist along the whole length of the tail (Fig. 2D, 3F). The axoneme is covered directly by partially wavy plasma membrane at the proximal end close to the centriole (Fig. 2C), while on the rest of the tail it appears fairly smooth and fits snugly around the axoneme (Fig. 3F).

DISCUSSION

The shape and general morphology of *Haliotis asinina* sperm are typical of the "primitive type" or "ect-aquasperm" described for mollusks that reproduce by external fertilization, *e.g.*, chitons, bivalves (Frazen, 1970; Baccetti, 1979) and scaphopods (Dufresne-Dube *et al.*, 1983). Spermatozoa of these mollusks usually possess short, cone-shaped heads and simple tails that lack mid-pieces. In contrast, mollusks whose sperm fertilize the eggs internally tend to have elongated and sometimes also spiraling heads, and tails that have definitive mid-pieces containing mitochondria or their derivatives; and frequently glycogen particles in residual cytoplasmic masses still remaining around parts of the tails (Franzen, 1956; 1983; Anderson & Personne, 1976; Baccetti & Afzelius, 1976; Healy, 1996).

The heads of sperm in *Haliotis asinina* appear to be shorter and more globular in comparison to those of temperate abalone species, such as *H. rufescens* (Lewis *et al.*, 1980), whose sperm tend to have elongate bullet-shaped heads. There also appears to be more clear areas or intranuclear vacuoles within the nucleus where the chromatin mass is lacking. The chromatin in *H. asinina* appears to be "granular type" in which large chromatin granules of 50-60 nm are packed tightly side-by-side. During spermiogenesis, these large chromatin granules are derived from the periodic thickening of formerly uniform chromatin fibers whose original size in the earliest round spermatid stage is about 20-30 nm (unpublished observation). This granular pattern of chromatin condensation could also be perceived in other primitive gastropods, such as trochids (Healy 1989; Hodgson *et al.*, 1990), scaphopods (Dufresne-Dube *et al.*, 1983), and bivalves (Bozzo *et al.*, 1993; Cacas & Subirana, 1994; Johnson *et al.*, 1996). In contrast, in the internally fertilized sperm of most meso- and all neogastropods, opisthobranchs and pulmonates, the chromatin condensation is of "fibrillar-lamellar" type in which the pattern of chromatin condensation goes through three successive phases: granular, fibrillar and lamellar structures, that finally become tightly packed in myelin-like whorls (Healy, 1987; 1988; Jaramillo *et al.*, 1986; Gallardo &

Garrido, 1989; Amor & Durfort, 1990; Sretarugsa *et al.*, 1991; Caceres *et al.*, 1994). It is possible that these two different patterns of chromatin condensation may be linked to the qualitative difference of basic nuclear proteins, especially protamines, which appear to be more variable among primitive, externally fertilized mollusks and the more advanced, internally fertilized mollusks; whereas histones appear to be more conserved (Subirana *et al.*, 1973; Balhorn *et al.*, 1979; Van Helden *et al.*, 1979; Chiva *et al.*, 1991; Daban *et al.*, 1991; Caceres *et al*, 1994). Much work remains to be done in mollusk in characterizing and correlating the variation of protamines with the abovementioned patterns of chromatin condensation.

The acrosome of *Haliotis asinina* is cup-shaped with much less elongation and invagination from nuclear side, in comparison to those of temperate abalone species (Lewis *et al.*, 1980) and other primitive gastropods (Hodgson *et al.*, 1990). The acrosomal material is uniformly homogeneous in contrast to the two clearly separated areas found in *H. rufescens* (Lewis *et al.*, 1980). The acrosomal core is composed of short thick crystalline-like axis embedded within moderately dense matrix that occupies the whole subacrosomal space. In comparison to other primitive gastropods and temperate abalone species, the core is much shorter in *H. asinina*. The crystalline material is probably consisted of actin and its associated proteins as reported for other mollusks (Baccetti, 1979; Shiroya *et al.*, 1986; Tilney *et al.*, 1987). This acrosomal core might participate in the extension of acrosomal process during acrosomal reaction and fertilization.

The tail of *Haliotis asinina* sperm consists of an axonemal core of 9+2 doublets of microtubules surrounded directly by a plasma membrane. This type of simple tail is also observed in other primitive gastropods (Healy 1989; Hodgson *et al.*, 1990), scaphopods (Dufresne-Dube *et al.*, 1983) and bivalves (Bozzo *et al.*, 1993; Cacas & Subirana, 1994; Johnson *et al.*, 1996), all of which reproduce by external fertilization. In contrast, the mollusks that reproduce by internal fertilization possess tails akin to those of mammalian sperm (Jaramillo *et al.*, 1986; Gallardo & Garrido 1989; Amor & Durfort, 1990; Sretarugsa *et al.*, 1991; Caceres *et al.*, 1994). Such tails usually have midpieces that contain large cylindrical or helical mitochondria. Fibrous sheathes often surround the axoneme to provide sturdy support that could allow stronger movement than the simple tails found in abalone and other primitive gastropods. Indeed, in the latter there are only five globular mitochondria located at the posterior end of the nucleus, surrounding the proximal and distal centrioles. These mitochondria could probably generate a smaller quantity of energy for the less motile sperm of these species.

Another remarkable feature in the sperm of *Haliotis asinina*, which has not been reported in sperm of other mollusks, is the presence of zig-zag filaments in the cytoplasm at the posterior corner of the head. It appears that these filaments link mitochondria to the posterior part of the plasma membrane, and some surround the lower half of the nucleus. Because of their zig-zag nature and solid core structure, they are probably not microtubules, but their exact composition has not yet been identified. We speculate that these filaments could play some roles in controlling the shape of the nucleus as well as the position of mitochondria.

ACKNOWLEDGMENTS

This investigation was supported by The Thailand Research Fund (Contract BRG4080004 and Senior Research Scholar Fellowship to Prasert Sobhon).

LITERATURE CITED

AL-HAJJ, H.A. & ATTIGA, F.A. 1995. Ultrastructural observations of euspermiogenesis in *Cerithium caeruleum* (Prosobranchia: Cerithiidae) from the Jordan Gulf of Aqaba. *Invertebrate Reproduction and Development*, 28: 113-124.

AMOR, M.J. & DURFORT, M. 1990. Changes in nuclear structure during eupyrene spermatogenesis in *Murex brandaris*. *Molecular Reproduction and Development*, 25: 348-356.

ANDERSON, W.A. & PERSONNE, P. 1976. The molluscan spermatozoon: dynamic aspects of its structure and function. *American Zoologist*, 16: 293-313.

AZEVEDO, C., & CORRAL, L. 1985. The fine structure of the spermatozoa of *Siphonaria algesirae* (Gastropoda, Pulmonata). *Journal of Morphology*, 186: 107-117.

BACCETTI, B. 1979. The spermatozoon. Pp. 305-329. In: Fawcett, D.W. & Bedford, J.M. (eds.), *The spermatozoon maturation, motility, surface properties and comparative aspects*. Urban-Schwarzenberg, Baltimore. Pp. 1-441.

BACCETTI, B. & AFZELIUS, B.A. 1976. Biology of the sperm cell. *Monographs on Development Biology*, Vol. 10, S. Karger, Basel. Pp. 1-254.

BALHORN, R., LAKE, S. & GLEDHILL, B.L. 1979. Electrophoretic analysis of nuclear membrane isolated from the sperm of the black abalone *Haliotis cracherodii*. *Experimental Cell Research*, 123: 414-475.

BOZZO, M.G., RIBES, E., SAGRISTA, E., POQUET, M. & DURFORT, M. 1993. Fine structure of the spermatozoa of *Crassostrea gigas* (Mollusca, Bivalvia). *Molecular Reproduction and Development*, 34: 206-211.

CACAS, M.T. & SUBIRANA, J.A. 1994. Chromatin condensation and acrosome development during spermiogenesis of *Ensis ensis* (Mollusca, Bivalvia). *Molecular Reproduction and Development*, 37: 223-228.

CACERES, C., RIBES, E., MULLER, S., CORNUDELLA, L. & CHIVA, M. 1994. Characterization of chromatin-condensing proteins during spermiogenesis in a neogastropod mollusc (*Murex brandaris*). *Molecular Reproduction and Development*, 38: 440-452.

CHIVA, M., DABAN, M., ROSENBERG, E. & KASINSKY, H.E. 1991. Protamines in polyplacophoras and gastropods as a model for evolutional changes in molluscan sperm basic proteins. Pp. 27-30. In: Baccetti, B. (ed.). *Comparative spermatology 20 years after*, Vol. 75. Raven Press, Seina, Italy.

DABAN, M., CHIVA, M., ROSENBERG, E., KASINSKY, H.E. & SUBIRANA, J.A. 1991. Protamines in prosobranchian gastropods (Mollusca) vary with different modes of reproduction. *Journal of Experimental Zoology*, 257: 265-283.

DUFRESNE-DUBE, L., PICHERAL, B. & GUERRIER, P. 1983. An ultrastructure analysis of *Dentalium vulgare* (Mollusca, Scaphopoda) gametes with special reference to early events at fertilization. *Journal of Ultrastructure Research*, 83: 242-257.

FRANZEN, A. 1955. Comparative morphological investigations into spermiogenesis among Mollusca. *Zoologiska Bidreg fran Uppsala*, 30: 282-304.

FRANZEN, A. 1956. On spermiogenesis, morphology of the spermatozoon and biology of fertilization among invertebrates. *Zoologiska Bidreg fran Uppsala*, 31: 356-482.

FRANZEN, A. 1970. Phylogenetic aspects of the morphology of spermatozoa and spermiogenesis. Pp. 29-46. In: Baccetti, B. (ed.). *Comparative spermatology*. Academic Press, New York.

FRANZEN, A. 1983. Ultrastructure studies of spermatozoa in three bivalve species with notes on evolution of elongated sperm nucleus in primitive spermatozoa. *Gamete Research*, 7: 199-214.

GALLARDO, C.S. & GARRIDO, O.A. 1989. Spermiogenesis and sperm morphology in the marine gastropod *Nucella crassilabrum* with an account of morphometric patterns of spermatozoa variation in the family Muricidae. *Invertebrate Reproduction and Development*, 15: 163-170.

HEALY, J.M. 1983. An ultrastructural study of basommatophoran spermatozoa (Mollusca: Gastropoda). *Zoologica Scripta*, 12: 57-66.

HEALY, J.M. 1987. Spermatozoan ultrastructure and its bearing on gastropod classification and evolution. *Australian Zoologist*, 24: 108-113.

HEALY, J.M. 1988. Sperm morphology and its systemic importance in the Gastropoda. *Malacological Review*, Supplement 4: 251-266.

HEALY, J.M. 1989. Ultrastructure of spermiogenesis in the gastropod *Calliotrapis glyptus* Watson (Prosobranchia: Trochidae) with special reference to the embedded acrosome. *Gamete Research*, 24: 9-19.

HEALY, J.M. 1996. Molluscan sperm ultrastructure: correlation with taxonomic units within the Gastropoda, Cephalopoda and Bivalvia. Pp. 99-113. In: Taylor, J. (ed.). *Origin and evolutionary radiation of the Mollusca*. Oxford University Press, London.

HEALY, J.M., & WILLAN, R.C. 1984. Ultrastructure and phylogenetic significance of notaspidean spermatozoa (Mollusca, Gastropoda, Opisthobranchia). *Zoologica Scripta*, 13: 107-128.

HODGSON, A.N. 1986. Invertebrate spermatozoa: structure and spermatogenesis. *Archives of Andrology*, 17: 105-114.

HODGSON, A.N., HELLER, J. & BERNARD, R.T.F. 1990. Ultrastructure of the sperm and spermatogenesis in five South African species of the trochid genus *Oxystele* (Mollusca, Prosobranchia). *Molecular Reproduction and Development*, 25: 263-271.

HUAQUIN, L. & BUSTOS-OBREGON, E. 1981. Ultrastructural analysis of spermatid differentiation in *Concholepas concholepas*. *Archives de Biologie*, Bruxelles, 92: 259-274.

JARAMILLO, R., GARRIDO, O. & JORQUERA, B. 1986. Ultrastructural analysis of spermiogenesis and sperm morphology in *Chorus giganteus* (Lesson, 1829) (Prosobranchia: Muricidae). *The Veliger*, 29: 217-225.

JOHNSON, M.J., CASSE, N. & LE PENNEC, M. 1996. Spermatogenesis in the endosymbiont-bearing bivalve *Loripes lucinalis* (Veneroida: Lucinidae). *Molecular Reproduction and Development*, 45: 476-484.

KITAJIMA, E.W. & PARAENSE W.L. 1976. The ultrastructure of mature sperm of the fresh-water snail *Biomphalaria glabrata* (Mollusca Gastropoda). *Transactions of the American Microscopical Society*, 95: 1-10.

LEWIS, C.A., LEIGHTON, D.L. & VACQUIER, V.D. 1980. Morphology of abalone spermatozoa before and after the acrosome reaction. *Journal of Ultrastructure Research*, 72: 39-46.

PASTISSON, C. & LACORRE, I. 1996. Fine structure of the germinating cells during the spermiogenesis of *Arion rufus* (Mollusca, Pulmonate Gastropoda). *Molecular Reproduction and Development*, 43: 484-494.

SHIROYA, Y., HOSOYA, H., MABUCHI, I. & SAKAI, Y.T. 1986. Actin filament bundle in the acrosome of abalone spermatozoa. *Journal of Experimental Zoology*, 239: 105-115.

SINGHAGRAIWAN, T. & DOI, M. 1993. Seed production and culture of a tropical abalone, *Haliotis asinina* Linné. The Eastern Marine Fisheries Development Center, Department of Fisheries, Ministry of Agriculture and Cooperatives, Thailand. 33 pp.

SRETARUGSA, P., NGOWSIRI, U., KRUATRACHUE, M., SOBHON, P., CHAVADEJ, J. & UPATHAM, E.S. 1991. Spermiogenesis in *Achatina fulica* as revealed by electron microscopy. *Journal of Medical and Applied Malacology*, 3: 7-18.

SUBIRANA, J.A., COZCOLLUELA, C., PALAU, J. & UNZETA, M. 1973. Protamines and other basic proteins from spermatozoa of molluscs. *Biochimistry et Biophysica Acta*, 317: 364-379.

TILNEY, L.G., FUKUI, Y. & DEROSIER, D.J. 1987. Movement of the actin filament bundle in *Mytilus* sperm: a new mechanism is proposed. *Journal of Cell Biology*, 104: 981-993.

VAN HELDEN, P.D., STRICKLAND, V.N., BRANDT, W.F. & VON HOLT, C. 1979. The complete amino acid sequence of histone H2B from the mollusc *Patella granatina*. *European Journal of Biochemistry*, 93: 71-78.

WALKER, M. 1970. Some unusual features of the sperm of *Nucella lapillus* (L.). Pp. 383-392. In: Baccetti, B. (ed.). *Comparative spermatology*. Academic Press, New York.

WALKER, M. & MACGREGOR, H.C. 1968. Spermatogenesis and the structure of the mature sperm in *Nucella lapillus* (L.). *Journal of Cell Science*, 3: 95-104.

ScienceAsia 26 (2000) : 149-158

Effect of Mammalian Gonadotropin Releasing Hormone Agonist, Human Chorionic Gonadotropin and Pituitary Homogenate on Spermiation in *Rana tigerina* and *Rana catesbeiana*

J Chavadej[a,*], N Vichatrong[b], P Sretarugsa[a] and P Sobhon[a]

[a] Department of Anatomy, Faculty of Science, Mahidol University, Bangkok 10400 Thailand.

[b] Department of Physical Therapy, Faculty of Allied Health Science, Chulalongkorn University, Bangkok 10330, Thailand.

* Corresponding author

Received 3 Feb 2000
Accepted 20 Jul 2000

ABSTRACT Frog pituitary extract, mammalian gonadotropin releasing hormone agonist(GnRHa) and human chorionic gonadotropin (hCG) were injected subcutaneously and intraperitoneally to determine the optimal doses required to elicit spermiation in adult male frogs, *Rana tigerina* and *R. catesbeiana*, during the breeding season. Pituitary extract showed the most pronounced effect in stimulating sperm release at dosages of 1 gland per frog in *R.tigerina* and 2 glands per frog in *R.catesbeiana*. GnRHa gave marked stimulating effect in both *R. tigerina* and *R. catesbeiana* at dosages of 10 and 25 μg/kg body weight, respectively. The induction of sperm release in both species of frogs could also be detected after the injection of hCG at the dosage of 50 and 200 IU per frog. The optimal doses of GnRHa were also tested for their stimulatory effect on spermiation during other seasons. *R. catesbeiana* could be stimulated to spermiate throughout the year, but with the reduction in sperm concentration during pre-, post- and non-breeding seasons. In contrast, *R. tigerina* could be induced to spermiate only during breeding season.

KEYWORDS: *Rana tigerina, Rana catesbeiana*, spermiation, gonadotropin, GnRHa.

INTRODUCTION

The reproductive cycles of amphibians have been studied by many investigators.[1,2] It is generally accepted that gonadotropic activity of pituitary gland which modulates the reproductive cycle is regulated by hypothalamus[3], through the release of gonadotropin-releasing hormone (GnRH). GnRH has been demonstrated to stimulate the secretion of follicle-stimulating hormone (FSH) and luteinizing hormone(LH) in some species of frogs, such as *Rana catesbeiana*.[4] The testicular function is, in turn, controlled by LH and FSH[2], whose levels were markedly increased during the proliferation of secondary spermatogonia, primary and secondary spermatocytes in *Rana esculenta*.[2] In addition to native hormones, gonadotropin-releasing hormone agonist (GnRHA) could also stimulate primary spermatogonial multiplication and testicular androgen production in *R. esculenta*.[5]

There were many reports on the study of the effect of hormone priming on spermiation.[1,6] The stimulation of sperm release by GnRH administration could be demonstrated in *Hyla regilla*.[7] The effectiveness of various hormones, ie. frog pituitaries, human chorionic gonadotropin (hCG), LH, FSH and LH/FSH-RH on eliciting spermiation in bullfrogs, *R. catesbeiana* had also been reported.[8,9] Similarly, pituitary preparation, gonadotropins and hCG could stimulate the sperm release in *Rana pipiens*.[10,11]

Most anurans have exhibited a high spermatogenic activity in the breeding season as observed in *Rana temporaria*[12], *Bufo arenarum*[13] and *Bufo regularis*[14]. In contrast, Loumbourdis and Kyriakopoulou[15] studied the testicular activity in an Indian frog, *Rana ridibunda*, and found spermatogenesis to be continuous throughout the year. It remains to be seen whether frogs with discontinuous-type spermatogenesis could be induced to spermiate during various seasons.

In present study we investigate the effect of GnRHa, hCG and pituitary homogenate on stimulating sperm release in *R. tigerina* and *R. catesbeiana* during various phases of reproductive cycle. The results obtained may have application in controlling the reproduction of both species, which are indigenous (*R. tigerina*), and imported species (*R. catesbeiana*), for commercial culturing.

Materials and Methods

1. **The determination of effective dosages of various hormones on spermiation during breeding season**

R. tigerina aged more than 12 months old (weighing on the average 150-200 gm)and *R. catesbeiana* more than 18 months old (weighing on the average 350-400 gm) were obtained from the culture laboratory of the Faculty of Science, Mahidol University. The adult male frogs collected during breeding season (April-September) were used to study the effects of mammalian Gonadotropin releasing hormone agonist (Buserelin acetate), (GnRHa), hCG, and homoplastic pituitary homogenate on spermiation. Each hormone or pituitary extract was dissolved in distilled water and injected in a total volume of 0.1 ml. Ten frogs were used in each group of experiment.

1.1 GnRHa administration

In *R. tigerina*, the frogs were divided into five groups : group I were injected with distilled water to serve as control; groups II, III, IV and V received GnRHa 5 µg, 10 µg, 25 µg and 50 µg/kg body weight (bw), respectively.

In *R. catesbeiana*, the frogs were divided into four groups : group I were injected with distilled water to serve as control; groups II, III and IV received GnRHa 10 µg, 25 µg and 50 µg/kg bw, respectively.

All the experimental frogs received a single subcutaneous injection of GnRHa into the dorsal lymph sac.

1.2 hCG administration

In *R. tigerina* there were four groups : group I was the control ; groups II, III and IV received hCG 25 IU, 50 IU and 100 IU per frog, respectively.

In *R. catesbeiana* there were five groups : group I was the control ; groups II, III, IV and V received hCG 50 IU, 100 IU, 200 IU and 300 IU per frog, respectively.

All the experimental frogs received a single intraperitoneal injection .

1.3 Pituitary homogenate administration

Pars distalis of pituitary glands were collected from the frogs during the breeding season from July to August.The glands were homogenized and lyophilized, and pituitary powder were kept at -20°C. until use. The pituitary powder was completely dissolved in 0.1 ml distilled water and subcutaneously injected into the dorsal lymph sac. Each male *R. tigerina* received one homoplastic pituitary homogenate, whereas a male *R. catesbeiana* was given two homoplastic pituitary homogenate.

All the experimental frogs were examined for the spermiation responses by the cloacal aspiration carried out at interval beginning at 1 hour onwards after hormone treatment. The number of frog responding to the stimulation, the volume of semen released, and the concentration of semen were quantitated.

2. **The effect of the optimal dose of GnRHa on spermiation during various seasons**

The optimal doses of GnRHa that caused spermiation during the breeding season in both species were used to induce spermiation in adult *R. tigerina* and *R. catesbeiana* during the post-breeding (October-November), non-breeding (December-January) and pre-breeding (February-March) seasons. The observations and quantitations of spermiation response were done in the same manner as described above.

3. **Statistical Analysis**

The mean values obtained from each experimental group were compared with the normal control values. In addition, comparison among different dosages of each hormone as well as different kinds of hormones were statistically tested by using non-parametric equivalent, the Mann-Whitney test. A probability value less than or equal to 0.01 or 0.05 was chosen to indicate statistical significance.

Results

1. **The effects of GnRHa, hCG and pituitary homogenate on spermiation during breeding season**

1.1 GnRHa

In *R. tigerina*, GnRHa at 10 µg/kg bw could stimulate the sperm release in 100% of specimens at the first two hours. This effect was then decreased to 60% in the third hour. In contrast, the other doses of GnRHa (5, 25 and 50 µg/kg bw) showed less stimulating effect. The high concentration of GnRHa, particularly 50 µg/kg bw, could only stimulate 20% of frogs to spermiate at the beginning, while the proportion of positive response was gradually increased to 60% and 80% in the second and third hours, respectively (Fig 1A). The same trend of spermiation response could be observed in *R. catesbeiana*, where 10 µg/kg bw dose showed marked effect at the first two hours. The higher doses of 25

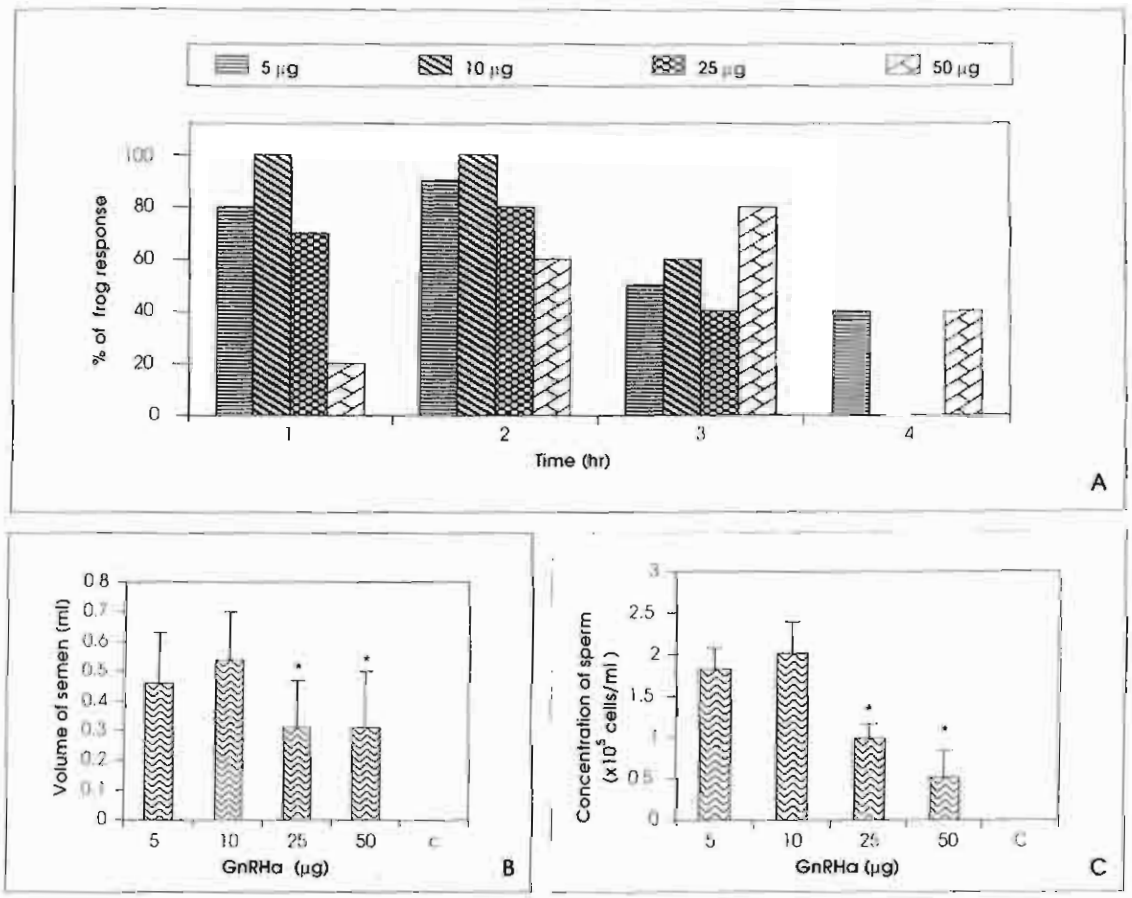

Fig 1. A. Histograms showing percentages of induced spermiation among male *R. tigerina* after being treated with various doses of GnRHa at 5, 10, 25 and 50 µg/kg bw

B,C: The changes in total volume of semen and concentration of sperm collected at the end of the experiment (4 hr, respectively) after the administration of 5, 10, 25 and 50 µg/kg bw of GnRHa.

* indicates $p < 0.05$ vs 10 ug GnRHa injected group.

and 50 µg /kg bw showed less effect at the first two hours, but later the effect increased to reach the peak at only 80-90% at 4-5 hours (Fig 2A).

The total volume of pooled semen of *R. tigerina* collected after the fourth hour in the group receiving the dosage 10 µg/kg bw gave the highest value (0.54±0.16 ml), whereas the total volume obtained from other doses remained relatively low (Fig 1B). The mean difference of the total volume in the 10 µg/kg bw GnRHa group is statistically significant ($P \leq 0.05$) when compared to the groups receiving 25 and 50 µg/kg bw GnRHa. In *R. catesbeiana*, after the end of the experiment at seventh hour the dosage of 25 µg/kg bw GnRHa gave the highest value of semen volume (1.86±0.4 ml, Fig 2B). This mean value, however, did not show any significant difference from 10 and 50 µg/kg bw GnRHa injected group.

The average concentration of *R. tigerina's* sperm obtained from 10 µg /kg bw GnRHa injection showed the highest value (2.02±0.38 x 10^5 cell/ml), whereas the mean concentrations of the other groups remained relatively low (1.83 ± 0.25 , 0.98±0.18 and 0.51±0.32 x 10^5 cells/ml) (Fig 1C). The high concentration of sperm collected from 10 µg/kg bw GnRHa injected group is significantly different ($P \leq 0.05$) from those of the other two dosages (25 and 50 µg/kg bw GnRHa groups). In *R. catesbeiana*, the dose of 25 µg/kg bw of GnRHa gave the maximal concentration of sperm (2.98 ± 0.36 x 10^5 cells/ml) (Fig 2C), while the doses of 10 µg and 50 µg/kg bw of GnRHa showed less effect. The mean concentrations of sperm from these two groups are 2.01±0.32 and 1.90±0.25 x10^5 cells/ml, respectively. These mean differences of the average concentration are statistically significant ($P \leq 0.001$) when compared to the value of 25 µg /kg bw injected group . None of the semen from the control group showed any spermatozoa.

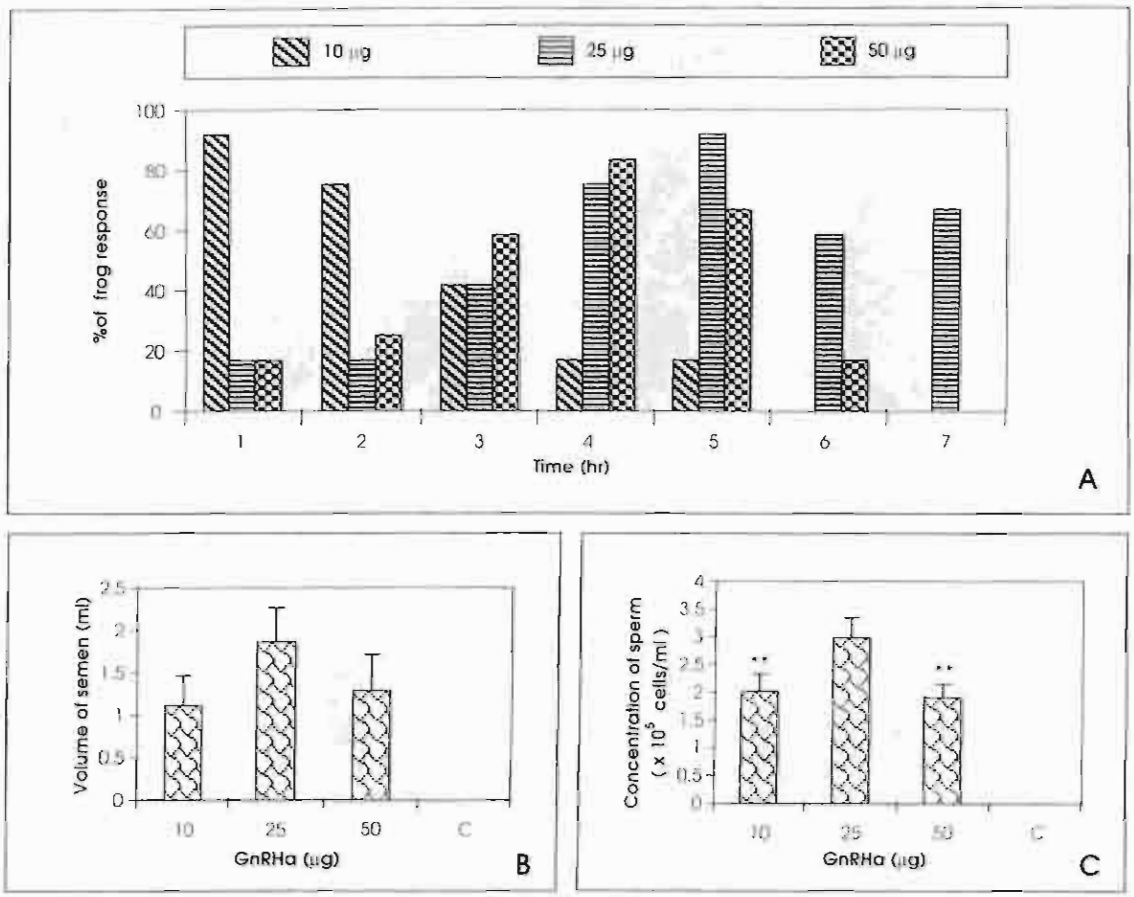

Fig 2. A: Histograms showing percentages of induced spermation among male *R. catesbeiana* after being treated with various doses of GnRHa at 10, 25 and 50 µg/kg bw

B,C: The changes in total volume of semen and concentration of sperm collected at the end of the experiment (7 hr., respectively) after the administration of 10, 25 and 50 µg/kg bw of GnRHa

** indicates p< 0.001 vs 25 ng GnRHa injected group.

1.2 hCG

The induction of sperm release in *R. tigerina* can also be detected after the hCG administration. The number of frogs responded to the dose at 50 IU/frog is 100% at the first two hours, and then abruptly decreased to 20% at the third hour (Fig 3A). In contrast, there is a noticeable lower percentage of frog response at the dosage of 25 and 300 IU/frog (57% and 50%, respectively). No positive responses was observed at any time after the treatment in the control group.

In *R. catesbeiana*, hCG at 50 IU/frog could not elicit spermation while hCG at 200 IU/frog gave the highest response (88%) at the first hour (Fig 4A). The other two doses of hCG at 100 IU and 300 IU/frog showed less effect (33% and 38%, respectively).

In *R. tigerina*, the mean value of the total semen volume collected over the entire period of the experiment is highest in the 100 IU/frog group (Fig 3B). This mean total volume (0.6±0.14 ml) is significant different (P≤0.001) from those injected with 25 and 50 IU hCG/frog. In *R. catesbeiana*, the highest total volume of semen could be obtained in the group treated with 200 IU hCG/frog (Fig 4B). However, this value is not significantly different from the other two groups (100 and 300 IU/frog of hCG).

In *R. tigerina*, the average concentration of semen collected in 100 IU/frog group is slightly higher (13.9± 2.2 x10⁵ cells/ml) than in other groups (7.6±1.5, 10.8± 2.3 x10⁵ cells/ml). However, statistically the sperm concentration of this group is not significantly different from the groups injected with 25 and 50 IU/frog (Fig 3C). In *R. catesbeiana*, the average concentration of sperm following administration of 200 IU hCG/frog was less (6 ± 2 x10⁵ cells/ml) than those injected with 100 and 300 IU hCG/frog (10 ± 3 and 9 ± 2 x 10⁵ cells/ml, respectively) (Fig 4C). Moreover, sperm concentration obtained from the group injected with 200 IU/frog is significantly different (P≤0.05) from the others.

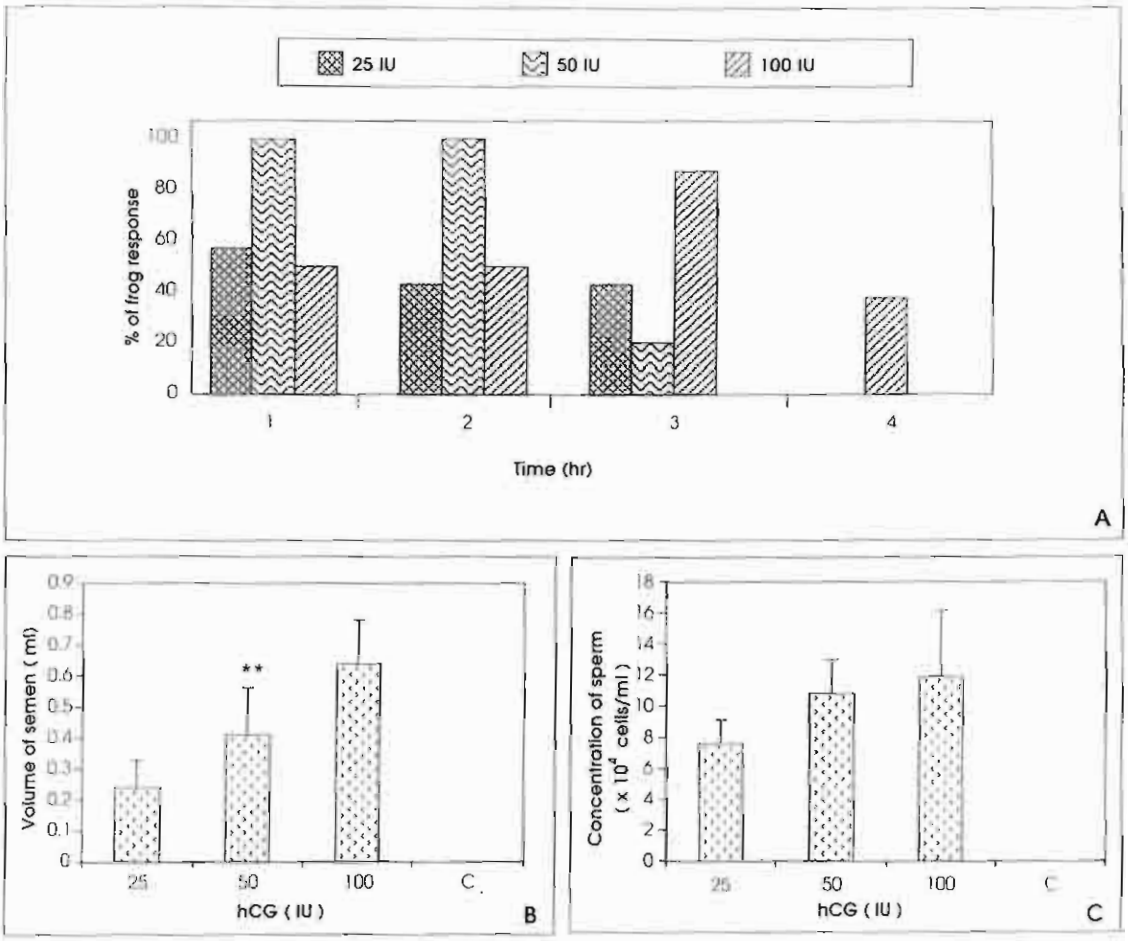

Fig 3. A. Histograms showing percentages of induced spermiation among adult male *R. tigerina* after being treated with hCG at 25, 50 and 100 IU.

B,C. The changes in total volume of semen and concentration of sperm collected at the end of the experiment (4 hr, respectively) after 25, 50 and 100 IU hCG administration.

** indicates $p < 0.001$ vs 100 IU hCG injected group.

1.3 Pituitary homogenate

Pituitary homogenates have very pronounced effect on spermiation. All the experimental *R. tigerina* (100%) responded to this treatment within the first two hours. Total response could also be detected in *R. castesbeiana* at the second and fourth hours, respectively. The total volume and concentration of semen of *R. tigerina* collected at one hour after injection are 0.7 ml and 3.09 x 10^5 cells/ml, respectively. The volume of semen collected from *R. castesbeiana* rose to 0.48 ml with the concentration of 2.16 x 10^5 cells/ml in the first hour.

2. Spermiation response to the optimal doses of GnRHa administered outside the breeding season

The dose of 10 µg/kg bw GnRHa has a remarkable effect on *R. tigerina*'s spermiation in both pre-breeding and breeding seasons. All the experimental frogs (100%) can release the sperm after this hormone administration. As the frogs progressed to post-breeding season, the percentage of response is reduced to 25%. None of them could spermiate in non-breeding season (Fig 5A). The average volumes of semen collected from pre-breeding, breeding and post-breeding seasons are 0.24±0.17, 0.51± 0.2 and 0.14±0.05 ml, respectively (Fig 5B). The concentration of sperm obtained during pre-breeding, breeding and post-breeding are 0.12± 0.05, 1.86±0.58 and 0.06± 0.02 x10^5 cells/ml, respectively (Fig 5C). Thus, there is a remarkable reduction in the number of sperm released when compared to those obtained in breeding season. The differences of mean values are statistically significant ($P \leq 0.05$).

The dose of 25 µg/kg bw GnRHa can stimulate spermiation in *R. castesbeiana* throughout the year

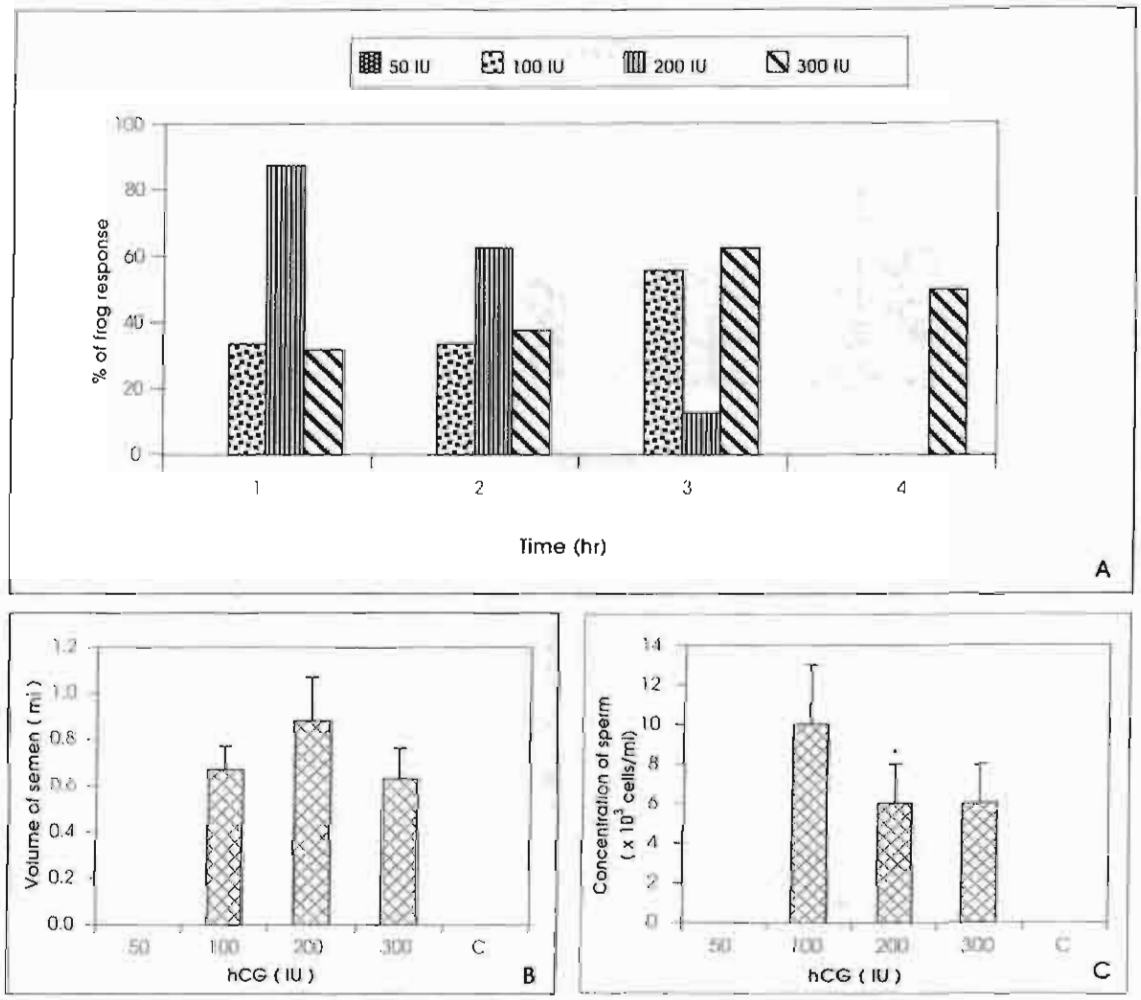

Fig 4 A: Histograms showing percentages of induced spermiation among adult male *R. catesbeiana* after being treated with hCG at 50, 100, 200 and 300 IU

B,C: The changes in total volume of semen and concentration of sperm collected at the end of the experiment (4 hr, respectively) after 50, 100, 200 and 300 IU hCG administration.

* indicates $p < 0.05$ vs 100 IU hCG injected group.

(Fig 6A). The volumes of semen collected from different periods are indistinguishable from those obtained from breeding season (Fig 6B). In contrast to the volume of semen, the concentration of sperm collected in pre-, post- and non-breeding seasons are significantly lower than the value recorded in the breeding season, with $P \leq 0.05$ (Fig 6C).

Discussion

Effects of administration of GnRHa, hCG and pituitary homogenate on spermiation

The present study revealed that GnRH agonist (GnRHa) and hCG could be used to elicit the sperm release in *R. tigerina*, a native rice field frog of Thailand. There was a significant difference among various doses of GnRHa in their effectiveness: the 10 μg/kg bw of GnRHa gave a better response than the lower and higher three doses. In *R. catesbeiana*, the frogs that have been imported from north America for commercial culturing in Thailand, the highest of both volume and sperm concentration could be obtained from the administration of GnRHa at 25 μg/kg bw. Similar effect was also reported in bullfrogs cultured in the temperate region[8] and in another species of frogs, *Hyla regilla*[7]. In contrast to these optimal doses, the higher doses of GnRHa up to 50 μg/kg bw could not elicit any substantial spermiation within the first hour in both species of frogs, and the peak response occurred at three hours after treatment. The GnRH agonist may act through the anterior pituitary gland which, in turn, induces

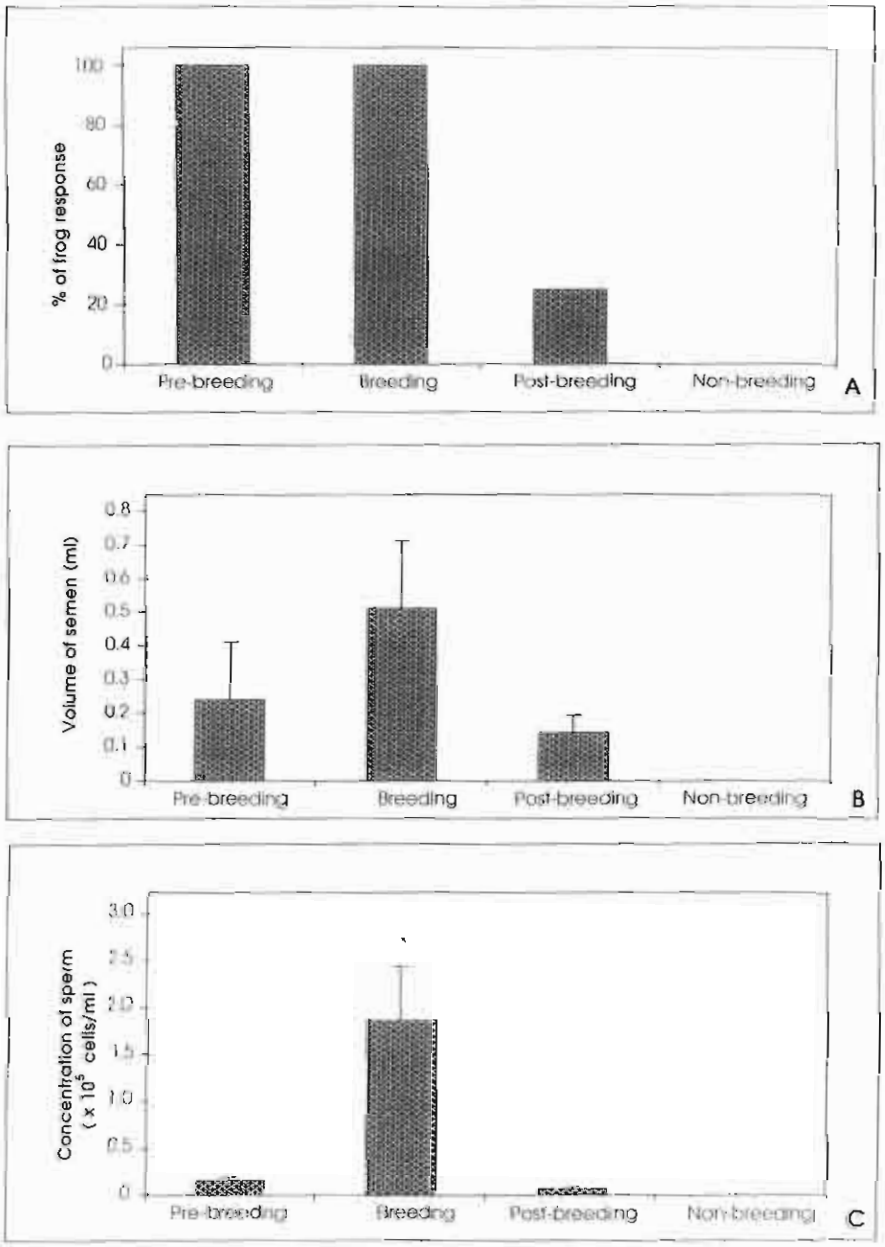

Fig 5 A Histograms showing changes in the percentages of spermiation of *R. tigerina* in different seasons after administration of the most effective doses of GnRHa (10 µg/kg bw).

B,C The changes in volume of semen and concentration of sperm collected from different seasons after injections with the most effective doses of GnRHa.

* indicates $p < 0.05$ vs other seasonal periods

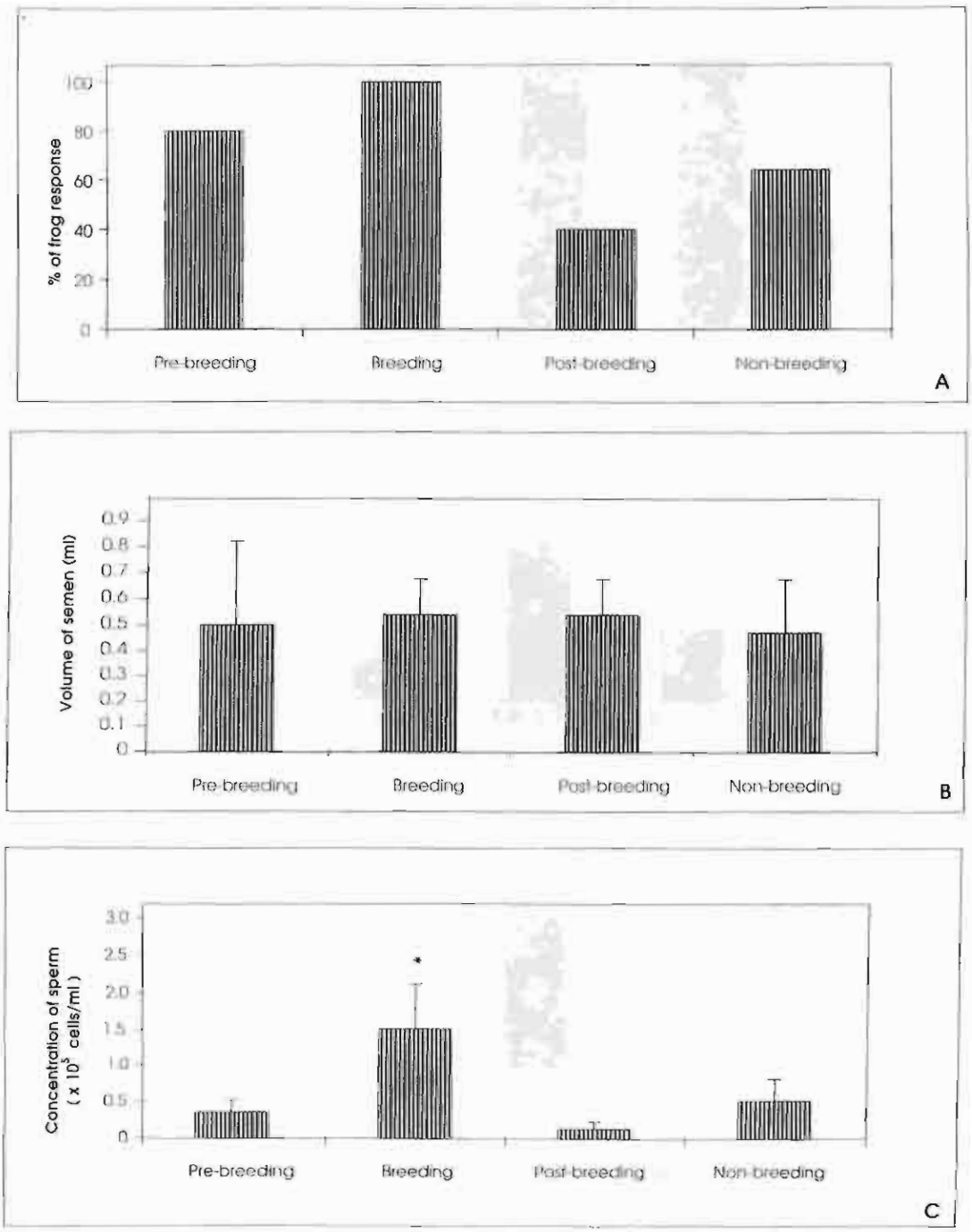

Fig 6. A Histograms showing changes in the percentages of spermiation of *R. catesbeiana* in different seasons after administration of the most effective doses of GnRHa (.25μg/kg bw)

B,C The changes in volume of semen and concentration of sperm collected from different seasons after injections with the most effective doses of GnRHa

* indicates $p<0.05$ vs other seasonal periods

the sperm release in the experimental frogs. The direct effect of GnRH on testicular activity has also been reported in *R. esculenta* and *R. pipiens*.[6,16,17,18]

The volume of semen and concentration of sperm in *R. tigerina* after the administration of GnRHa at dosage 50 µg/kg bw were also remarkably decreased in comparison with the results from the dosages of 10 or 25 µg/kg bw The high dose of GnRHa may lead to the desensitization of the pituitary gland which, in turn, could not maintain the level of circulating gonadotropins. There was an evidence done in rhesus monkey which indicated that the constant infusion of exogenous GnRH could reduce pituitary response in a phenomenon generally known as "down regulation".[19] The restoration of gonadotropin secretion, however, was achieved in the same animals by the intermittent administration of GnRH. In the present study, a single injection of high dose of GnRHa to the frogs would probably create the condition of prolonged exposure to this hormone. Therefore, it might result in the decrease in the response of pituitary gland at the beginning of the experiment. Furthermore, the development of pituitary refractoriness after continuous infusion of GnRH for a short duration was also found in rat[20] and sheep[21]. This phenomenon may also be resulted in part from a reduction in the available receptors for GnRH.

The administration of pituitary homogenate showed significant effect on spermiation in both species of frogs. This may be due mainly to the stimulatory effects of LH and FSH. It was reported that mammalian LH and FSH could induce spermiation in frogs.[8,10] The sperm release could also be induced by hCG, in which the doses of 50 and 100 IU/frog could induce 85-100% response in *R. tigerina* and *R. catesbeiana*, respectively. Similar effect was also reported in *R. catesbeiana* after receiving 200 IU hCG.[8] The activity of hCG in inducing spermiation in frogs is probably due to its LH-like action which could act directly at the gonadal level.[22] There was an evidence which showed that the hCG receptors existed in the testicular tissue.[23]

The effect of high doses of hCG (100 and 300 IU/frog), however, appeared to delay the maximal response, especially in *R. catesbeiana* which showed only 60% of response after three hours of injection. The delayed effect of high dose of hCG might occur from the loss of receptors in the gonads and the phenomenon of "down regulation" as discussed earlier. Conti *et al.*[24] who studied rat ovary, had found that there was a receptor loss after hCG administration, and there seemed to be an inverse correlation between the number of receptors and the dose of hCG.

Effect of the optimal dose of GnRHa on spermiation outside the breeding season

The present study also showed that the exogenous GnRHa could have the effect on spermiation outside the breeding season in *R. catesbeiana*. However, the percentage of frogs responding to GnRHa decreased during the post-and non-breeding periods. The testicular activities of bullfrogs were well correlated with the level of gonadotropin throughout the year.[25] Histological investigation of testes of *R. catesbeiana* from natural habitat in the state of Missouri,USA, revealed that spermatozoa in seminiferous tubules were reduced in number after breeding period but they never reached zero level.[26] Similar testicular picture was found in bullfrogs cultured in Thailand.[27] The spermiation response in *R. catesbeiana* throughout the year may be due to their continuous type of spermatogenic cycle.

In contrast, the spermiation could not be successfully induced in *R. tigerina* outside breeding season. The negative response to GnRHa in *R. tigerina* could be explained by the work of van Oordt,[28] who have shown that the sensitivity of the germinal cells to gonadotropic hormones were least sensitive during autumn and winter. Our earlier observation also showed that in *R tigerina*, the testicular tissue usually break down during the non-breeding periods, and late stages germ cells were completely absent.[29] Similarly, the seminiferous tubules of a tropical frogs, *R. tigrina* Daud, in the period apart from the breeding season contained very few cell nests and most of which were spermatogonia.[30] These frogs are, hence, considered to have discontinuous spermatogenic cycle.

Acknowledgements

The authors wish to recognize the assistance in graphic work by Associate Professor Sukumal Chongthammakun. Appreciation is expressed to Professor Maleeya Kruatrachue for her valuable comments on the research.

This work was supported by the National Center for Genetic Engineering and Biotechnology, the National Science and Technology Development Agency (Grant # 01-35-006) and the Thailand Research Fund (Senior Research Scholar Fellowship to P Sobhon), Bangkok, Thailand.

References

1. Callard IP, Callard GV, Lance V, Bolaffi JL and Rosset JS (1978) Testicular regulation in nonmammalian vertebrates. *Biol Reprod*, 18, 16-43.
2. Licht P (1979) Reproductive endocrinology of reptiles and amphibians gonadotropins. *Ann Rev Physiol* 41, 337-51.
3. Thornton VF and Geschwind II (1974) Hypothalamic control of gonadotropin release in amphibia : evidence from studies of gonadotropin release *in vitro* and *in vivo*. *Gen Comp Endocrinol* 23, 294-301.
4. Daniels E and Licht P (1980) Effects of gonadotropin-releasing hormone on the levels of plasma gonadotropins (FSH and LH) in the bullfrog, *Rana catesbeiana*. *Gen Comp Endocrinol* 42, 455-63.
5. Rastogi RK, Iela L, Saxena PK and Chieffi G (1976) The control of spermatogenesis in the green frog, *Rana esculenta*. *J Exp Zool* 96, 151-66.
6. Di Matteo L., Minucci S, Fasano S, Pierantoni R, Varriale B and Chieffi G (1988) A gonadotropin-releasing hormone (GnRH) antagonist decreases androgen production and spermatogonial multiplication in frog (*Rana esculenta*) : indirect evidence for the existence of GnRH or GnRH-like material receptors in the hypophysis and testis. *Endocrinology* 122, 62-7.
7. Licht P (1974) Induction of sperm release in frogs by mammalian gonadotropin-releasing hormone. *Gen Comp Endocrinol* 23, 352-54.
8. Easley KA, Culley DD, Nelson JR, Horseman D and Penkala JE (1979) Environmental influences on hormonally induced spermiation of the bullfrog, *Rana catesbeiana*. *J Exp Zool* 207, 407-16.
9. McCreery BR, Licht P, Barnes R, Rivier JE and Vale WW (1982) Action of agonistic and antagonistic analogs of gonadotropin releasing hormone (Gn-RH) in the bullfrog *Rana catesbeiana*. *Gen Comp Endocrinol* 46, 511-20.
10. Robbins SL and Parker F Jr (1952). Studies on the mechanism of the spermatic release of the male north American frog (*Rana pipiens*) reaction to various hormones. *J Clin Endocrinol Metab* 12, 354-60.
11. Mckinnell RG, Pisciano DJ and Kreig RE (1976) Fertilization and development of frog eggs after repeated spermiation induced by human chorionic gonadotropin. *Lab Animal Sci* 26, 932-35.
12. Van Oordt PJWJ (1956) Regulation of spermatogenetic cycle in the common frog (*Rana temporaria*). van Der Wiel, Arnhem.
13. Burgos MH (1992) Regulación hormonal de los caracteres sexuales secundarios en el sapo macho. *Rev Soc Agent Biol* 26, 193-71.
14. Inger RF and Greenberg B (1963) The annual reproductive pattern of the frog, *Rana erythraea* in Sarawak. *Physiol Zool* 36, 21-33.
15. Loumbourdis NS and Kyrizakopoulou-Sklavounou P (1991) Reproductive and lipid cycles in the male frog *Rana ridibunda* in northern Greece. *Comp Biochem Physiol* 4, 357-63.
16. Sogal SJ and Adejawoo LA (1979) Direct effect of LHRH on testicular steroidogenesis in *Rana pipiens*. *Biol Bull* 157, 397.
17. Pierantoni R, Fasano S, Di Matteo L, Minucci S, Varriale B and Chieffi G (1984a) Stimulatory effect of a GnRH agonist (buserelin) in vitro and in vivo testosterone production by the frog (*Rana esculenta*) testis. *Mol Cell Endocrinol* 38, 213-19.
18. Pierantoni R, Iela L, d'Istria M, Fasano S, Rastogi RK, Delrio G (1984b) Seasonal testosterone profile and testicular responsiveness to pituitary factors and gonadotropin releasing hormone during two different phases of the sexual cycle of the frog (*Rana esculenta*). *J Endocrinol* 102, 387-92.
19. Belchetz PE, Plant TM, Nakai Y, Keogh EJ and Knobil E (1978) Hypophysial responses to continuous and intermittent delivery of hypothalamic gonadotropin-releasing hormone. *Science* 202, 631-33.
20. Schuiling GA and Van Rees GP (1974) Evidence of an extra-hypothalamic inhibitory influence on the secretion of gonadotropins in the female rat. *Neuroendocrinology* 15, 73-8.
21. Piper EL and Foote WC (1970) The effect of 17-beta-estradiol on corpus luteum function in sheep. *Biol Reprod* 2, 48-52.
22. Russo J and Burgos MH (1969) Effect of HCG on the enzymic activity of toad testes. *Gen Comp Endocrinol* 13, 185-88.
23. Hsueh AJ, Dufau ML and Catt KJ (1977) Gonadotropin-induced regulation of luteinizing hormone receptors and desensitization of testicular 3'5'-cyclic AMP and testosterone response. *Proc Natl Acad Sci USA*, 74, 592-95.
24. Conti M Harwood JP, Dufau ML and Catt KJ (1977) Regulation of luteinizing hormone receptors and adenylate cyclase activity by gonadotrophin in the rat ovary. *Mol Pharmacol* 13, 1024-32.
25. Licht P, McCreery BR, Branes R and Pang R (1983) Seasonal and stress related changes in plasma gonadotropins, sex steroids and corticosterone in the bullfrog, *Rana catesbeiana*. *Gen Comp Endocrinol* 50, 124-45.
26. Schroeder EE (1974) The reproductive cycle in the male bullfrog, *Rana catesbeiana* in Missouri. *Trans Kans Acad Sci* 77, 31-5.
27. Chavadej J, Jeratcungrattana A, Sretarugsa P and Sobhon P (2000) Structure and development of the testis of Bullfrog, *Rana catesbeiana* and their changes during seasonal variation. *ScienceAsia* 26, 69-80.
28. van Oordt CJ and van Oordt PGWJ (1955) The regulation of spermatogenesis in the frog. *Mem Soc Endocrinol* 4, 25.
29. Sretarugsa P, Nakiem V, Sobhon P, Chavadej J, Kruatrachu M and Upatham ES (1997) Structure of the testis of *Rana tigerina* and its changes during development and seasonal variation. *J Sci Soc Thailand* 23, 75-86.
30. Saidapur SK and Nadkarni VB (1975) Seasonal variation in the structure and function of testis and thumb pad in the frog *Rana tigrina* (Daud). *Indian J Exp Biol* 13, 432-48.

Journal of Helminthology (2001) 75, 43–50 DOI: 10.1079/JOH2001041

Fasciola gigantica: surface topography of the adult tegument

T. Dangprasert[1], W. Khawsuk[1], A. Meepool[1], C. Wanichanon[1], V. Viyanant[2], E.S. Upatham[2], S. Wongratanacheevin[3] and P. Sobhon[1]*

[1]Department of Anatomy and [2]Department of Biology, Faculty of Science, Mahidol University, Rama VI Road, Bangkok 10400, Thailand: [3]Department of Microbiology, Faculty of Medicine, Khon Kaen University, Khon Kaen 40002, Thailand

Abstract

Adult *Fasciola gigantica* are leaf-shaped with tapered anterior and posterior ends and measure about 35 mm in length and 15 mm in width across the mid section. Under the scanning electron microscope its surface appears rough due to the presence of numerous spines and surface foldings. Both oral and ventral suckers have thick rims covered with transverse folds and appear spineless. On the anterior part of the ventral surface of the body, the spines are small and closely-spaced. Each spine has a serrated edge with 16 to 20 sharp points, and measures about 20 μm in width and 30 μm in height. In the mid-region the spines increase in size (up to 54 μm in width and 58 μm in height) and number, especially towards the lateral aspect of the body. Towards the posterior end the spines progressively decrease in both size and number. The tegumental surface between the spines appears highly corrugated with transverse folds alternating with grooves. At higher magnifications the surface of each fold is further increased with a meshwork of small ridges separated by variable-sized pits or slits. There are three types of sensory papillae on the surface. Types 1 and 2 are bulbous, measuring 4–6 μm in diameter at the base with nipple-like tips, and the type 2 also have short cilia. Type 3 papillae are also bulbous and of similar size but with a smooth surface. These sensory papillae usually occur in clusters, each having between 2 and 15 units depending on the region of the body. Clusters of papillae on the lateral aspect (usually types 1 and 2) and around the suckers (type 3) tend to be more numerous and larger in size. The dorsal side of the body exhibits similar surface features, but the spines and papillae appear less numerous and are smaller. Corrugation and invaginations of the surface are also less extensive than on the ventral side of the body.

Introduction

Fascioliasis is a disease that infects both domestic and wild animals, and it is one of the major tropical diseases that afflicts both the temperate and tropical regions of the world. The causative parasite in temperate regions is *Fasciola hepatica*, whilst in the tropics it is *F. gigantica*. Fascioliasis causes significant economic losses estimated at US $2000 million per annum from its effect on domestic and economic animals (Boray, 1985). The disease can also cross-infect humans, and there have been reports of increasing incidents worldwide (Chitchung *et al.*, 1992; Maurice, 1994). The prevalences of infection are as high as 30–90% in Africa, 25–90% in Indonesia (Edney & Muchlis, 1962; Soesetya, 1975; Fabiyi, 1987). In Thailand, the prevalences of *F. gigantica* in cattle and buffaloes range between 4 and 24%, with

*Author for correspondence
Fax: 662 2479880
E-mail: scpso@mahidol.ac.th

highest incidences in the north and north-east, and the lowest in the south (Pholpark & Srikitjakara, 1989; Sukhapesna *et al.*, 1990, 1994; Sobhon *et al.*, 1998). It is clear that the disease is a major impediment to economic progress, which is exacerbated in less developed countries, particularly towards subsistence farmers who have limited resources to treat their herds.

Fascioliasis can be partially controlled by periodic treatment of the animals in endemic areas with a repertoire of drugs. Triclabendazole has been reported to be highly effective, although resistance of liver flukes to this drug has been reported (Overend & Bower, 1995). In view of the cost and possible resistance of liver fluke to the action of drugs, a better alternative would be the development of vaccines to either completely prevent the infection or arrest worm development at certain stages of the life cycle.

The tegument is the interfacing layer that helps the liver flukes to maintain their homeostasis which is essential for their survival in the hostile environment of the host. The tegument plays a key role in the absorption and exchange of nutritive and waste molecules, the regulation of ionic equilibrium between the interior of the parasite and the surrounding host fluid, and in protecting the parasites from the immune responses of the host. Understanding the structural organization of the tegument is essential in developing any rational drugs or vaccines, which might damage the parasites through their actions on the tegument. Despite few observations on the fine surface features of *F. hepatica* (Bennett 1975a,b), no studies have previously been undertaken on *F. gigantica*. In the present study, the detailed surface features of adult *F. gigantica* tegument are investigated by using scanning electron microscopy (SEM).

Materials and methods

Adult specimens of *Fasciola gigantica* were collected from the bile ducts in the liver and gall bladder of cattle and water buffaloes killed at local abattoirs. Flukes were washed several times in 0.85% normal saline before being transferred into Minimum Essential Medium (MEM), with three changes. Flukes were kept in MEM supplemented with 10 $\mu g\ ml^{-1}$ penicillin and 100 units ml^{-1} streptomycin until processed for SEM.

Entire adult worms were fixed in 2.5% glutaraldehyde in 0.1 M sodium cacodylate buffer containing calcium acetate, pH 7.2, at 4°C for at least 2 h. They were washed three times with the same buffer, post-fixed in 1% osmium tetroxide in 0.1 M sodium cacodylate buffer, pH 7.2, at 4°C for 3 h, and washed in three changes of distilled water. Subsequently, they were dehydrated through increasing concentrations of ethanol, and dried in a Hitachi HCP-2 critical point drying machine using liquid carbon dioxide as a transitional medium. After drying, specimens were mounted on aluminum planchets and coated with gold in an ion-sputtering apparatus, Hitachi E-102, with a setting at 10–15 mA for 4 min. Specimens were examined in a Hitachi scanning electron microscope (SEM) S-2530 operating at 30 kV.

Results

Ventral surface

On the surface of the anterior region, spines are medium-sized and closely-spaced, each measuring about 20 μm in width and 30 μm in height and having a serrated edge with 16–20 sharp points (fig. 1E,G,H). At higher magnifications the surface of the spines, except their edges, appears highly corrugated and invaginated with small ridges and pits (fig. 1G,H). The surface area between the spines appears corrugated with transverse folds alternating with grooves (fig. 1E,G). At higher magnifications the folds are, in turn, composed of a meshwork of interlacing microfolds or small ridges separated from one another by variable-sized pits or slits (fig. 1I). In some areas there are groups of bulbous papillae, which are assumed to be sensory receptors (figs 1E–G, 2A–C). Each papilla appears as a small dome or bulb 4–6 μm in diameter at the base. The first two types of papillae, types 1 and 2, have nipple-like tips, with type 2 also having short cilia on their tips (fig. 2E,G). The third type of papillae, type 3, is fungiform in shape with a smooth top and highly pitted base (fig. 2F). On the anterior and lateral surfaces, type 1 and 2 papillae may appear singly or in a group of two to three units (fig. 1E). In contrast, both the oral and ventral suckers have thick muscular rims covered with wide transverse folds, surrounded by rows of type 3 papillae in large clusters, and pores of gland cells (fig. 1A–D).

On the surface of the middle region of the body, the spines increase in size (up to 54 μm in width and 58 μm in height) as well as number, particularly towards the edges of the body. The majority of spines, because of their large size, have blunt rather than sharp serrated edges (fig. 1F). The area between the spines appears highly corrugated with ridges separated by pits and slits. This area also contains large groups of papillae with similar characteristics to those found on the anterior region. Towards the lateral aspect of the body, the spines and clusters of papillae become very prominent in both size and number (fig. 2A–C). Each cluster of papillae is a large aggregate of 10–15 units (fig. 2C,D). Most of the papillae in the clusters are types 1 and 2 (fig. 2D,E,G).

On the surface of the posterior region of the body, the spines progressively decrease both in size and number, and they become widely separated (fig. 3A–C). The spines are usually short but still covered with highly invaginated surface (fig. 1E,F). Clusters of papillae are, however, still prominent; and each may contain as many units per group as those on the lateral aspect of the middle region (fig. 1C–E). The area between the spines also appears highly folded and invaginated, but the ridges are not as well developed as those on the anterior and middle regions. The posterior tip of the body has very few spines and appears smooth (fig. 3B).

Dorsal surface

Generally, the anterior and middle regions of the dorsal surface exhibit similar features to those of the ventral surface, but they tend to have smaller-sized spines and fewer papillae (fig. 3G,H). Spines on the

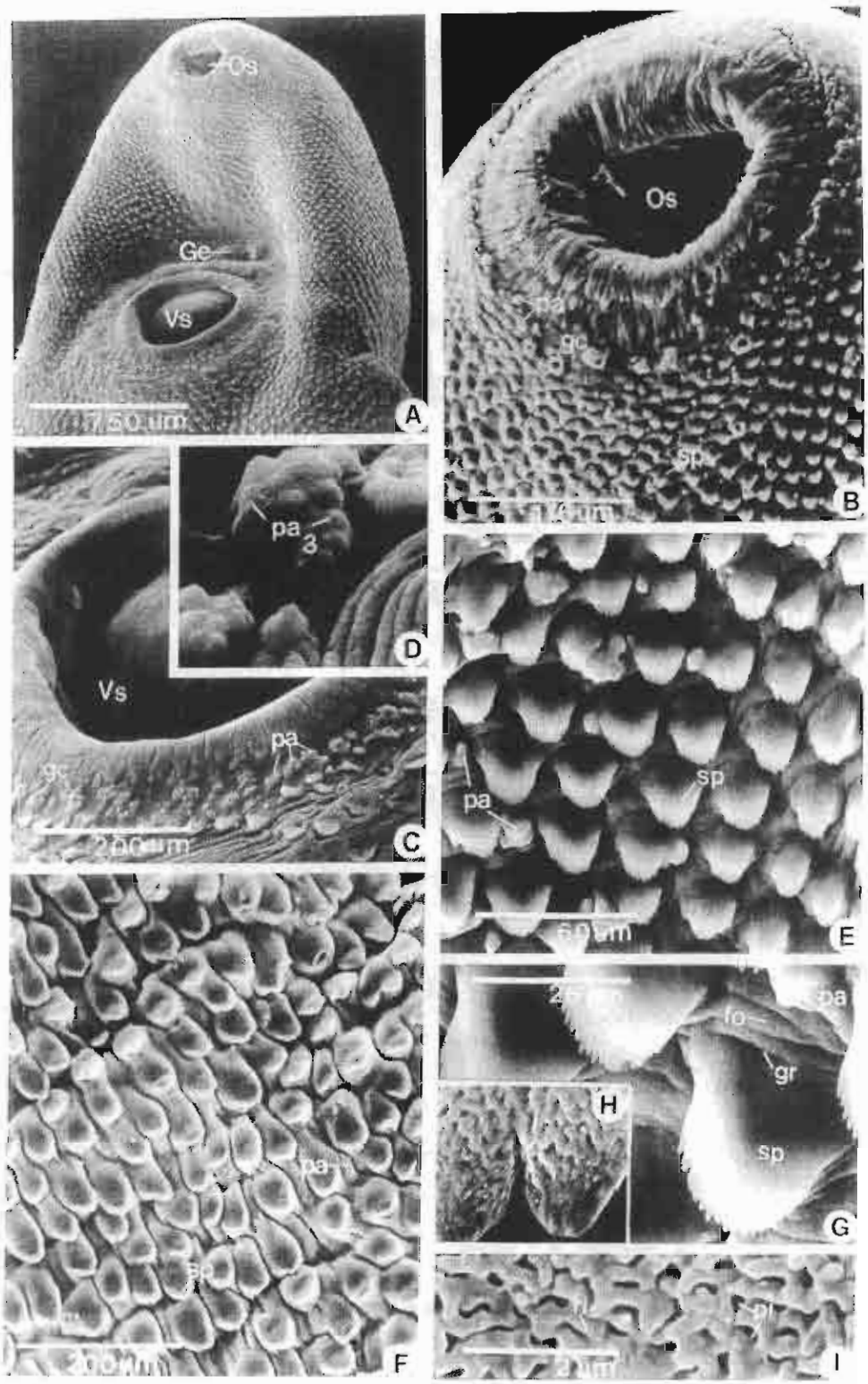

Fig. 1. A–D. The anterior ventral surface of adult *Fasciola gigantica*, with oral (Os) and ventral suckers (Vs) surrounded by rows of ventral papillae (pa) with papilla cluster (pa_3) in D, flat spines (sp), pores of glands (gc) and opening of genital canal (Ge). E and F. The anterior and middle surface regions, respectively, with closely-spaced spines (sp) and clusters of papillae (pa). G and H. Serrated spines with highly corrugated surface. Between the spines the surface appears as a series of alternating folds (fo) and grooves (gr). I. Surface of fold with small ridges (ri) separated by pits and slits (pi).

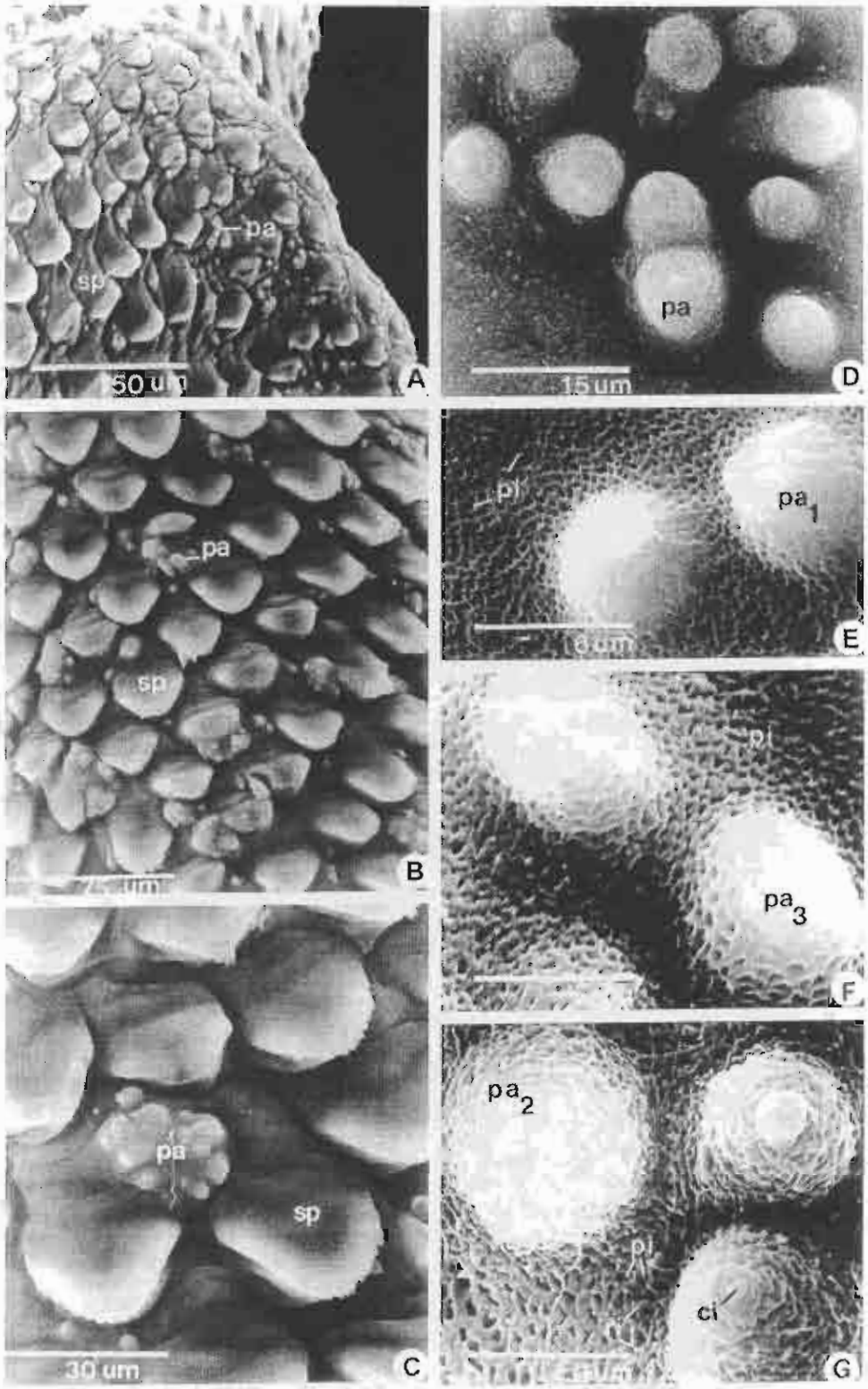

Fig. 2. A–C. The anterior-lateral (in A) and middle-lateral (in B) regions of the ventral surface of *Fasciola gigantica*, with numerous flattened and highly serrated spines (sp), and large clusters of papillae (pa). D. A large cluster of papillae. E. Type 1 papillae (pa1) with nipple-like tips. F. Type 3 papillae (pa_3) fungiform in shape, with smooth surface. G. Type 2 papillae (pa_2) with short cilia (ci) on the nipple-like tips.

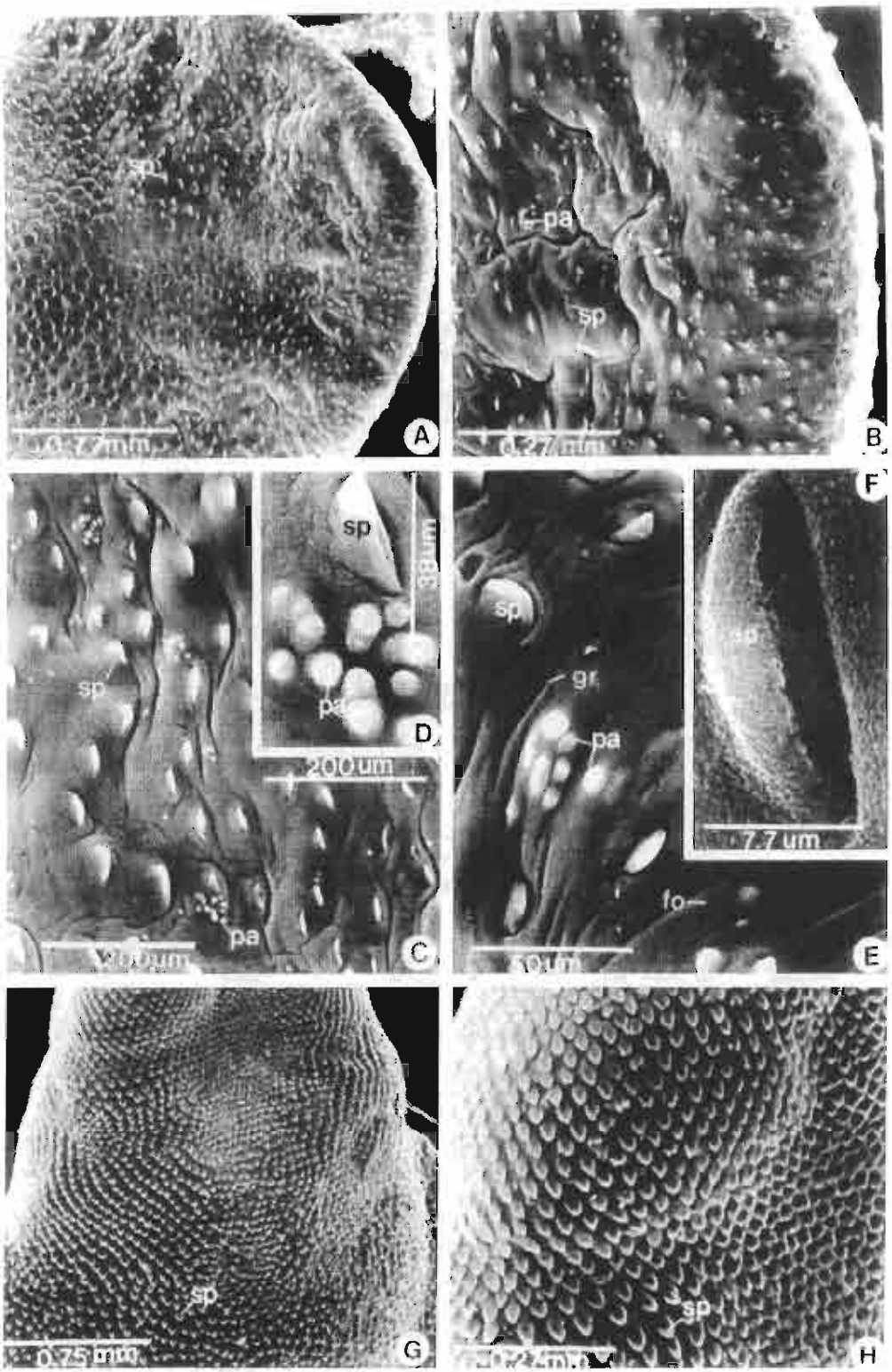

Fig. 3. A–C. The posterior part of the ventral surface and the tip of *Fasciola gigantica* with short, flattened, widely-spaced spines (sp) and clusters of papillae (pa). D. Large cluster of papillae. E. Large cluster of papillae and surface folds (fo) and grooves (gr). F. Spine with highly corrugated surface. G and H. The anterior dorsal surface with numerous spines but fewer papillae.

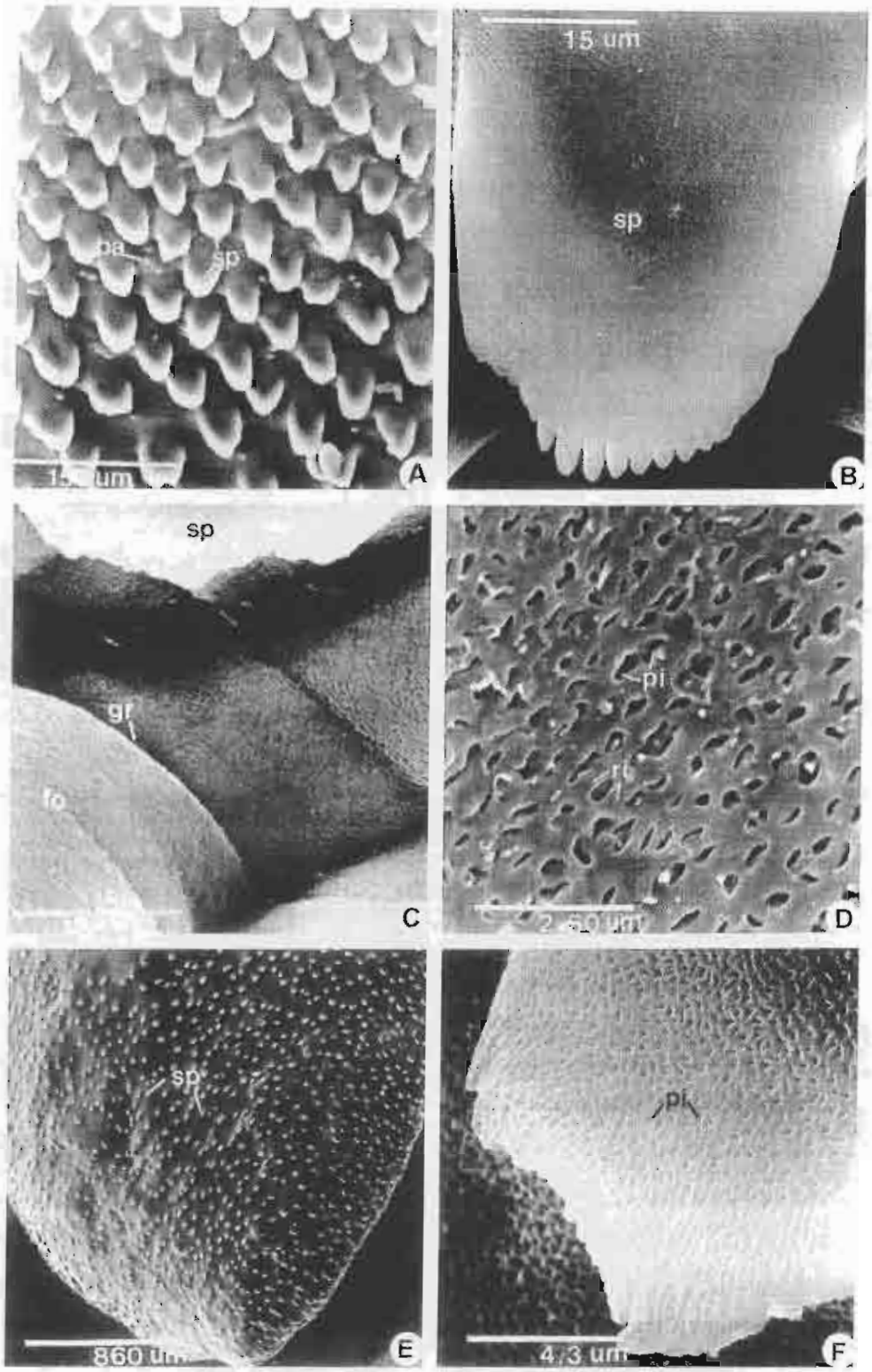

Fig. 4. A. The middle region of the dorsal surface of *Fasciola gigantica*, with flat serrated spines (sp) close together. B. Spine C. Surface between the spines, highly corrugated with folds (fo) and grooves (gr). D. Surface of fold, with flat ridges (ri) separated by pits and slits (pi). E. The posterior dorsal surface, with short widely separated spines. F. Spine with highly invaginated surface and unserrated edge.

anterior and middle regions are still serrated (fig. 4A,B), whilst those located towards the lateral and posterior regions are smaller and not well serrated. The surface area between the spines appears highly convoluted with folds and grooves (fig. 4C), but ridges on each fold tend to be flattened when compared with those on the anterior and middle regions of the ventral surface (fig. 4D).

The posterior region of the dorsal surface possesses fewer, smaller, and widely-spaced spines (fig. 4E). Each spine is short and unserrated, but still covered with a highly invaginated surface (fig. 4F). The area between the spines is invaginated with large pits, whilst the ridges are not well developed. Unlike the ventral surface, the posterior end of the dorsal surface has only a small number of papillae.

Discussion

The most remarkable features of the surface topography of fully mature *F. gigantica* are the presence of a highly corrugated surface which consists of series of alternating grooves and folds, and the presence of spines. The surface of each fold is increased further by a meshwork of microfolds or ridges separated by pits and slits. This increased surface area could enhance the effectiveness of absorption and exchange of materials by the tegument, a characteristic which is also observed in other trematodes, such as *F. hepatica* (Bennett, 1975b), *Opisthorchis viverrini* (Apinhasmit *et al.*, 1993), and the schistosomes (Hockley, 1973; Hockley & McLaren, 1973, 1977; Jinxin & Yixun, 1981; Sobhon & Upatham, 1990). The development of ridges and pits varies in different regions of the worm surface. The ventral and lateral surfaces tend to have more complex ridges and pits than the dorsal surface, and the anterior and middle regions also tend to have more developed ridges and pits than the posterior region. This suggests different degrees of absorptive capacities in various regions of the tegument, a characteristic which is similar to other helminths (Bennett, 1975b; Hockley & McLaren, 1977; Sobhon & Upatham, 1990; Apinhasmit *et al.*, 1993). Another distinguishing surface feature is the presence of numerous spines covering all parts of the body's surface. We have not yet examined the surface of metacercaria and juvenile stages of this species, but juveniles of *F. hepatica* possess large serrated spines on their entire surface (Bennett, 1975a,b), while those of *O. viverrini* possess serrated spines on the anterior and single-pointed spines on the posterior parts of the body (Scholz *et al.*, 1992; Apinhasmit *et al.*, 1993). These spines may facilitate the movement of juvenile flukes during their migration to the biliary system of the liver. Upon reaching the liver, mature *O. viverrini* become spineless (Apinhasmit *et al.*, 1993), and the loss of spines may be due to the decreased movement of the fluke in the bile ducts. In contrast, adults of *F. gigantica* and *F. hepatica* still retain spines on the surface which implies that they may have more movement in the bile ducts of the liver. Their more active movement in the biliary tree of the liver may explain why they cause more severe fibrosis of the bile ducts in comparison with *O. viverrini*. However, for most of the time adult *F. gigantica* probably remain attached to the wall of the bile ducts using their relatively large and muscular ventral suckers, which are surrounded by smooth fungiform (type 3) papillae which could act as pressure receptors. On the other hand, type 1 and 2 papillae, which are distributed elsewhere on the surface of the bodies, may act as tactile receptors.

Acknowledgement

This project was supported by Thailand Research Fund (Senior Research Scholar Fellowship to P. Sobhon).

References

Apinhasmit, W., Sobhon, P., Saitongdee, P. & Upatham, E.S. (1993) *Opisthorchis viverrini*: changes of the tegumental surface in newly excysted juvenile, first-week and adult flukes. *International Journal for Parasitology* **23**, 829–839.

Bennett, C.E. (1975a) Surface features, sensory structures and movement of the newly excysted juvenile *Fasciola hepatica*. *Journal of Parasitology* **61**, 886–891.

Bennett, C.E. (1975b) Scanning electron microscopy of *Fasciola hepatica* during growth and maturation in the mouse. *Journal of Parasitology* **61**, 892–898.

Boray, J.C. (1985) Flukes of domestic animals. pp. 179–278 *in* Gaafar, S.M., Howard, W.E., Marsh, R.E. (*Eds*) *Parasites, pests and predators*. New York, Elsevier.

Chitchung, S., Ratanaikom, N. & Mitranun, W. (1992) *Fasciola hepatica* in human pancreas: a case report. *Journal of Parasitology and Tropical Medicine Association of Thailand* **5**, 113.

Edney, J.M. & Muchlis, A. (1962) Fascioliasis in Indonesian livestock. *Communication Veterinarae* **6**, 49–52.

Fabiyi, J.P. (1987) Production losses and control of helminths in ruminants of tropical regions. *International Journal for Parasitology* **17**, 435–442.

Hockley, D.J. (1973) Ultrastructure of tegument of *Schistosoma*. *Advances in Parasitology* **11**, 233–305.

Hockley, D.J. & McLaren, D.J. (1973) *Schistosoma mansoni*: change in the outer membrane of the tegument during development from cercaria to adult worm. *International Journal for Parasitology* **3**, 13–25.

Hockley, D.J. & McLaren, D.J. (1977) Scanning electron microscopy of eight species of *Schistosoma*. *Transactions of the Royal Society of Tropical Medicine and Hygiene* **71**, 292.

Jinxin, M. & Yixun, H. (1981) Scanning electron microscopy of Chinese (mainland) strain *Schistosoma japonicum*. *Chinese Medical Journal* **94**, 63–70.

Maurice, J. (1994) Is something lurking in your liver? *New Scientist* **1917**, 26–31.

Overend, D.J. & Bower, F.L. (1995) Resistance of *Fasciola hepatica* to triclabendazole. *Australian Veterinary Journal* **72**, 275–276.

Pholpark, M. & Srikitjakara, L. (1989) The control of parasitism in swamp buffalo and cattle in north-east Thailand. pp. 244–249 in *International Seminar on Animal Health and Production Service for Village Livestock*. Khon Kaen, Thailand.

Scholz, T., Ditrich, O. & Giboda, M. (1992) Study on the surface morphology of the developmental stages of the liver fluke, *Opisthorchis viverrini* (Trematoda:

Opisthorchidae). *Annales de Parasitologie Humaine et Comparee* 67, 82–90.

Sobhon, P. & Upatham, E.S. (1990) Snail hosts, life-cycle, and tegumental structure of oriental schistosomes. UNDP/World Bank/WHO Special Programme for Research and Training in Tropical Diseases. pp. 57–88.

Sobhon, P., Anantavara, S., Dangprasert, T., Viyanant, V., Krailas, D., Upatham, E.S., Wanichanon, C. & Kusamran, T. (1998) *Fasciola gigantica*: studies of the tegument as a basis for the developments of immunodiagnosis and vaccine. *Southeast Asian Journal of Tropical Medicine and Public Health* 29, 387–400.

Soesetya, R.H.B. (1975) The prevalence of *Fasciola gigantica* infection in cattle in East Java, Indonesia. *Malaysian Veterinary Journal* 6, 5–8.

Sukhapesna, V., Tantasuvan, D., Sarataphan, N. & Sangiumluksana, S. (1990) A study on epidermiology of liver fluke infection in buffaloes. *Thai Journal of Veterinary Medicine* 20, 527–534.

Sukhapesna, V., Tantasuvan, D., Sarataphan, N. & Imsup, K. (1994) Economic impact of fascioliasis in buffalo production. *Journal of the Thai Veterinary Medical Association* 45, 45–52.

(Accepted 21 August 2000)

RESEARCH ARTICLE

ScienceAsia 26 (2000) : 137-148

Fasciola gigantica: Ultrastructure of the Adult Tegument

P Sobhon[a,*], T Dangprasert[c], S Chuanchaiyakul[d], A Meepool[a], W Khawsuk[a], C Wanichanon[a], V Viyanant[b] and ES Upatham[b]

[a] Department of Anatomy, Faculty of Science, Mahidol University, Bangkok 10400, Thailand.
[b] Department of Biology[2], Faculty of Science, Mahidol University, Bangkok 10400, Thailand.
[c] Department of Anatomy, Pramongkutklao College of Medicine, Bangkok 10400, Thailand.
[d] Department of Anatomy, Faculty of Medicine, Srinakarinviroj University, Bangkok 10110, Thailand.
* Corresponding author. E-mail: scpso@mahidol.ac.th

Received 27 Apr 2000
Accepted 6 Jun 2000

ABSTRACT The tegument of adult *Fasciola gigantica* can be divided into four layers based on ultrastructural characteristics. The first layer includes ridges and pits which are covered by a trilaminate membrane about 8 nm thick, underlined by a dense lamina about 15 nm thick. The membrane is coated externally by the glycocalyx which consists of two layers: the inner dense homogeneous layer about 10-15 nm, and the outer fibrillar layer about 100-300 nm thick which is intensely stained with ruthenium red. The cytoplasm is composed of densely-packed microtrabecular network, and contains many ovoid granules (G_1) whose size is about 90 x 180 nm, and numerous discoid granules (G_2) whose size is about 40 x 250 nm. G_1 contain dense ruthenium red-positive matrix while G_2 contain translucent matrix, and both are surrounded by a trilaminate membrane. G_1 close to the surface invariably exocytose their content into bottoms of the pits, while some G_2 are fused and have their membrane joined up with the surface membrane. It is, therefore, suggested that G_1 contribute to the formation of glycocalyx while G_2 are the main contributor to the surface membrane. The second layer of the tegument is a narrow zone of cytoplasm that contains high concentrations of G_1, G_2 granules and lysosomes. The third layer is the widest middle portion of the tegument which contains numerous and evenly distributed mitochondria. Both G_1 and G_2 granules are present but in much fewer number than in the first and second layers. The fourth layer is the innermost zone that rests on and couples with the 120-140 nm thick basal lamina. Its cytoplasm is loosely packed and contains numerous infoldings of the basal plasma membrane which have mitochondria in close association. It contains fairly large numbers of G_1 and G_2 granules which are produced and transported to the tegument by one type of tegumental cells lying in rows underneath the muscular layers. Spines in the tegument are numerous, each is a wedge-shaped crystalline structure with the lattice spacing about 4 nm, and its rootlets are firmly implanted in the basal lamina.

KEYWORDS: *Fasciola gigantica*, tegument, ultrastructure, transmission electron microscopy

INTRODUCTION

Fasciolosis due to *Fasciola gigantica* causes significant economic loss in animal production in the tropics. The disease can also infect humans, and there are reports of increasing incidence worldwide.[1] The prevalence of infection of animal are as high as 30-90% in Africa, 25-90% in Indonesia.[2,3] In Thailand the prevalence of infection in cattle and buffaloes are 4-24%, with the highest incidence in the North and Northeast, and the lowest in the South.[4,5] Hence, the disease is one of the major impediments to economic progress in developing countries. Fasciolosis could be partially controlled by periodic treatment of animals in endemic areas with drugs, among which triclabendazole was reported to be highly effective, even though resistance has been observed. In view of the cost and possible emergence of drug resistance, a better preventive measure would be the development of vaccines which could either completely prevent the infection or arrest the development of the parasites at certain stages of their life cycle.

The tegument of the parasite is one of the major targets for vaccines since it produces and releases a number of antigens that can stimulate the immune responses in hosts.[6,7] Furthermore, the tegument plays roles in maintaining the parasites' homeostasis, such as the absorption and exchange of nutritive and waste molecules, and the regulation of ionic equilibrium between the interior of the parasites and the surrounding host fluid.[8] A complete understanding of the structural organization of the tegument is hence crucial in developing any rational drugs or vaccines that can damage the parasites through their actions.

on the tegument. Up to now, all work on the tegument ultrastructure have been carried out in *Fasciola hepatica*.[10,11] Though the basic structure of the tegument of *F. gigantica* is expected to be similar to that of *F. hepatica*, there is evidence that the two species exhibit differences in their resistance to drugs and potential vaccine candidates.[14] Hence there could be variations in the tegument ultrastructure that have not yet been observed. In this study, we report the tegument ultrastructure of adult *F. gigantica*.

Materials and Methods

Specimen Collection

Adult *F. gigantica* were collected from the bile ducts and gallbladders of cattle and water buffaloes killed at the abattoirs. The flukes were washed several times in 0.85% normal saline before being transferred into Minimum Essential Medium (MEM) with three changes. The flukes were kept in MEM supplemented with 10mg/ml penicillin and 100 unit/ml streptomycin until prepared for TEM.

Conventional Transmission Electron Microscopy (TEM)

The adult flukes were sliced into thin strips while being fixed in 2.5 % glutaraldehyde in 0.1 M sodium cacodylate buffer containing 0.1 M calcium acetate, pH 7.2, at 4°C for 2 h. Then they were washed three times with the same buffer, post-fixed in 1 % osmium tetroxide in 0.1 M sodium cacodylate buffer, pH 7.2, at 4°C for 3 h, and washed in distilled water. Finally, the specimens were fixed in 0.5% aqueous solution of uranyl acetate, pH5, containing 45mg/ml sucrose, for 30 min, at 4°C. The specimens were washed three times in distilled water, then dehydrated in graded series of ethanol (50-100%), for 20 min at each step. Subsequently, they were infiltrated twice in propylene oxide for 20 min each; and the solution was later sequentially replaced with the mixture of propylene oxide and Araldite-502 at the ratio of 2:1 for 1 h and 1:2 overnight at room temperature. Finally, the specimens were infiltrated with pure Araldite for at least 12 h at room temperature, and then polymerized at 45°C and 60°C for 2 days each. Thin section were cut and collected either on naked or formvar-coated 200-mesh copper grids, and stained with methanolic 1.8% uranyl acetate and lead citrate, for 30 min each. The sections were viewed in a Hitachi H-300 TEM, operating at 75 kV.

Ruthenium Red Staining

Ruthenium red is a low-mol.wt polycationic compound which binds electrostatically to polyanions such as proteoglycans and staloglycoproteins.[15] This method is used to exhibit glycocalyx and the structure that contains negatively-charged acidic carbohydrates.[16,17] Another group of parasite specimens was thus stained with ruthenium red.[15] Briefly, the specimens were fixed and stained for 1 h at room temperature in a solution containing equal proportions of 4% glutaraldehyde in 0.2 M cacodylate buffer pH 7.2, and 1500 ppm aqueous solution of ruthenium red (Polysciences Co). After washing three times with the same buffer, the flukes were post-fixed for 3 h at room temperature in a solution containing equal proportions of 2 % osmium tetroxide in 0.2 M cacodylate buffer pH 7.2, and an aqueous solution of 1500 ppm ruthenium red. The specimens were rinsed briefly with the same buffer, and then dehydrated and processed for TEM as already described. Both unstained and counterstained sections with uranyl acetate and lead citrate were examined in TEM.

Results

Ultrastructure of the Tegument

When examined in cross section, the tegument can be divided into four layers based on the presence of various organelles and the density of the tegumental cytoskeleton (Fig 1A-C; 2A, B). The first and outer most layer is the microvillus-like zone which actually represents cross sections of ridges or microfolds intervened by oblong pits as visualized in SEM.[9] The crevices or grooves between major folds may run deep down in the tegument, such that in these areas the surface membrane of the ridges are compressed together (Fig 2B). The cytoplasm of the first layer consists of tightly packed microtrabeculae of very thin filaments (Fig 2C, D), and contains moderate number of granules. In conventional TEM preparation the surface membrane appears unilaminate with 8 nm in thickness, and coated on the exterior by a thin layer of homogeneous glycocalyx about 10-15 nm in width (Fig 2D; 3C). By contrast, in ruthenium red-stained sections, glycocalyx appears as a fibrillar layer with thickness as much as 100-300nm (Fig 4D, E). On the cytoplasmic side, the surface membrane is underlined by a lamina of condensed cytoplasm about 15 nm thick (Fig 2D).

The second layer is a narrow zone of cytoplasm under the first layer, which is characterized by the presence of a high concentration of tegumental granules and lysosome-like bodies (Fig 1A; 2B, C).

Figure 1

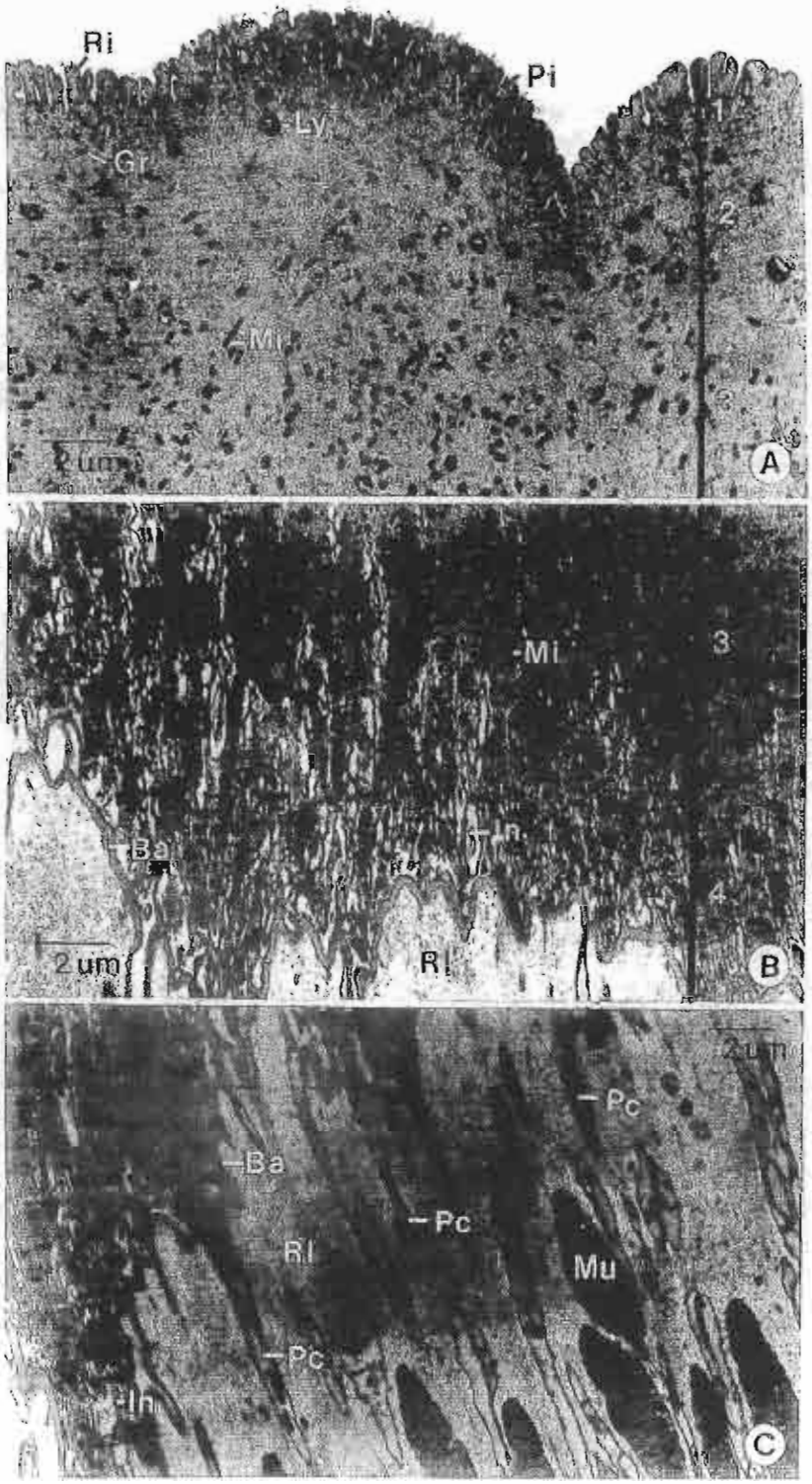

Fig 1 (A) (B) (C) low power conventional TEM micrographs illustrating the division across the width of the adult *T. gigantica* tegument into 4 zones (1, 2, 3, 4). Notice the cross sections of ridge (Ri) and pits (Pi) in zone 1, high concentration of granules (Gr) and lysosomes (Ly) in zone 2, myofibrillar (Mi) in zone 3, basal plasma membrane infoldings (In) in zone 4.
(C) A TEM micrograph showing basal (Ba), circular (Rl), limiting and muscle (Mu) of the body wall traversed by tegumental cells processes (Pc).

Figure 2

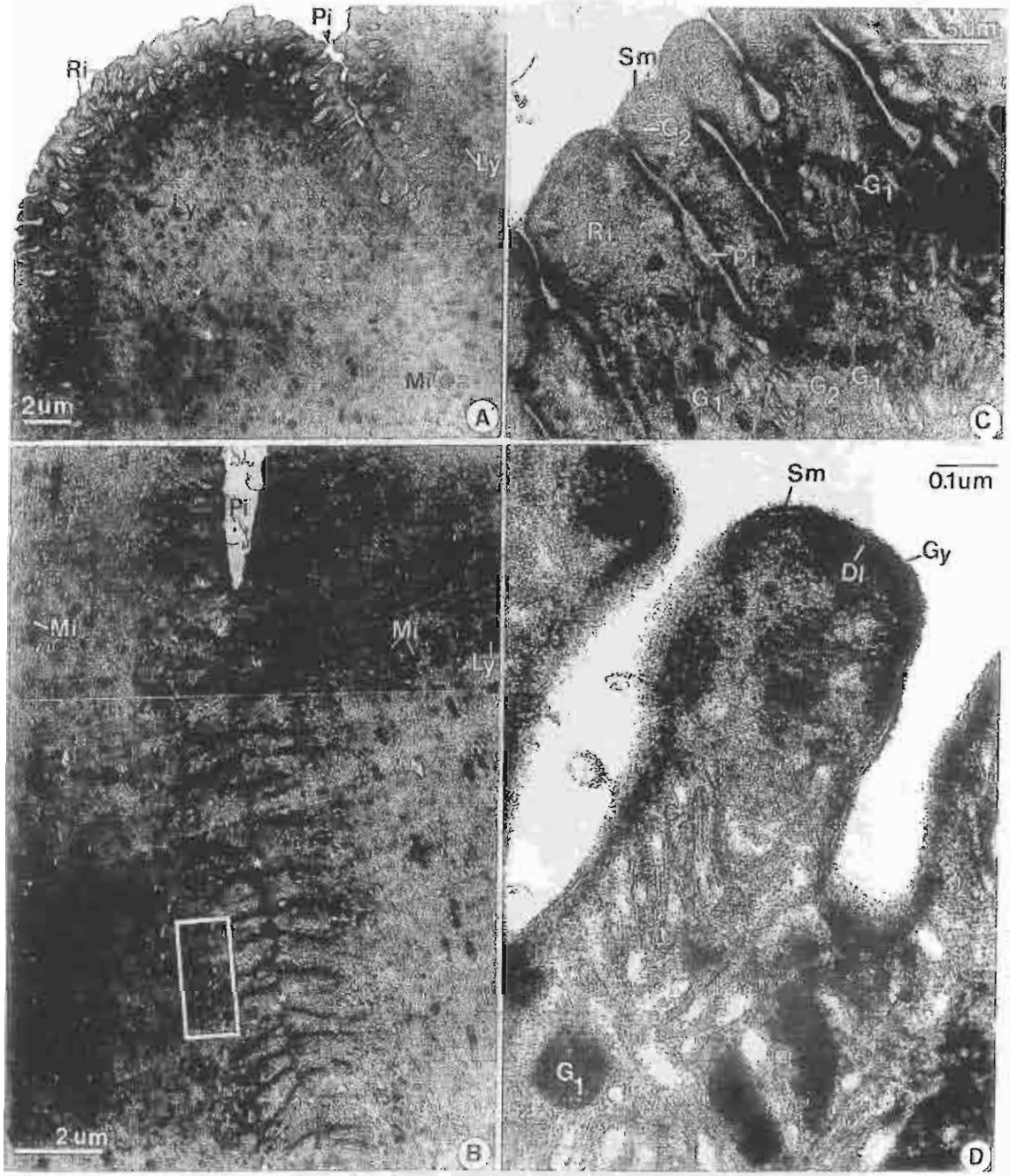

Fig 2. A, B) Zone 1 and 2 of the tegument, exhibiting cross sections of ridges (Ri) and pits (Pi) and deep cuticles (stars). Zone 2 has both concentrations of tegumental granules (no single C and lysosomes (Ly).

C, D) Medium and high magnification of zone 1 exhibiting subtegumental surface membrane (Sm) underlined by dense formation of cytoplasm (Dl), and covered by thin glycocalyx (Gy). A large number of G1 granules are present in this zone which there are very few G2 granules.

Fig 3. A, B)

Figure 3

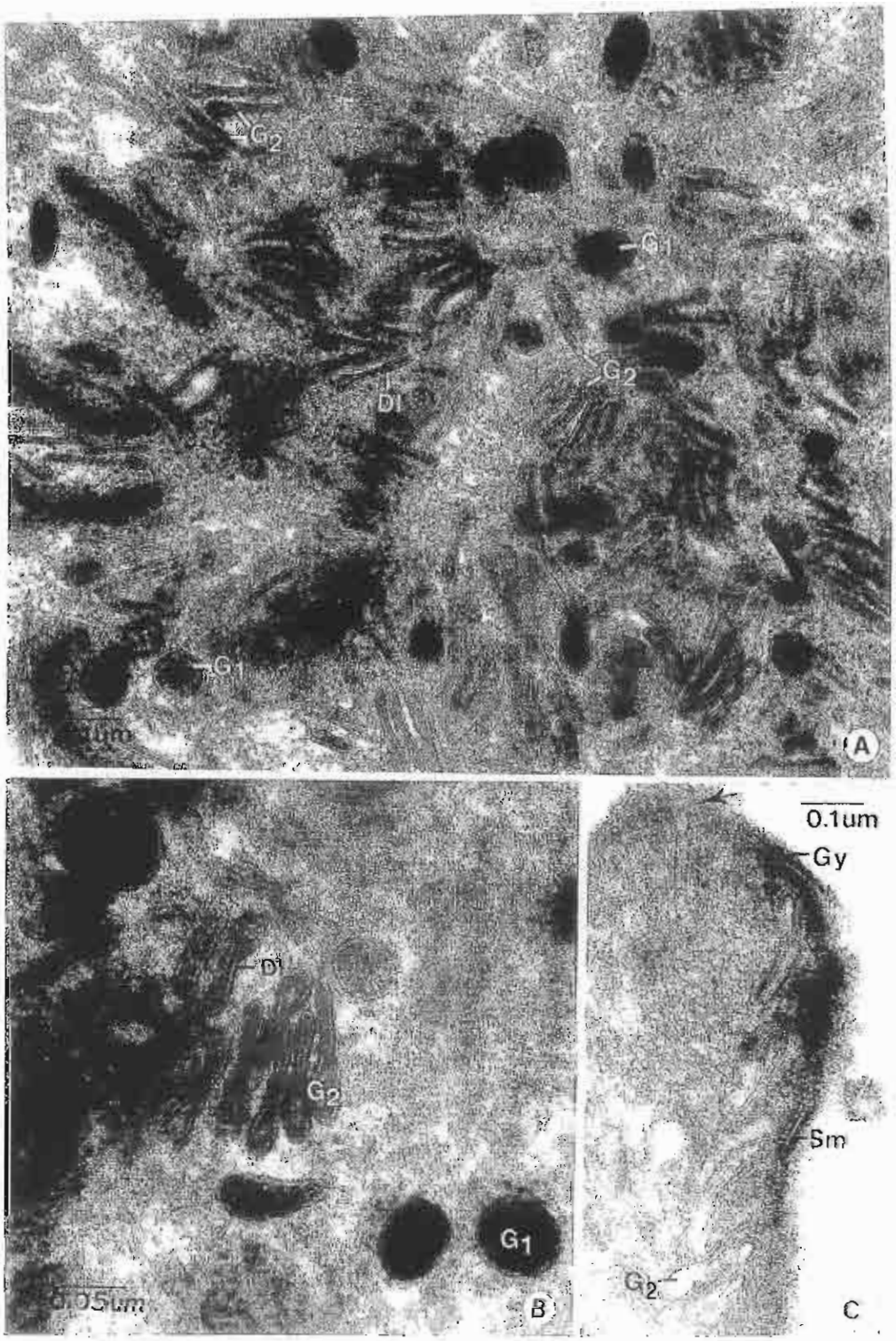

Fig 3. A, B) High magnification of zone 2 (taken from box of area in Fig. 2B) illustrating a high concentration of G_1 granules and fewer numerous G_2 granules. Most G_1 contain homogeneous dense matrix, while some G_2 contain dark brown matrix G_2 has dumbbell shape and contain pale matrix and then membrane is surrounded by dense lamina (D1).
C) A high magnification micrograph of a ridge showing the lesion of zone 3, with the surface membrane (arrow).

At high magnifications there appear to be two types of tegumental granules (Fig. 2C, 3A). The first type (G_1) is a dense ovoid granule that is measured approximately 90 nm wide by 180 nm long. G_1 contains homogeneously dense ruthenium red-positive matrix and is surrounded by a trilaminate membrane (Fig 2C, D; 3A, B; 4A, D). Some G_1 granules appear very close to the surface membrane at the bottoms of the pits (Fig 2D; 4B, C), and a few appear to join with the membrane and exocytose their content into the pits (Fig 4A-C). The second type is a discoid granule (G_2) which is measured about 40 nm wide by 250 nm long. This granules is surrounded by a trilaminate membrane, and at the central part its membrane is closely apposed, while both ends become enlarged such that the granule assumes a mild dumbbell shape (Fig 2D, 3A, B). G_2 granule contains light homogeneous matrix, while the cytoplasmic side of its membrane has a thin dense lamina lining (Fig 3B). While G_2 are more numerous than G_1, both are concentrated in this zone. A large number of G_2 flow up to the first layer to join up with the membrane lining the sides of ridges and pits (Fig 2D, 3C). The second layer also contains lysosome-like bodies arranged in rows parallel to the surface (Fig 1A; 2A, B).

The third layer is the middle and widest zone of the tegumental cytoplasm (Fig 1A, B). It consists of uniformly packed microtrabecular network, and contains numerous mitochondria but only few lysosomes (Fig 1A, B). G_1 and G_2 tegumental granules are evenly distributed throughout the layer, and appear less concentrated than in the second layer. Mitochondria have dense matrix and only few cristae running parallel to their longitudinal axes.

The fourth or basal layer rests on the basal and reticular laminae (Fig 1B, C). Its cytoplasm contains loosely-packed microtrabecular network and long narrow lightly-stained channels, running vertically towards the surface of the tegument. At high magnification these channels are actually oblong spaces between the tortuous infoldings of the basal plasma membrane. The basal plasma membrane is trilaminate and coupled by hemidesmosomes to the basal lamina, whose homogeneous matrix continues to fill the narrow spaces between the infoldings. G_1 are the most frequently observed granules in the third layer, while G_2 are relatively scarce.

Spines

Spines are the most prominent feature of the adult tegument. Each spine has the main part of its body embedded within the whole thickness of the tegument with its apical part jutting out from the surface (Fig 5A, B). The spine is composed of a wedge-shaped crystalline structure, with each spacing between the lattice about 4 nm (Fig 4C, D). The tip of the spine is covered only by the surface membrane, while the edges are covered by thin sheet of tegumental cytoplasm that ae invaginated. The edge of the spine and adjoining cytoplasm have no specialized coupling other than the presence of a rather compact mass of cytoplasm that contains relatively high concentration of mitochondria (Fig 5C, E). In contrast, at the basal end the crystalline lattices are fragmented into "rootlets" that are firmly embedded in the matrix of the basal lamina (Fig 5F).

The Basal and Reticular Laminae

The basal lamina is a thin layer of fairly dense matrix about 120-140 nm in width, whose components are made of closely-packed fine filaments enmeshed within a gel-like ground substance (Fig 1B; 5F). The filaments are so fine and tightly packed together that they are hardly resolved individually even at high magnification. The basal lamina is tightly adhered to the tegument's basal plasma membrane, and its matrix continues to fill the spaces between the basal membrane infoldings (Fig 1B). Small plaques of hemidesmosomes distributed at irregular intervals help to couple the tegument's basal membrane and the lamina together. On its internal surface the basal lamina binds with the reticular lamina (Fig 1B, C; 5F) whose major components are uniform fibers similar in character to the reticular fibers present in the basement membranes of higher vertebrates.

Tegumental Cells

Tegumental cells lie in rows underneath the longitudinal muscle layer, and send their processes containing bundles of microtubules outwards between the muscle cells to joint up with the tegument (Fig 1C). Each cell has a large round vesicular nucleus containing a thin strip of heterochromatin along the inner surface of the nuclear envelope, and a few small blocks scattered within the interior of the nucleus, while most of the remaining chromatin appears as euchromatin. The nucleus also has a very prominent nucleolus (Fig 6A). The cytoplasm contains numerous mitochondria, rough endoplasmic reticulum, free polysomes and few areas of Golgi complexes (Fig 6A-C). Both G_1 and G_2 tegumental granules could be observe within a single cell (Fig 6B, C); however, G_2 are the more numerous and they are closely aggregated near the Golgi complexes (Fig 6A). In addition to these

Figure 4

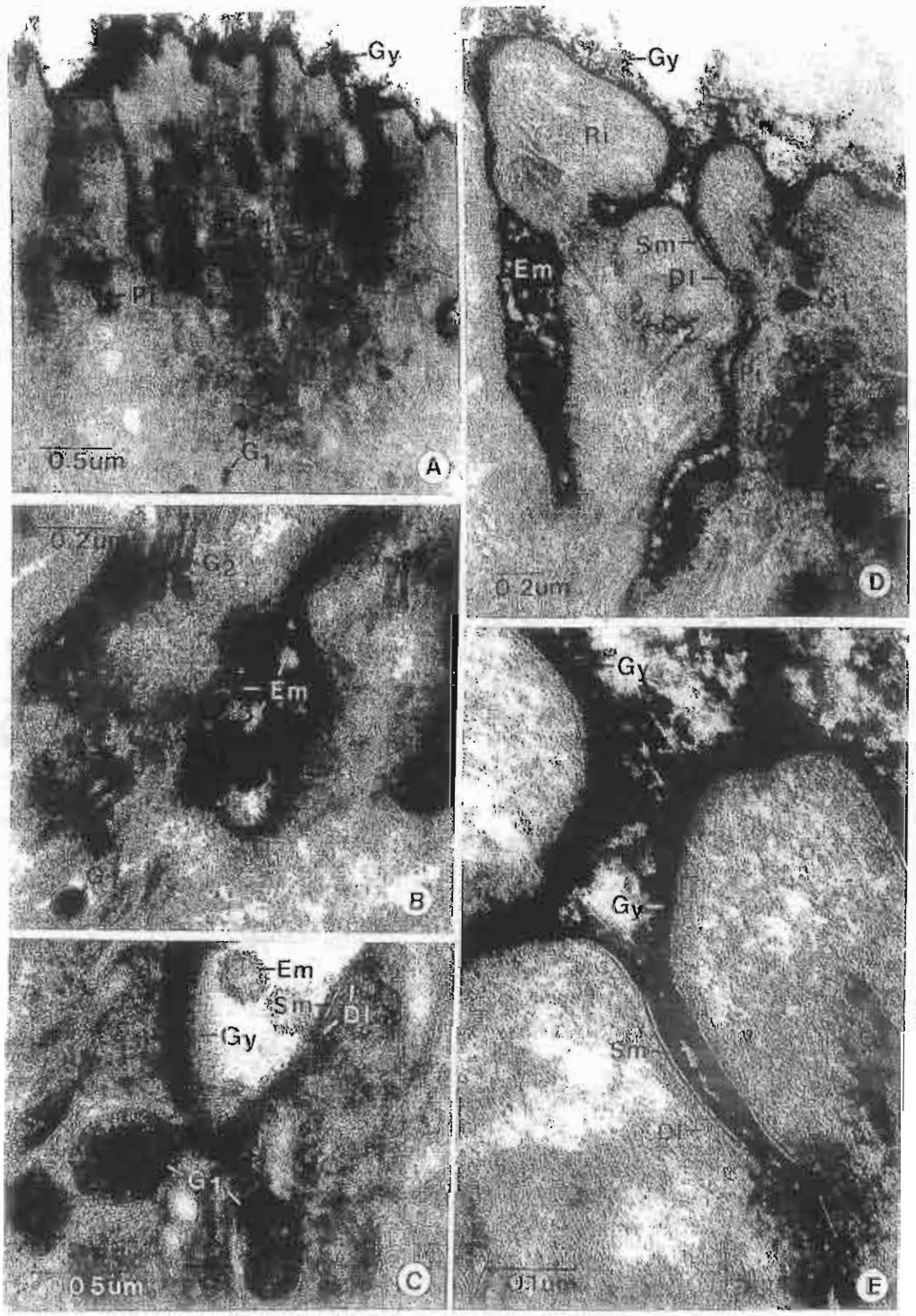

Fig 4. (A, B, C) Micrographs of ruthenium red-fixed sections, uncontrastained (A) and contrastained with lead citrate and uranyl acetate (B, C) illustrating intense staining of ruthenium red on the glycocalyx (Gy) lining the pits (Pl) and the sulcus (Sc) and (G) granules closed to the surface. (G1) indicates the exocytosis and release of matrix (Em) of (G) granules into the pit.
(D, E) The contrastained ruthenium red fixed sections illustrating thick (100-300nm) non uniform glycocalyx on the surface of cuticle, and exocytosed matrix of (G) in the pit (Sc). The surface cuticle (Sm) and underlying dense lamina (Dl) are clearly seen.

Figure 5

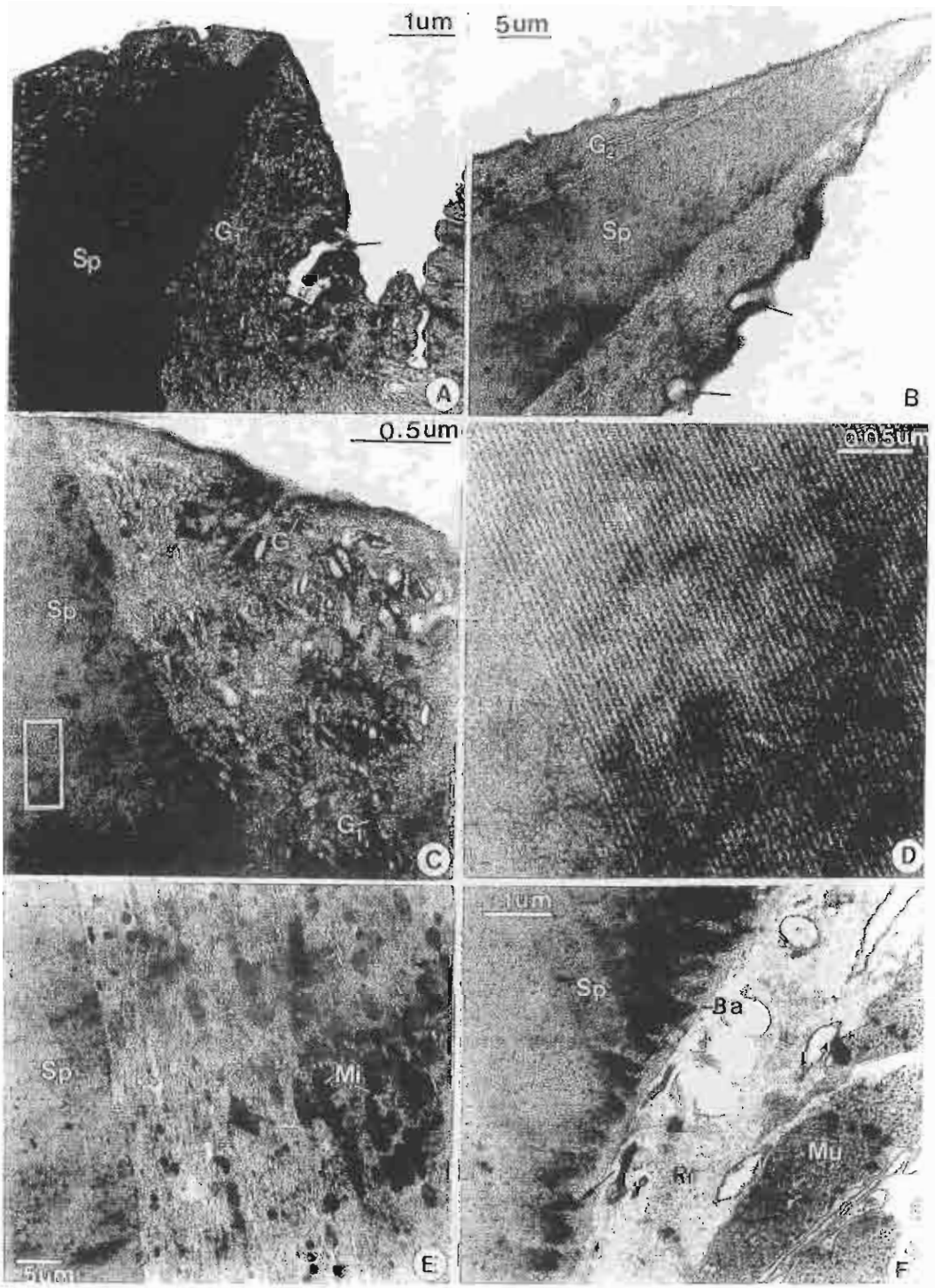

Fig 5 A, B) Micrographs of the spines (Sp) whose tips are covered by the surface membrane and whose edges by sequestered cytoplasm that are incorporated (arrow).

C, D, E) The middle of the spines showing crystalline structure with lattice space about 7nm apart (boxed area in A, B). The side of the spine is covered by dense cytoplasm containing numerous mitochondria (Mi).

F) The base of a spine (Sp) which is fragmented into nodules (arrow) that are embedded in matrix of the basal lamina (Ba).

Figure 6

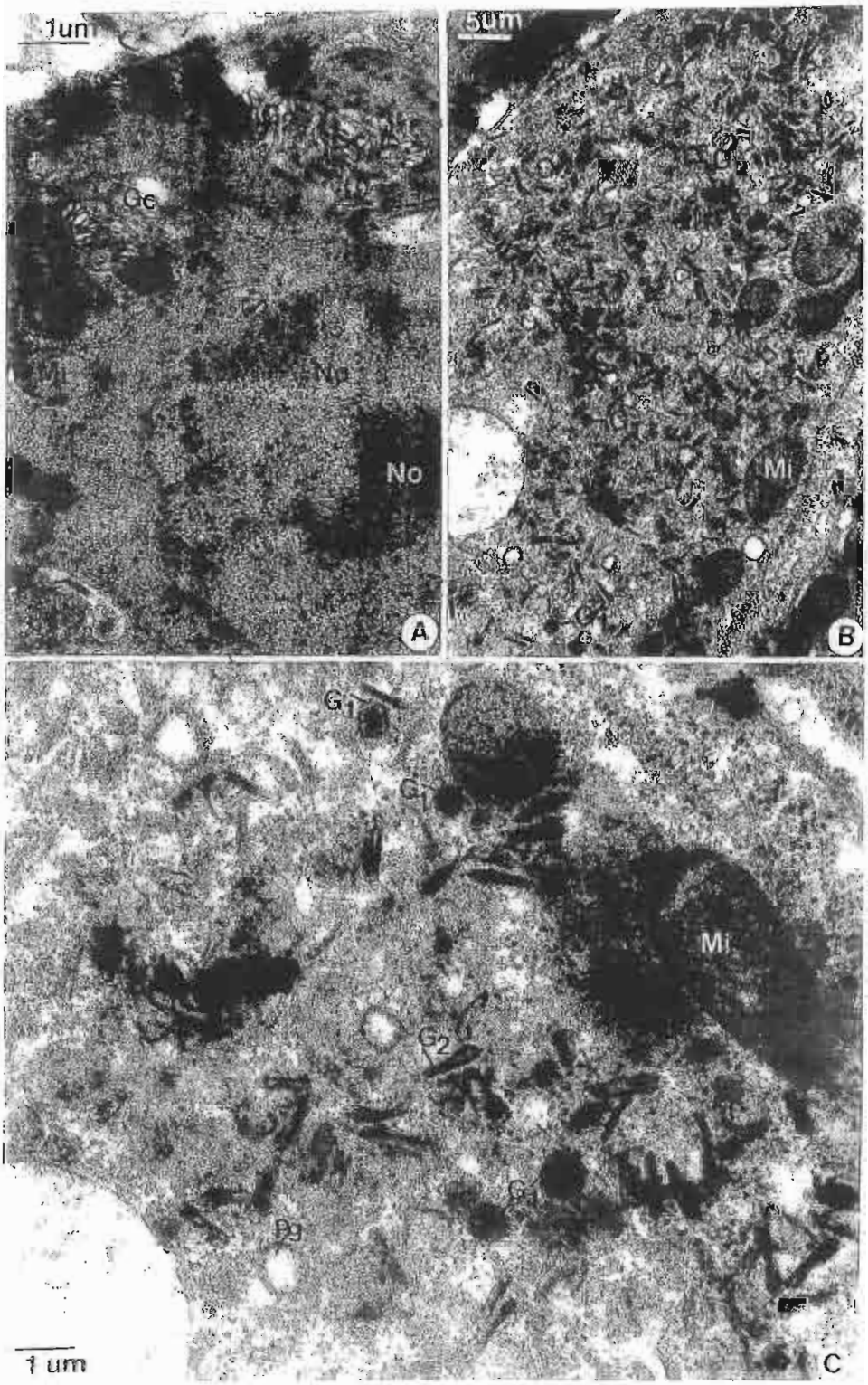

Fig 6. A, B, C: Micrographs of neuroserial cells showing the nucleus (No) containing nucleoli, euchromatin and prominent nucleolus (Nol). The Golgi complex areas (Gc) contain high concentration of G_1 granules. In the cytoplasm (in B, C) both G_1 and G_2 granules are present within the same cell with G_1 predominate in number.

tegumental granules, there are spherical-shaped granules whose content are very lightly stained, and some may actually appear empty (Fig 6B, C). These granules could be the precursor of G_1 whose matrix has not yet been highly concentrated.

Discussion

Ultrastructure of the Tegument

Trematode parasites that live in the mammalian hosts' circulation or biliary system need to absorb nutrient molecules from either the blood or bile, as demonstrated in schistosomes' tegument which can absorb substantial amount of small nutrient molecules such as glucose, fructose and amino acids.[18,19] Simultaneously the tegument of these parasites can also protect them from hosts' immune attacks by evolving evasion mechanisms that include the rapid turn over of the surface membrane to prevent the attachment of immune effector cells, and by immune mimickry or disguise through the adsorption of hosts' antigens onto the parasites' surfaces. In addition, the fluid environment in the host body, especially the bile, is vastly different in terms of ionic composition from that of the parasites' bodies. Hence another important role of the tegument is the regulation of ions and fluid balance, which will keep the homeostatic equilibrium within the parasites' bodies. Adult *F. gigantica* tegument, as reported in the present study, exhibits all the ultrastructural features to subserve these critical functions.

The First Layer

Based on their ultrastructural features the tegument of adult *F. gigantica* could be divided into four layers of specialized functions. The first and outermost region of the tegument contains highly folded parts, namely, ridges and pits. The membrane covering these structures is trilaminate and coated with a substantial layer of glycocalyx, a typical feature found in all bile and lumen-dwelling trematodes, including, *F. hepatica*[20-22] *Clonorchis sinensis*[23] and *Opisthorchis viverini*.[24] The vast amount of membrane covering the ridges and pits helps to increase the surface area for absorption and exchanging of materials. Glycocalyx may provide the first line of defense because of its substantial thickness and insolubility. In conventional TEM, glycocalyx appears only as a thin layer (about 10-15 nm in thickness) which may be due to the failure of the fixative to preserve the glycocalyx in its entirety. By contrast, when the parasites were simultaneously treated with ruthenium red which acts as both stain and fixative[11,17] the glycocalyx appears as thick as 100-300 nm, and consists of two definite layers, ie, the thin inner homogeneous layer apposed to the surface membrane and the thick outer fibrillar layer. The latter may be more labile and could be preserved only by extra treatment with ruthenium red. Glycocalyx may be quite resistant to the emulsifying action of the bile and, therefore, able to confer a certain degree of protection to *F. gigantica*. High affinity to ruthenium red is indicative that glycocalyx of adult *F. gigantica* is highly negatively charged. The anions present may be contributed mainly by sialic acids, as it has been shown that ruthenium red can bind strongly to this sugar.[17] The presence of abundant negative charges on the surface could be another factor that helps to defend the parasites against hosts' immune attacks by repelling the attachment of the hosts' immune effector cells, which also bear high electronegativity on their own surfaces.[11,25] Moreover, the presence of a large quantity of large negatively-charged molecules, like glycoproteins, may be instrumental in retaining and concentrating small molecules including sugars and amino acids and various ions. Thus, the glycocalyx may be viewed as a hydrated shell around the parasites' bodies that helps to protect as well as concentrate nutrient molecules, in order to make them readily available for the absorption by the tegument.

Glycocalyx is probably derived from G_1 granules present in abundance within the second layer of the tegument. Ruthenium red stain shows similar binding to the glycocalyx as well as the matrix of G_1 granules lying close to the surface. These granules invariably join up with the surface membrane at the bottom of the pits, and exocytose their matrix into the lumen of pits. This material could be later incorporated into the surface membrane, thus forming part of the new glycocalyx. In *F. hepatica*, similar granules which were termed T_0 by Hanna,[26] were also thought to be contributing to the formation of glycocalyx in metacercaria and juvenile parasites, particularly during their invasive migration through the host's tissues. Once *F. hepatica* juveniles reach their final destination and take up permanent residence in bile ducts of the liver T_0 granules were replaced by a similar set of adult-type granules (T_1). In comparison to T_0, the number of T_1 in adult tegument is drastically decreased, while another set of so call T_2 granules became the majority of tegumental granules in adult. Each T_2 granule is surrounded by a trilaminate membrane and associated thin layer of glycocalyx that express adult-type antigens on the surface.[26-28] These adult antigens are much less immunogenic than juvenile

antigens.[27,28] In contrast to *F. hepatica*, we have shown that in the tegument of adult *F. gigantica* G_1 granules, which are probably equivalent to T_1 granules, are still quite numerous; and the ruthenium red staining implicates that the secretion of these granules into the pits may form the major part of glycocalyx.

The surface membrane of an adult *F. gigantica* is trilaminate and supported internally by a thin lamina of dense cytoplasm, while the cytoplasm underneath the lamina is composed of tightly packed microtrabeculae and bundles of larger fibrils. Within this interstice there are numerous G_2 granules that may be equivalent to T_2 granules of *F. hepatica* tegument. In fortuitous sections several G_2 granules were seen joined up with the surface membrane, and evert their cisternal side outwards, thus turning into the exterior surface of the tegument's surface membrane, which may later become coated with the glycocalyx material released from G_1 granules. The matrix inside the cisternae of G_2 granules could become part of the thin homogenous layer of glycocalyx that may be coupled with the more fibrillar components derived from the secretion of G_1 granules. On the cytoplasmic side, which is now turned into the cytoplasmic face of the surface membrane, the dense cytoplasm covering the membrane of the G_2 granules could coalesce and form the dense lamina underlining the surface membrane. The surface membrane and associated glycocalyx of the adult *F. gigantica* tegument probably maintain a high turnover rate, since there are always a vast amount of G_2 granules accumulated in the first and the second layers of the tegument, as well as a still relatively large number of G_1 granules in the second layer. Such rapid turnover and renewal of the surface membrane could be a part of the mechanism for self defense against the detergenic action of bile and the host's immune attacks, as it has been shown that bile also contains copious amount of antibodies, especially IgA.[29]

The Second Layer

The most prominent characteristic of this layer is the presence of a very high concentration of G_1 and G_2 granules, particularly G_2 granules. Therefore, this layer could be viewed as the storage area for the new membrane (G_2) and glycocalyx (G_1) material. Another prominent feature of this layer is the presence of a large number of lysosomal granules, which implies that there may be absorption of large molecules via the endocytotic pathway within the tegument. In addition to nutritive substances, some of these large molecules could be antibodies forming immune complexes with the surface antigens. Once attached to the surface membrane these large molecules or immune complexes could be internalized and broken down by the fusion with lysosomes, which could be another part of parasites' defense mechanism against the hosts' immune attacks.

The Third Layer

This is the widest layer of the tegument. Its cytoskeleton is less tightly packed, and it has the highest concentration of mitochondria which are evenly distributed throughout the layer. G_1 and G_2 granules are present but appear to be much fewer than in the second layer. This layer may, therefore, be involved mainly in supplying energy to other layers. The concentration of mitochondria and their positioning within the tegument of this parasite are quite different from that of schistosomes and a human liver fluke, *O. viverrini*. In schistosomes most of mitochondria are concentrated in the basal layer,[30] while in *O. viverrini* they are localized close to the surface plasma membrane.[24] The distribution of energy for various metabolic processes in the tegument of these two species could be carried out by these eccentrically-located mitochondria because of the relative thinness of their tegument. In contrast, *F. gigantica* has a much thicker tegument because of the worms' very large size. The increased energy requirement dictates that the parasites' tegument must possess a very large number of mitochondria that are positioned strategically in the middle zone, so that energy could be sufficiently distributed to other layers.

The Fourth Layer

This layer exhibits the most unique features in having highly convoluted infoldings of the basal plasma membrane, with closely-associated mitochondria. These features resemble the basal cytoplasm of ion-transport epithelium in mammals, such as, the kidney proximal and distal tubules. Based on these similarities the fourth layer could be involved in the transport of ions which will help to maintain the ionic equilibrium within the parasites' bodies with regards to the bile.

Tegumental Cells

In *F. hepatica*, Hanna[26] and Burden et al[31] reported that there is one type of cell which synthesize T_0 granules in metacercaria and in the very early juvenile stage, while the parasites are migrating through the hosts' abdominal cavities. T_0 cells transform into T_1 cells which produce granules with similar feature but with greater density when the

parasites reach the liver. Both T_0 and T_1 granules were thought to give rise to the juveniles', and later adults' glycocalyx, that enables the parasites to evade the killing by hosts' immune responses. When parasites become established in the bile duct at about 12 weeks there is another type of tegumental cells which produce T_2 granules, which are the main contributor to the formation of the adult parasites' surface membrane and glycocalyx. These T_2 cells supersede T_1 cells, and as a result the number of T_1 granules in the tegument of the adult parasites is drastically decreased. In *F. gigantica* the number of G_1 granules in the adult tegument is still relatively high in comparison with the T_1 granules of *F. hepatica*. In contrast to the two types of tegument cells reported in the adult *F. hepatica* we observed only one type of cells in adult *F. gigantica*. These cells produce both G_1 and G_2 granules, even though the productions of G_2 predominate in the adult stage. Both types of granules are found in close association with microtubules within the processes of the cells that extend outwards to join up with the tegument. Hence, we believe that these granules are translocated form cell soma to the tegument by the sliding action of microtubules.

Acknowledgements

This research was supported financially by the Thailand Research Fund (Senior Research Scholar Fellowship to P Sobhon).

References

1. Maurice J (1994) Is something lurking in your liver? *New Scientist* 1917, 26-31.
2. Edney JM, Muchlis A (1962) Fasciolasis in Indonesian livestock. *Communication Veterinaire* 6, 49-52.
3. Soeseiya RHB (1975) The prevalence of *Fasciola gigantica* infection in cattle in East Java, Indonesia. *Malaysian Vet J* 6, 5-8.
4. Fabiyi JP (1987) Production losses and control of helminthes in ruminants of tropical regions. *Int J Parasitol* 17, 435-42.
5. Sukhapesna V, Tantasuvan D, Sarataphan N, Imsup K (1994) Economic impact of fasciolasis in buffalo production. *J Thai Vet Med Assoc* 45, 43-52.
6. Sobhon P, Anantavara S, Dangprasert T, Viyanant V, Krailas D, Upatham ES, Wanichanon C, Kusamran T (1998) *Fasciola gigantica*: studies of the tegument as a basis for the developments of immunodiagnosis and vaccine. *Southeast Asian J Trop Med and Pub Hlth* 29, 387-400.
7. Overend DJ, Bower FI (1995) Resistance of *Fasciola hepatica* to triclabendazole. *Aus Vet J* 72, 275-6.
8. Sobhon P, Anantavara S, Dangprasert T, Meepool A, Wanichanon C, Viyanant V, Upatham ES, Kusamran T, Chompoochan T, Thammasart S, Prasittisuk P (1996) *Fasciola gigantica*: identification of adult antigens, their tissue sources and possible origin. *J Science Soc Thai* 27, 312-7.
9. Fairweather I, Lawence T, Threadgold LT, Hanna REB (1999) Development of *Fasciola hepatica* in the mammalian hosts. In: *Fasciolosis* (Edited by Dalton JP), pp 47-111, CABI Publishing, Wallingford, UK.
10. Bennett CE, Threadgold LT (1975) *Fasciola hepatica*: Development of tegument during migration in mouse. *Exp Parasitol* 38, 38-55.
11. Threagold LT (1976) *Fasciola hepatica*: Ultrastructure and histochemistry of the glycocalyx of the tegument. *Exp Parasitol* 39, 119-34.
12. Threagold LT, Brennan G (1978) *Fasciola hepatica*: Basal infolds and associated vacuoles of the tegument. *Exp Parasitol* 46, 300-16.
13. Burden DJ, Bland AP, Hughes DL, Hammet NC (1982) *Fasciola hepatica*: development of the tegument of normal and γ-irradiated flukes during infection in rats and mice. *Parasitol* 86, 137-45.
14. Estuningsith SE, Smooker PM, Wiedosari E, Widjajanti S, Vaiano S, Partoutomo S, Spithill TW (1997) Evaluation of antigens of *Fasciola gigantica* as vaccines against tropical fasciolosis in cattle. *Int J Parasitol* 27, 1419-28.
15. Luft JH (1971) Ruthenium Red and Violet I. Chemistry, purification, methods of use for electron microscopy and mechanism of action. *Anat Rec* 171, 347-68.
16. Luft JH (1971) Ruthenium Red and Violet II. Fine structure localization in animal tissues. *Anat Rec* 171, 369-416.
17. Rambourg A (1971) Morphological and histochemical aspects of glycoproteins at the surface of animal cells. *Int Rev Cytol* 31, 57-114.
18. Fripp PJ (1967) The sites of (C^{14}) glucose assimilation in *Schistosoma haematobium*. *Comp Biochem Physiol* 23, 893-8.
19. Senft AW (1968) Studies in proline metabolism by *Schistosoma mansoni*. I. Radioautography following *in vitro* exposure to radioproline C^{14}. *Comp Biochem Physiol* 27, 251-61.
20. Threadgold LT (1967) Electron-microscope studies of *Fasciola hepatica* III. Further observations on the tegument. *Exp Parasitol* 46, 300-16.
21. Theadgold LT (1984) Parasitic platyhelminths. In: *Biology of the tegument* (Edited by Bereiter-Hahn J, Matoltsy AG, Richards KS), pp 132-85, Springer-Verlag, Berlin.
22. Hanna REB (1980) *Fasciola hepatica*: Glycocalyx replacement in the juvenile as a possible mechanism for protection against host immunity. *Exp Parasitol* 50, 103-44.
23. Fujino T, Ishii Y, Choi DW (1979) Surface ultrastructure of the tegument of *Clonorchis sinensis* newly excysted juvenile and adult worms. *J Parasitol* 65, 579-90.
24. Apinhasmit W, Sobhon P, Saitongdee P, Menayotin S, Upatham ES (1994) *Opisthorchis viverrini*: ultrastructure of the tegument of the first-week juveniles and adult flukes. *Int J Parasitol* 24, 613-21.
25. Lumsden RD (1972) Cytological studies on the absorptive surface of cestodes. VI. Cytochemical evaluation of electrostatic charge. *J Parasitol* 58, 229-34.
26. Hanna REB (1980) *Fasciola hepatica*: An immunofluorescent study of antigenic changes in the tegument during development in the rat and sheep. *Exp Parasitol* 50, 155-70.
27. Hanna REB (1980) *Fasciola hepatica*: Autoradiography of protein synthesis, transport and secretion by the tegument. *Exp Parasitol* 50, 297-304.
28. Hanna REB, Trudgett AG (1983) *Fasciola hepatica*: development of monoclonal antibodies and their use to characterize a glycocalyx antigen in migrating flukes. *Parasite Immunol* 5, 409-425.
29. Hughes DL, Hanna REB, Symonds HW (1981) *Fasciola hepatica*: IgG and IgA levels in the serum and bile of infected cattle. *Exp Parasitol* 52, 271-9.
30. Sobhon P, Upatham ES (1990) The tegument of adult parasites. In: *Snail hosts, life cycle, and tegumental structure of oriental schistosomes*, pp57-107. UNDP/World Bank/WHO Special Programs for Research and Training in Tropical Diseases, Geneva.

Invertebrate Reproduction and Development, 39:1 (2001) 55–66
Balaban, Philadelphia/Rehovot
0168-8170/00/$05.00 © 2001 Balaban

Ultrastructure of the differentiating male germ cells in *Haliotis asinina* Linnaeus

PRASERT SOBHON[1*], SOMJAI APISAWETAKAN[1], VICHAI LINTHONG[1], VIRIYA PANKAO[1], CHAITIP WANICHANON[1], ARDOOL MEEPOOL[1], MALEEYA KRUATRACHUE[2], EDWARD SUCHART UPATHAM[2,3] and TANATE PUMTHONG[4]

[1]*Department of Anatomy,* [2]*Department of Biology, Faculty of Science, Mahidol University, Rama VI Road, Bangkok, Thailand 10400*
Tel. (662) 245-5198; Fax (662) 247-9880; email: scpso@mahidol.ac.th
[3]*Department of Medical Science, Faculty of Science, Burapha University, Chonburi, Thailand*
[4]*The Coastal Aquaculture Development Center, Department of Fisheries, Prachuabkirikhun Province, Thailand 77000*

Received 25 September 2000; Accepted 7 March 2001

Summary

Male germ cells in the testis of *H. asinina* can be divided into 14 stages based on the ultrastructure and patterns of chromatin condensation. The spermatogonium is a spherical or oval-shaped cell with diameter about 8 μm. Its nucleus contains mostly euchromatin with only a thin rim of heterochromatin along the inner facet of the nuclear envelope. Primary spermatocytes (PrSc) are divided into six stages, i.e., leptotene (LSc), zygotene (ZSc), pachytene (PSc), diplotene (DSc), diakinesis (DiSc) and metaphase (MSc). The early cells are round and become increasingly larger, ranging in size from 12 to 14 μm from LSc to PSc; then their sizes gradually decrease from 10 to 7 μm from DSc to MSc. LSc contains small blocks of heterochromatin that are scattered throughout the nucleus. These heterochromatin blocks are increasingly thickened and lengthened in ZSc, and achieve their maximum sizes in PSc. DSc decreases in size, resulting in the close clumping of chromatin blocks; while in DiSc and MSc long and large blocks of chromosomes are formed and then move to be aligned along the equatorial region. In the nuclei of all stages of PrSc, heterochromatin blocks are formed by the tight aggregation of 30 nm chromatin fibers. The secondary spermatocyte (SSc) is a round cell about 8 μm in diameter. They are aligned in rows that separate spermatids from primary spermatocytes. Their nuclei contain criss-crossing chromatin cords in a reticulate pattern, whose individual 30 nm fibers are loosely packed. All spermatids are freed from the epithelium, and can be divided into four stages: St_1 is a large round cell (about 5–6 μm), and its nucleus contains evenly dispersed 30 nm chromatin fibers. In St_2 the nucleus decreases in size by a half and becomes oval; thus the chromatin fibers are packed closer together, particularly around the axis of condensation. In St_3 the nucleus is elongated with individual chromatin fibers enlarged to about 40 nm in cross section, and they are packed tightly together. In St_4 (about 3×2 μm) the nucleus is increasingly elongated with the acrosome covering the anterior pole. Individual chromatin fibers are enlarged to 60 nm and appear in cross-section as closely aligned dense granules. The spermatozoon has a cone-shaped

*Corresponding author.

head (about 3×1.5 μm) that contains completely condensed chromatin covered by the cup-shaped acrosome with the subacrosomal core. Each spermatozoon has globular mito-chondria surrounding a pair of centrioles at the neck region and the tail consists of the axonemal microtubules surrounded by the plasma membrane.

Key words: *Haliotis asinina*, male germ cells, ultrastructure, chromatin

Introduction

Despite extensive ultrastructural studies of the male germ cells in several mollusc species (Franzen, 1955; Fawcett, 1970; Anderson and Personne, 1976; Buckland-Nicks and Chia, 1976; Dorange and Le Pennec, 1989), no rigorous categorization of the various stages of the male germ cells during spermatogenesis and spermiogenesis in *Haliotis* spp. has been undertaken, apart from the presumption that they comprise four major classes, i.e., spermatogonium, spermatocytes, spermatids and spermatozoa (Tomita, 1968; Young and De Martini, 1970; Takashima, 1978). The aim of the present study is to classify various stages of the male germ cells in *H. asinina*, a major species of tropical abalone found along the coast of Thailand, based on ultrastructural features and the pattern of chromatin organization. Such basic information could be useful in the collection and estimation of the maturity of male gamete for use in the aquaculture of this species.

Materials and Methods

Collection of abalone specimens

Adult abalones over 24 months old were collected from a land-based culture system at Coastal Aquaculture Development Center, Department of Fisheries, Prachaubkirikhun Province, Thailand. They were kept in concrete tanks housed in the shade and well flushed with mechanically circulated sand-filtered seawater and provided with an air delivery system to maintain the stable controlled environment. The optimum level of salinity is about 22.5–32.5 ppt and the temperature about 22–26°C (Singhagraiwan and Doi, 1993). They were fed with macroalgae (usually *Gracilaria* spp. and *Laminaria* spp.), supplemented with artificial food.

Transmission electron microscopy (TEM)

For TEM studies, testes were cut into small pieces and fixed in a solution of 3% glutaraldehyde in 0.1 M sodium cacodylate buffer, pH 7.8, at 4°C overnight. The specimens were post-fixed in 1% osmium tetroxide in 0.1 M sodium cacodylate buffer at 4°C for 2 h. Then they were dehydrated in graded series of ethanol (50% to 100%) for 30 min each, cleared in two changes of propylene oxide, infiltrated in the mixtures of propylene oxide and Araldite 502 resin at the ratios of 3:1 for 1 h 2:1 for 2 h and 1:2 overnight; then in pure Araldite 502 resin for at least 6 h, and finally polymerized at 30°C, 45°C and 60°C for 24, 48 and 48 h, respectively. Ultrathin sections were cut and stained with lead citrate-uranyl acetate and viewed under a Hitachi TEM H-300 at 75 kV. In each stage at least 20 large cells with full cross sectional profiles of the nuclei were selected for measurement of the cell and nuclear sizes. The width of the chromatin fibers was measured from the electron micrograph negatives using catalase crystal with the lattice spacing of 8.75 nm as the standard.

Results

Connective tissue scaffold and spermatogenic unit

The detailed histology of *H. asinina* testis and its connective scaffold has been extensively described in our previous work (Sobhon et al., 1999; Apisawetakan et al., in press). Basically, the testis is surrounded by the connective tissue capsule that gives off connective tissue sheets, termed trabeculae, at regular intervals.

Fig. 1. (Opposite) A, D. TEM micrographs showing the undulating basal lamina (Ba) that separates the gonadal compartment containing germ cells (LSc) and supporting cells (Se) from the trabecular compartment (Tr), which contains hemolymph capillary (Ca), branches of granulated cells (Gr) and muscle cells (Mu). B, E. Supporting cells (Se), showing the cytoplasm that is extremely rich in mitochondria (Mi). Nu, nucleus; Sc, spermatocytes. C, F. A spermatogonium whose nucleus contains mostly euchromatin (Ec), with only a thin rim of heterochromatin (Hc) along the nuclear envelope and small blocks in the central area. The nucleolus (no) is prominent and contains pale central granular area surrounded by dense periphery. In F, chromatin fibers have two levels: the thin zigzag 10 nm fibers (1) and 30 nm fibers whose cross sections appear as very dense dots (2). Heterochromatin (Hc) is formed by the tight aggregation of 30 nm fibers.

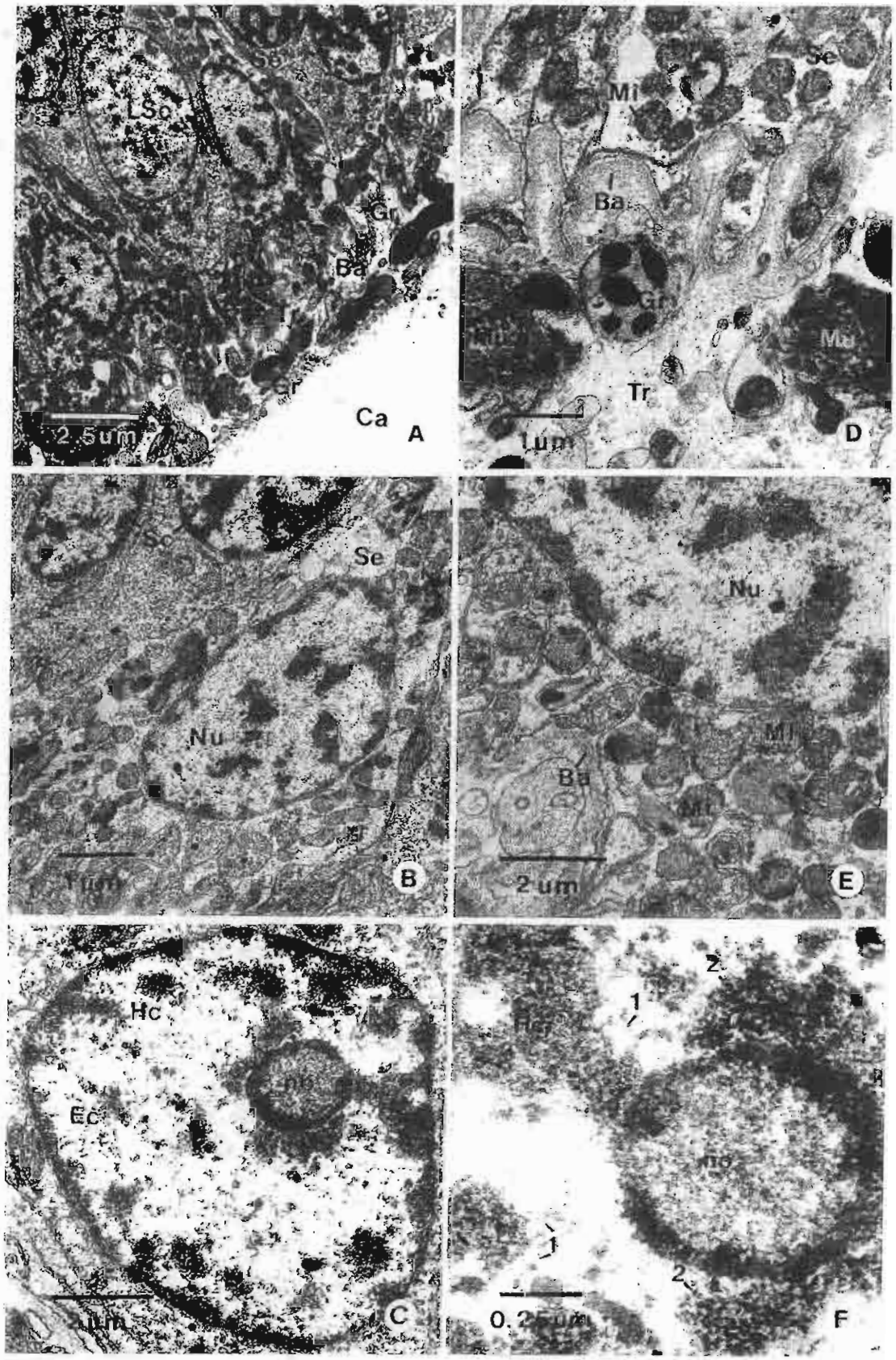
Lsc
Se
Gr
Ba
Ca
2.5um
A
Mi
Se
Ba
Gr
Mu
Tr
1um
D
Sc
Se
Nu
1um
B
Nu
Mi
Ba
Mi
2 um
E
Hc
Ec
1um
C
Hc
1
2
1
2
0.25um
F

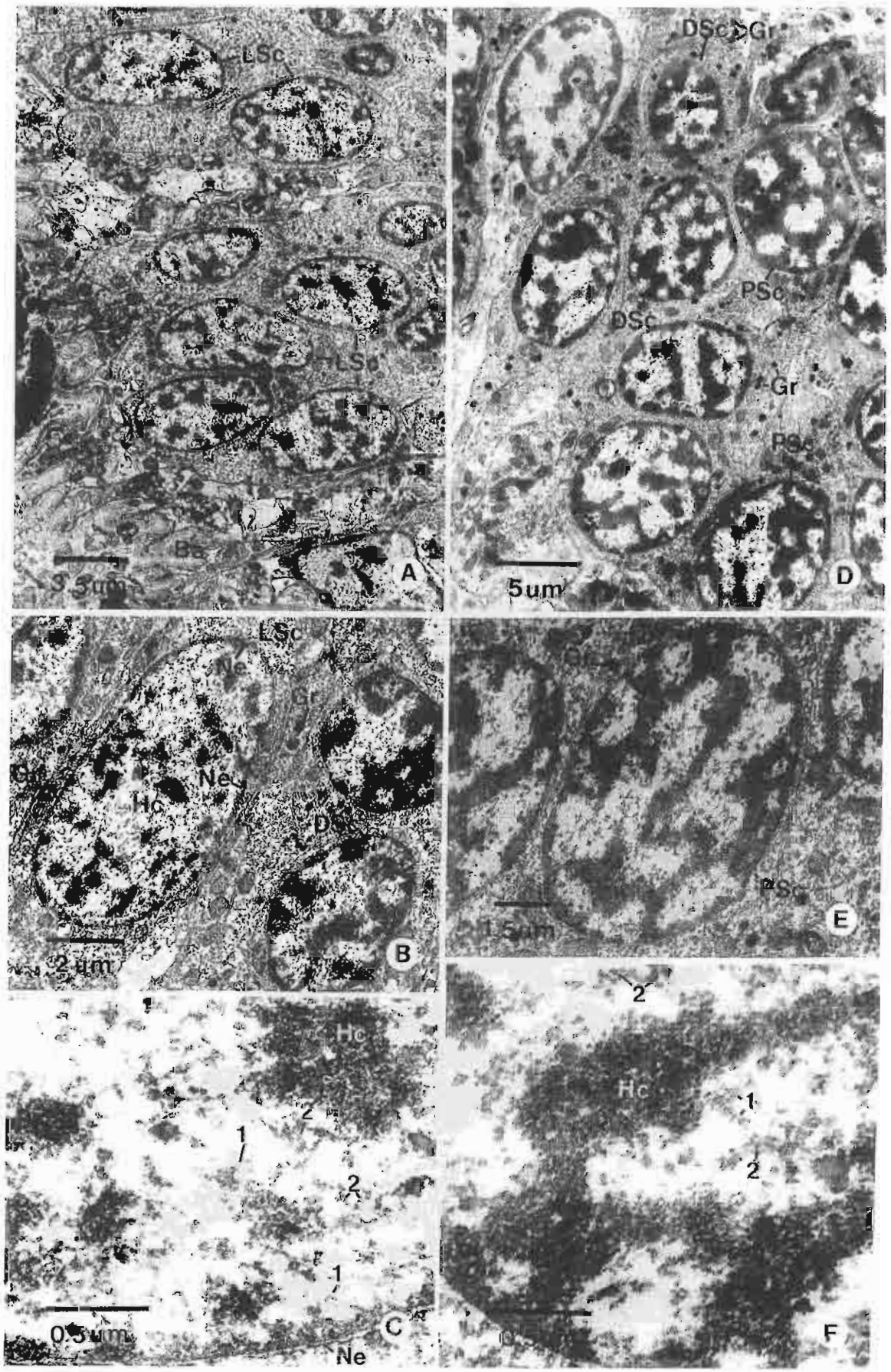
LSc
LSc
Ba
3.5um
A
DSc
Gr
PSc
DSc
Gr
PSc
5um
D
LSc
Ne
Gr
Gr
Ne
Hc
DSc
2um
B
Gr
PSc
1.5um
E
Hc
2
1
2
1
0.5um
C
Ne
2
Hc
1
2
F

Each trabecula contains a small hemolymph vessel in the center surrounded by muscle cells, fibroblasts, connective tissue fibers and some granulated cells. A trabecula forms the axis from which male germ cells proliferate, together forming a spermatogenic unit. Germ cells are separated from the connective tissue proper of a trabecula by a thin undulating sheet of basal lamina (Fig. 1A, D). Spermatogonia and early stage primary spermatocytes lie close to the basal lamina (Fig. 1A,D, 2A), while late stage primary spermatocytes are located at some distance away. Secondary spermatocytes lie in a row at the outermost rim of a spermatogenic unit, and they are the final cells that still attached to the germinal epithelium (Fig. 3A). Smaller and denser spermatids are detached from the epithelium, freed from one another, and released into the lumnal compartment (Fig. 3A).

There are supporting cells situated at regular intervals on the basal lamina, which could be equivalent to Sertoli cells in the vertebrate testes. These cells are characterized by branching cytoplasm that is filled with numerous large mitochondria with very few other organelles (Fig. 1A, B, E). The nucleus of this cell contains thin strip of heterochromatin along the inner surface of the nuclear envelope and small irregular blocks scattered throughout (Fig. 1B,E).

Based on the cell sizes, the ultrastructure and chromatin condensation pattern, the male germ cells in the testis of *H. asinina* can be classified into 14 stages.

Spermatogenic cells

Spermatogonium (Sg) (Fig. 1C, F)

Sg is a spherical-shaped cell with a diameter of 8–10 μm. Its nucleus is round or slightly indented with a diameter of 6–7 μm. The nucleus contains mostly euchromatin with only a thin strip of heterochromatin attached to the inner surface of the nuclear envelope and small blocks in the central area. In the euchromatic area the chromatin fibers exist in two sizes, i.e., 10 and 30 nm fibers; the former appear as thin zigzag lines while the latter appear in cross sections as dense dots (Fig. 1F). The heterochromatin blocks are formed by tightly packed 30 nm fibers. The nucleolus is prominent and composed of a pale central granular area surrounded by dense fibrous ring (Fig. 1F). The cytoplasm contains abundant free ribosomes but only few mitochondria and no other organelles.

Primary spermatocytes (PrSc)

PrSc consists of six stages, i.e., leptotene (LSc), zygotene (ZSc), pachytene (PSc), diplotene (DSc), diakinetic (DiSc) and metaphase (MSc). The early cells (from LSc to PSc) are oval or round and become increasingly larger; then they (from DSc to MSc) are gradually decreased in size. The most distinctive differences among various stages of PrSc are the patterns of chromatin condensation and the relative amount of euchromatin versus heterochromatin.

Leptotene spermatocyte (LSc) (Fig. 2A–C)

This oval-shaped cell is larger than Sg with a diameter of 10–12 μm and also contains a large oval or round nucleus with the diameter about 8 μm. Most of the chromatin is in euchromatic form with only a small amount of heterochromatin appearing as a very thin rim along the nuclear envelope and small blocks scattered evenly throughout the nucleus (Fig. 2B,C). In the euchromatic area individual chromatin fibers exhibit two levels of organization, i.e., the 30 nm fibers which mostly appear in cross sections as dense dots, and the 10 nm fibers that appear as zig-zag lines. Heterochromatin blocks, regardless of their locations and forms, consist of tightly aggregated 30 nm fibers (Fig. 2C). The nucleolus is still present but not as prominent as in Sg. In addition to abundant ribosomes and an increasing number of mitochondria, the cytoplasm also contains a few dense granules which could be the precursor of a proacrosomal vesicle (Fig. 2B).

Zygotene spermatocyte (ZSc)

ZSc has approximately the same size as LSc. The distinguishing features of ZSc are the increase in size and density of heterochromatin blocks which are coupled by synaptonemal complexes. The chromatin

Fig. 2. A,B,C. Leptotene primary spermatocytes (LSc) showing ovoid nuclei, each containing a very thin rim of heterochromatin along the nuclear envelope (Ne) and many small heterochromatin blocks (Hc) scattered throughout the nucleus (in B). In C, the chromatin fibers appear in two levels: the thin zigzag 10 nm fibers (1) and 30 nm fibers whose cross sections appear as dense dots (2). Heterochromatin blocks (Hc) are composed of tightly packed 30 nm fibers. The cytoplasm of LSc contains abundant ribosomes, few mitochondria and small dense granules (Gr). Ba, basal lamina. D,E,F. Pachytene (PSc) and diplotene (DSc) primary spermatocytes, whose chromatin appear as thick branching heterochromatic cords that become more tightly packed in DSc (also shown in B). In E and F, PSc shows more heterochromatin than euchromatin; and chromatin fibers also exist at two levels, i.e., 10 and 30 nm fibers (1, 2 in F). The cytoplasm of LSc and DSc also contain small dense granules (Gr).

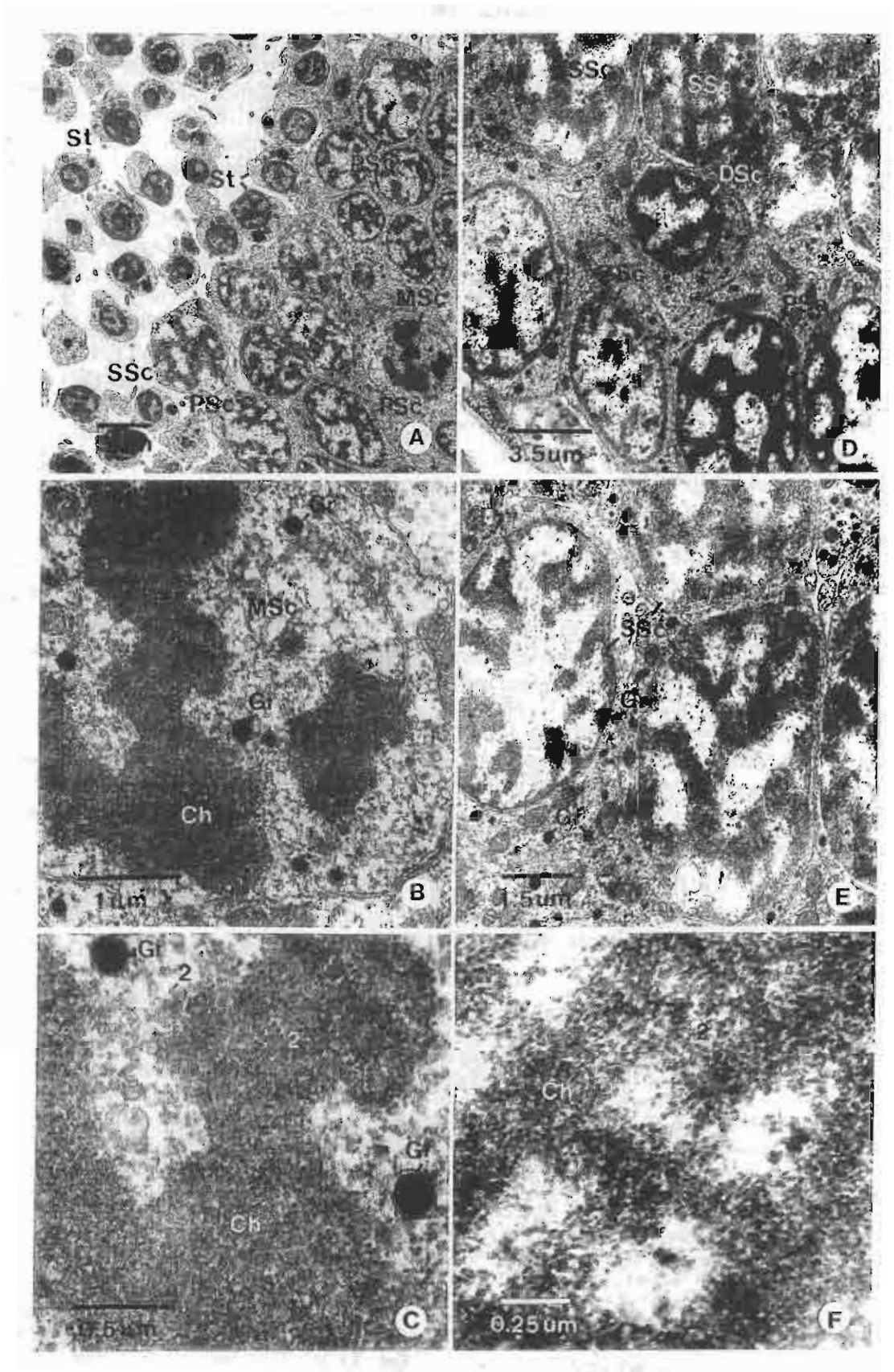
St
St
MSc
SSc
PSc
PSc
A
SSc
DSc
3.5um
D
Gr
MSc
Gr
Ch
1 um
B
SSc
Gr
Gr
1.5um
E
Gr
2
2
Gr
Ch
C
2
Ch
0.25 um
F

fibers and its packaging pattern are similar to that found in LSc. The nucleolus disappears completely. The cytoplasm has similar features as LSc.

Pachytene spermatocyte (PSc) (Fig. 2D, E, F)

PSc still has a round shape with slightly larger size than LSc (13–14 μm in size and 10–12 μm in nuclear diameter). It is characterized by the heterochromatin that appear as dense interconnecting cords consisting of tightly packed 30 nm fibers (Fig. 2E, F). In the cytoplasm, proacrosomal granules increase in number (Fig 2D, E).

Diplotene spermatocyte (DSc) (Fig. 2B)

This cell resembles PSc, except the sizes of the cell and its nucleus become smaller (about 10 and 8 μm, respectively), and the chromatin cords become increasingly thicker and packed closer together in the denser nucleoplasm. The cytoplasm has similar features to PSc.

Diakinetic (DiSc) and metaphase spermatocytes (MSc) (Fig. 3A–C)

These stages are about 7 μm in size, and they exhibit very large chromatin blocks that are parts of the completely formed chromosomes in DiSc, which are separated and then move to align at the equatorial region whilst the nuclear membrane disintegrates and completely disappears in MSc. Despite their tight aggregation, individual chromatin fibers in the chromosomes are the 30 nm type (Fig. 3C). The cytoplasm contains a large number of dense proacrosomal granules (Figs. 3B, C).

Secondary spermatocyte (SSc) (Fig. 3A, D, E)

SSc is a round or oval cell about 8 μm in diameter with the nucleus about 6 μm. They show thick chromatin cords that are criss-crossing one another, thus appearing as checker-board or XY figures (Fig. 3E, F). The individual chromatin fibers in the cords are loosely packed, but each still maintains the size of 30 nm (Fig. 3F). The cytoplasm of SSc contains a large number of dense proacrosomal granules (Fig. 3E).

Fig. 3. A. On the right is the epithelium of closely packed early germ cells consisting of pachytene (PSc), metaphase (MSc) primary spermatocytes and secondary spermatocyte (SSc), while on the left are early spermatids (St) that become separated from each other and from the epithelium. B,C. Metaphase primary spermatocyte containing large blocks of heterochromatin which are pieces of chromosomes (Ch). In C, the chromatin blocks are formed by the tight aggregation of 30 nm fibers. There are also numerous dense granules (Gr) in the cytoplasm. D,E,F. Secondary spermatocytes (SSc) whose nuclei contain thick chromatin cords in a reticulate pattern. In F, the 30 nm chromatin fibers (2), which form the cords, are loosely packed when compared to earlier stages.

Spermiogenic cells and spermatozoa

Spermatids (St)

There are four stages of spermatids, i.e., spermatid I (St_1), spermatid II (St_2), spermatid III (St_3) and spermatid IV (St_4) depending on the sizes, chromatin granulation and condensation. Successive stages vary from round and oval to ellipsoid, and ranging in sizes from 5-6 μm in St_1 to 3×2 μm in St_4.

Spermatid I (St_1) (Fig. 4A, B)

St_1 can be distinguished by its chromatin appearing as uniform but loosely packed 30 nm chromatin fibers (Fig. 4B, C). The cytoplasm of St_1 also contains a large number of proacrosomal granules that become concentrated in one side of the cell (Fig. 4A, B). Mitochondria are enlarged but still scattered in all areas of the cytoplasm (Fig. 4A).

Spermatid II (St_2) (Fig. 4D, E)

The general features of St_2 are similar to those of St_1 but the cell size is decreased to about 3.5 μm, the nucleus becomes oval, and is located eccentrically within the cell. The 30 nm chromatin fibers become more closely packed into clumps in the center of the nucleus as well as along the nuclear envelope, leaving light areas in between (Fig. 4D,E). At high magnification the chromatin clumping is formed by 30 nm fibers winding and condensing around the axis of condensation (Fig. 4F). In the cytoplasm, a large proacrosomal vesicle is formed on one side of the nucleus, perhaps by the fusion of the small proacrosomal granules found in earlier stages (Fig. 4D).

Spermatid III (St_3) (Fig. 5A–C)

The cell becomes reduced to about 3 μm and assumes a more oval shape with an eccentrically located nucleus. The cytoplasm moves to the posterior part. The chromatin begins to condense into dark connecting blocks with intervening light areas of nucleoplasm. Individual chromatin fibers in the chromatin blocks are enlarged and most appear in cross section as 40 nm tightly packed granules (Fig. 5C). A

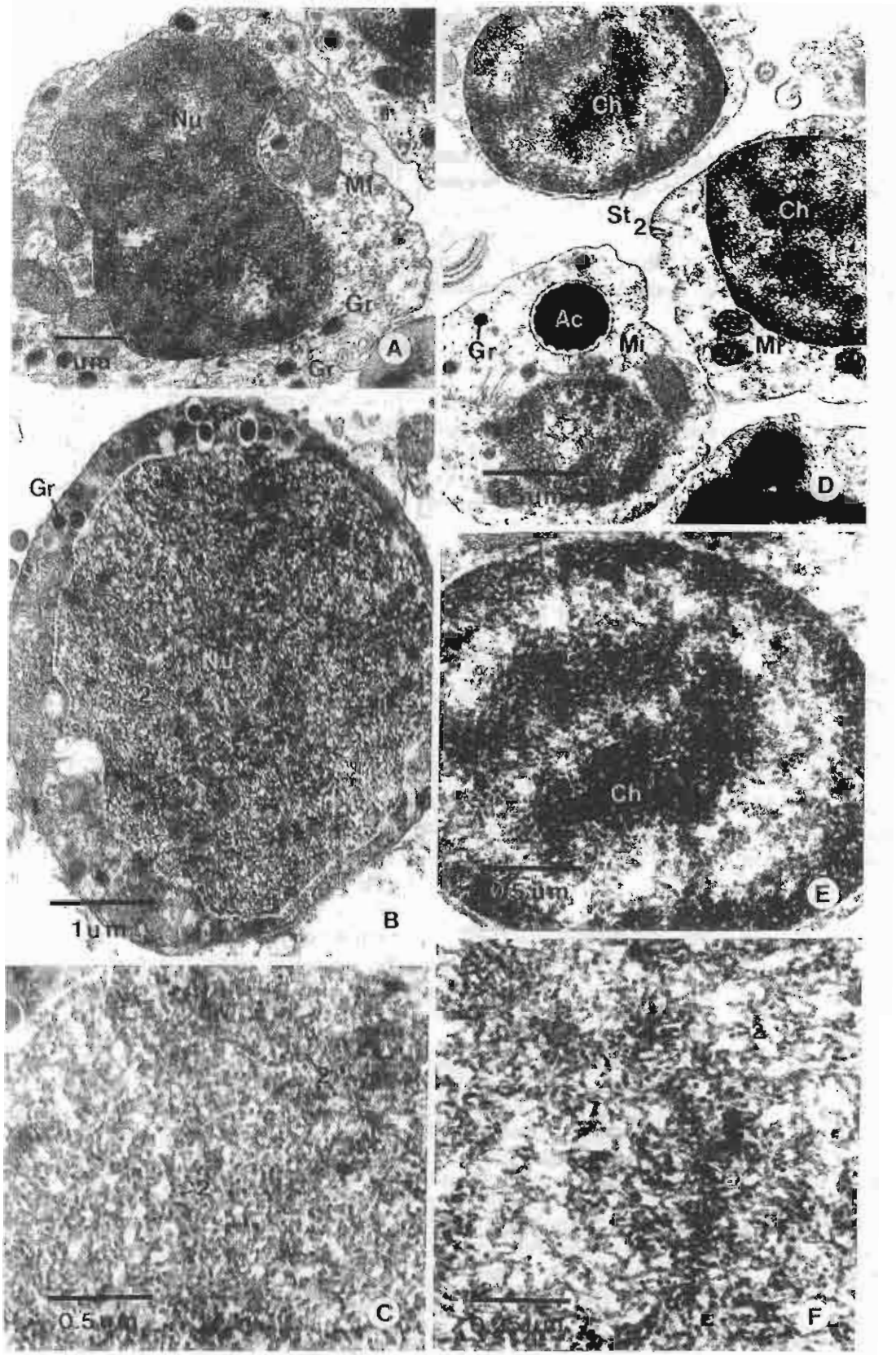
Nu
Mi
Gr
Gr
A
Ch
St2
Ch
Ac
Gr
Mi
Mi
D
Gr
Nu
1 µm
B
Ch
0.5 µm
E
0.5 µm
C
F

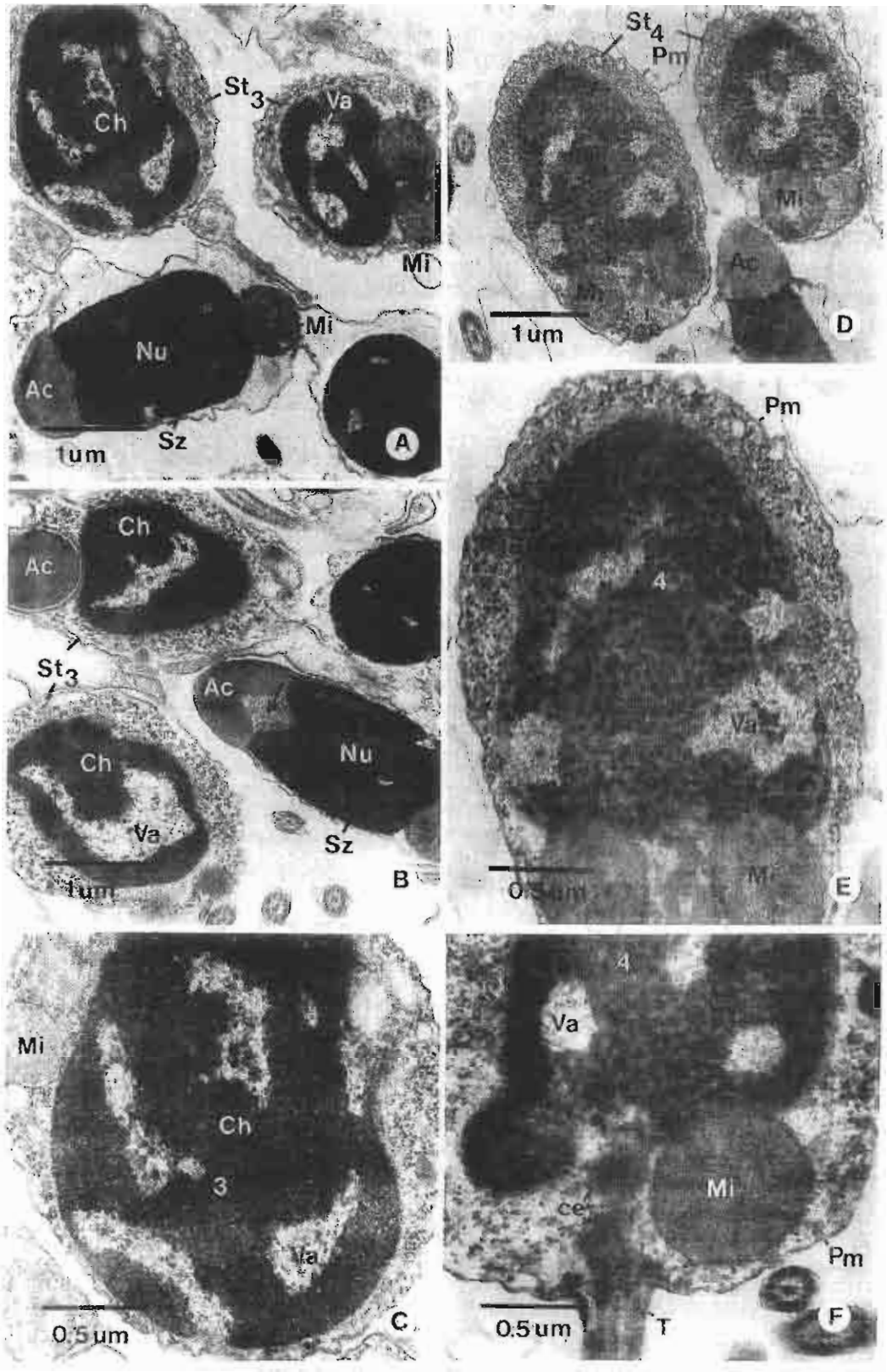
St3
Ch
Va
Mi
Nu
Mi
Ac
Sz
1um
A
St4
Pm
Mi
Ac
1um
D
Ch
Ac
St3
Ac
Nu
Ch
Va
Sz
1um
B
Pm
4
Va
M
0.5um
E
Mi
Ch
3
Va
0.5 um
C
4
Va
Mi
ce
Pm
0.5 um
T
F

single large proacrosomal vesicle becomes attached to one side of the nucleus (Fig. 5B), while mitochondria and centrioles are concentrated on the opposite side (Fig. 5A).

Spermatid IV (St_4) (Fig. 5D–F)

The cell becomes reduced in size to about 3× 2 μm and appears cone-shaped. Its chromatin becomes nearly condensed, thus the nucleus appears rather opaque; however, the outlines of individual chromatin fibers could still be observed as beaded structures, with each bead about 60 nm in diameter, connected by thin strands (Fig. 5E, F). At the caudal end of the nucleus the centrioles, which are surrounded by globular-shaped mitochondria, start to form the axonemal complex of the tail (Fig. 5F).

Spermatozoon (Sz)

An immature spermatozoon is a cone-shaped cell whose size is about 3×1.5 μm (Fig. 5A, B). There is a cup-liked acrosome with subacrosomal core apposing on the anterior tip of the electron dense nucleus (Fig. 5B). The tail is short with a pair of centrioles surrounded by globular-shaped mitochondria at the neck region from which the axonemal microtubules are generated. Full details of the mature spermatozoa of *H. asinina* has been recently described by our group (Apisawetakan et al., 2000)

Fig. 4. A, B, C. Stage I spermatids whose nuclei show evenly distributed 30 nm chromatin fibers (2) which are loosely packed. The cytoplasm contains numerous proacrosomal granules (Gr) and a few mitochondria (Mi). D, E, F. Stage II spermatids (St_2) showing the condensation of 30 nm chromatin fibers into clumps (Ch) separated from each other by clear nucleoplasm. At high magnification (in F) the clumping of 30 nm chromatin fibers (2) occur around the axis of condensation (ax). A very large acrosomal granule (Ac) is formed in every cell, while a few small granules (Gr) are also still present (in D).

Fig. 5. A, B, C. Stage III spermatids (St_3) whose nuclei show increasingly condensed chromatin (Ch), leaving only irregular electron lucent areas (Va) which contain very little chromatin fibers. At high magnification (in C) the 40 nm chromatin granules (3), which represent the closely packed chromatin fibers, could be observed in the condensing chromatin blocks (Ch). In each cell there is only one large proacrosomal vesicle (Ac) abutting on one side of the nucleus (in B). Two spermatozoa (Sz) with completely condensed chromatin are also present in A and B. Each has a cup-shaped acrosome (Ac) with the subacrosomal core (arrow) at the anterior end of the nucleus. D, E, F. Stage IV spermatids (St_4) whose nuclei contain dense chromatin which appear as evenly distributed beads about 60 nm in size (4). In reality these beads could be the cross sections of the enlarged chromatin fibers. Only small electron lucent areas (Va) are presented. Notice that there is still a narrow rim of cytoplasm surrounding the nucleus, while most of the cytoplasmic mass is translocated to the posterior end, which also contains the tail piece (T) developed from a pair of centrioles (ce) that are surrounded by globular-shaped mitochondria (Mi).

Discussion

Testicular structure and classification of cells in spermatogenesis

The first accounts of the testicular histology of an abalone species, *H. tuberculata*, were published by Stephenson (1924) and Croft (1929), who showed that the basic connective tissue framework of the testis is composed of fibrous capsule and trabecular sheets, from which germ cells appear to generate. Similar histological studies in other species were later performed by many investigators (Tomita, 1968; Young and De Martini, 1970; Takashima et al., 1978; Bevelander, 1988; Jarayabhand et al., 1994). Up to now most studies have not rigorously categorized the various stages of spermatogenesis in *Haliotis*, apart from suggesting broadly that there are four classes, i.e., spermatogonia, spermatocytes, spermatids and spermatozoa (Tomita, 1968; Young and De Martini, 1970; Takashima et al., 1978). In the present study, the process in *H. asinina* could be classified into 14 specific stages according to the size, shape, cytoplasmic features and the pattern of chromatin condensation. The spermatogonium is the earliest cell which gives rise to primary spermatocytes which pass through six stages as in the first meiotic division of vertebrate germ cells (Courot et al., 1970). Secondary spermatocytes are quite numerous in comparison to those in vertebrate testes, and they have heterochromatin that exhibits a checker-board pattern. Regardless of the changes in the packaging of chromatin into various patterns during primary and secondary spermatocyte stages, the individual chromatin fibers within the heterochromatin blocks are always the 30 nm type. These fibers invariably appear in cross sections as dense dots that are tightly packed together from PSc to MSc, but are more dispersed in SSc.

Cells in spermiogenesis and formation of spermatozoa

Four stages of spermatid development could be identified in *H. asinina* based on nuclear size, shape

and chromatin condensation patterns. The first two exhibit finely granulated chromatin which are the cross sections of 30 nm fundamental fibers. Individual chromatin fibers increase in size to 40 nm in St_3 and eventually, transform into enlarged beaded fibers, with individual beads about 60 nm in diameter in St_4. The change in size of chromatin from 30 nm highly coiled fibers to 60 nm beaded fibers could be modulated by the replacement of histones by the more basic protamine-liked protein. All fractions of histones could be detected in testicular cells of abalone and other molluscs, and these histones are similar to those found in mammalian cells (Daban et al., 1991; Caceres et al., 1994). On the other hand, it was found that in spermatozoa of most bivalves (Giancotti et al., 1983; Ausio et al., 1992) and abalone (Balhorn et al., 1979) there is a protamine-liked (PL) protein in addition to histones. This PL protein represents a group that appears to be intermediate basic proteins between histones and protamines (Ausio, 1999). It is possible that this highly positive PL protein may partially replace histones during the course of differentiation of male germ cells, probably in spermatid stage III (St_3) as judged from the change in chromatin fiber size from 30 to 40 nm. Subsequently, this protein may help to package DNA into tight coils which appear as large 60 nm beads. The exact point of replacement of histones by PL protein and how DNA is coiled up remain to be investigated further.

Our study has shown that the formation of the acrosome in *H. asinina* may begin earlier than in vertebrates, as a few dense proacosomal granules could be observed even in the LSc stage of primary spermatocytes. These granules are increased in number in PSc and later stages of primary spermatocytes. Consequently, St_1 is a relatively simple cell whose cytoplasmic mass is scanty and does not have a well-developed Golgi complex in contrast to a vertebrate spermatid at the same stage in which proacrosomal granules start to be synthesized. The large acrosomal vesicle becomes apparent in St_2 due to the coalescence of smaller granules. The definitive acrosome is formed in St_3 when the large single proacrosomal vesicle becomes attached to one side of the nucleus. The acrosome is fully formed in immature spermatozoa where it appears as a cup-shaped structure with a subacrosomal core, which is not as highly developed as in other abalone species (Shiroya et al., 1986; Usui, 1987) and bivalves (Tilney et al., 1987).

Another interesting finding is that there are supporting cells whose cytoplasm is highly branching and extremely rich in mitochondria, which implies that they are metabolically highly active. It is possible that these cells may play an important role in the development of primary spermatocytes with which they maintain close association. However, spermatids and immature spermatozoa are not embedded or anchored in the cytoplasm of supporting cells as in the case of vertebrate and neogastropod Sertoli cells (De Jong-Brink et al., 1977). Instead all spermatids are freed from each other while they are differentiating to spermatozoa and released into the lumen of the testicular compartment. A less intimate association between spermatids and supporting cells was also observed in other prosobranchia (Buckland-Nicks and Chia, 1986; Hodgson and Heller, 2000), which implies a less active role of supporting cells during spermiogenesis in the primitive gastropods.

Acknowledgements

This investigation was supported by the Thailand Research Fund (Senior Research Scholar Fellowship to Prasert Sobhon).

References

Anderson, W.A. and Personne, P., The molluscan spermatozoa: dynamic aspects of its structure and function. Am Zool., 16 (1976) 293–313.

Apisawetakan, S., Sobhon, P., Wanichanon, C., Linthong, V., Upatham, E.S., Kruatrachue, M., Jarayabhan, P. and Pumthong, T., Ultrastructure of spermatozoa in the testis of *Haliotis asinina* Linnaeus. J Med & Appl Malacol., 10 (2000) 101–109.

Apisawetakan, S., Chanpoo, M., Wanichanon, C., Linthong, V., Kruatrachue, M., Upatham, E.S., Pumthong, T. and Sobhon, P., Characterization of trabecular cells in the gonad of *Haliotis asinina* Linnaeus. J Shellfish Res., in press.

Ausio, J., Purification and biochemical characterization of the nuclear sperm-specific proteins of the bivalve mollusks *Agriodesma saxicola* and *Mytilimeria nuttalli*. Biol. Bull., 182 (1992) 31–40.

Ausio, J., Histone H1 and evolution of sperm nuclear basic protiens. J Biol Chem., 274 (1999) 31115–31118.

Balhorn, R., Lake, S. and Gledhill, B.L., Electrophoretic analysis of nuclear proteins isolated from the sperm of the black abalone *Haliotis crackeroidii*. Exp. Cell Res., 123 (1979) 414–417.

Bevelander, G., Abalone: gross and fine structure. Boxwood Press, California, 1988.

Buckland-Nicks J.A. and Chia F.S., Spermatogenesis of a marine snail, *Littorina sitkana*. Cell Tissue Res., 172 (1976) 503–515.

Buckland-Nicks J.A. and Chia F.S., Fine structure of Sertoli cells in three marine snails with a discussion on the

functional morphology of Sertoli cells in general. Cell Tissue Res., 245 (1986) 305–313.

Caceres, C., Ribes, E., Muller, S., Cornudella, L. and Chiva, M., Characterization of chromatin-condensing proteins during spermiogenesis in a neogastropod mollusc (*Murex brandaris*). Mol. Reprod. Dev., 38 (1994) 440–452.

Courot, M., Hochereau-de Reviers, M.T. and Ortavant, R., In: The Testis, A.D. Johnson (ed.), Academic Press, New York, 1970.

Croft, D.R., *Haliotis*. L.M.B.C. mem, Liverpool University Press, Vol. 29, 1929.

Daban, M., Chiva, M., Rosenberg, E., Kasinsky, H.E. and Subirana, J.A., Protamines in prosobranchian gastropods (Mollusca) vary with different modes of reproduction. J. Exp. Zool., 257 (1991) 265–283.

De Jong-Brink, M., Boer, H.H., Hommes, T.G. and Kodde, A., Spermatogenesis and the role of Sertoli cells in the freshwater snail *Biomphalaria glabrata*. Cell Tissue Res., 181 (1977) 37–58.

Dorange, G. and Le Pennec, M., Ultrastructural characteristics of spermatogenesis in *Pecten maximus* (Mollusca, Bivalvia). Invert. Reprod. Develop.,15 (1989) 109–117.

Fawcett, D.W., A comparative view of sperm ultrastructure. Biol. Reprod. Suppl., 2 (1970) 90–127.

Franzen, A., Comparative morphological investigations into the spermiogenesis among mollusca. Zool. Bidr. Uppsala., 30 (1955) 399–456.

Giancotti, V., Russo, E., Gasparini, M., Serrano, D., Del Piero, D., Thorne, A.W., Cary, P.D. and Crane-Robinson, C., Proteins from the sperm of the bivalve mollusc *Ensis minor*: co-existence of histones and a protamine-like protein. Eur. J. Biochem., 136 (1983) 509–516.

Hodgson, A.N. and Heller, J., Spermatozoon structure and spermiogenesis in four species of Melanopsis (Gastropoda, Prosobranchia, Cerithioidea) from Israel. Invert. Reprod. Develop., 37 (2000) 185–200.

Jarayabhand, P., Jew, N., Manasveta, P. and Choonhabandit, S., Gametogenic cycle of abalone *Haliotis ovina* Gmelin 1791 at Khangkao Island, Chon-buri province. Thai J. Aqua. Sci., 1 (1994) 34–42.

Shiroya, Y., Hosoya, H., Mabuchi, I. and Sakai, Y.T., Actin filament bundle in the acrosome of abalone spermatozoa. J. Exp. Zoo., 239 (1986) 105–115.

Singhagraiwan, T. and Doi, M., Seed production and culture of a tropical abalone, *Haliotis asinina* Linne. The Eastern Marine Fisheries Development Center, Department of Fisheries, Ministry of Agriculture and Cooperatives, Thailand, 1993.

Sobhon, P., Apisawetakan, S., Chanpoo, M., Wanichanon, C., Linthong, V., Thongkukiatkul, A., Jarayabhand, P., Kruatrachue, M., Upatham, E.S. and Pumthong, T., Classification of germ cells, reproductive cycle and maturation of gonads in *Haliotis asinina* Linnaeus. Science Asia, 25 (1999) 3–21.

Stephenson, T.A., Notes on *Haliotis tuberculata*. J. Marin. Biol. Assoc. UK, 13 (1924) 480–495.

Takashima, F., Okuno, M., Nichimura, K. and Nomura, M., Gametogenesis and reproductive cycle in *Haliotis diversicolor diversicolor* Reeve. J. Tokyo Univ. Fish., 1 (1978) 1–8.

Tilney, L.G., Fukui, Y. and De Rosier, D.J., Movement of the actin filament bundle in *Mytilus* sperm: A new mechanism is proposed. J. Cell Biol., 104 (1987) 981–993.

Tomita, K., The testis maturation of the abalone, *Haliotis discus hannai* Ino, in the Rebun Island, Hokkaido, Japan. Sci. Rep. Hokkaido Fish. Exp. Sta., 9 (1968) 56–61.

Usui, N., Formation of the cylindrical structure during the acrosome reaction of abalone spermatozoa. Gamete Res., 16 (1987) 37–45.

Young, J.S. and De Martini, J.D., The reproductive cycle, gonadal histology and gametogenesis of the red abalone, *Haliotis rufescens* (Swainson). Calif. Fish and Game., 56 (1970) 298–309.

Invertebrate Reproduction and Development, 39:1 (2001) 67–79
Balaban, Philadelphia/Rehovot
0168-8170/00/$05.00 © 2001 Balaban

Ultrastructure of female germ cells in *Haliotis asinina* Linnaeus

SOMJAI APISAWETAKAN[1], VICHAI LINTHONG[1], CHAITIP WANICHANON[1], SASIPORN PANASOPHONKUL[1], ARDOOL MEEPOOL[1], MALEEYA KRUATRACHUE[2], EDWARD SUCHART UPATHAM[2,3], TANATE PUMTHONG[4] and PRASERT SOBHON[1*]

[1]*Department of Anatomy,* [2]*Department of Biology, Faculty of Science, Mahidol University, Rama VI Road, Bangkok, Thailand 10400*
Tel. (662) 245-5198; Fax (662) 247-9880; email: scpso@mahidol.ac.th
[3]*Department of Medical Science, Faculty of Science, Burapha University, Chonburi, Thailand*
[4]*The Coastal Aquaculture Development Center, Department of Fisheries, Prachuabkirikhun Province, Thailand 77000*

Received 25 September 2000; Accepted 7 March 2001

Summary

Germ cells in the ovary of *H. asinina* are divided into six stages: oogonia and five stages of oocytes. The oogonium is a scallop-shaped cell 8–10 μm in diameter, closely adhered to a trabecula. Its nucleus exhibits small blocks of heterochromatin along the nuclear envelope and a small nucleolus. The cytoplasm contains abundant ribosomes. The stage I oocyte is a round cell 12–25 μm in diameter. Its nucleus contains numerous lampbrush chromosomes consisting of chromatin fibers with three sizes, i.e., 100–200, 40–60 and 7–12 nm in diameter. The cytoplasm has numerous mitochondria, few rough endoplasmic reticulum, and abundant ribosomes. The stage II oocyte is a round cell 25–35 μm in diameter. Its nucleus exhibits increasingly decondensed chromatin and a nucleolus, and the nuclear envelope exhibits numerous nuclear pores. The cytoplasm contains numerous and well-developed Golgi bodies, rough endoplasmic recticulum and abundant ribosomes. There are two types of secretory granules: both have a spherical shape, 350–450 nm in diameter, with an electron-dense and electron-lucent matrix, respectively. The stage III oocyte is a pear-shaped cell about 35×70 μm in size. Lampbrush chromosomes are almost completely unraveled. The two types of secretory granules are greater in number and cluster around the Golgi bodies. Larger and more electron-dense ovoid-shaped yolk granules start to appear. The stage IV oocyte is a flask-shaped cell about 50×80 μm in size. Its nucleus contains completely decondensed chromatin and a highly enlarged nucleolus. The cytoplasm is filled with lipid droplets (1.5–3 μm in diameter) and yolk granules (1.5–2.5 μm in diameter). The vitelline-cum-jelly coat starts to develop, and could be derived from the first type of secretory granules which are translocated to be exocytosed at the plasma membrane. The stage V oocyte is similar to the stage IV oocyte except its vitelline-jelly coat achieves maximum thickness and appears fibrous in comparison to the amorphous appearance at stage IV.

Key words: *Haliotis asinina*, female germ cells, ultrastructure

*Corresponding author.

Introduction

The histology of the ovary in various abalone species has been extensively studied since 1924 (Stephenson, 1924). In 1929, Croft (1929) showed that the basic connective tissue framework of the ovary in *H. tuberculata* is composed of a fibrous capsule that partly projects inwards as trabeculae which provide support for the developing germ cells. Similar conclusions were reached in the studies of other species including *H. discus hannai* (Tomita, 1967), *H. cracherodii* (Webber and Giese, 1969), *H. rufescens* (Young and DeMartini, 1970; Giorgi and DeMartini, 1977), *H. diversicolor diversicolor* (Takashima et al., 1978), *H. ovina* (Jarayabhand et al., 1994; Minh, 1998), and *H. asinina* (Apisawetakan et al., 1997; Sobhon et al., 1999). Recently, electron microscopic studies revealed that the outer gonadal capsule is lined by a single layer of mucus-secreting epithelium (Martin et al., 1983; Apisawetakan et al., in press) and not a cuticle as suggested earlier by Young and DeMartini (1970). Furthermore, the middle layer of the capsule consists of several alternated layers of muscle cells and collagen fibrils, intermingled with fibroblasts, granulated cells and nerve fibers. This is lined at the inner surface with a single layer of simple squamous epithelium which rests on the thick basal lamina that separates the connective tissue proper of the capsule and trabeculae from the germ cell compartment (Apisawetakan et al., in press).

There have also been several attempts to classify the female germ cells in the oogenetic processes. Tomita (1967) reported that there are seven stages of female germ cells, including oogonia and six stages of developing oocytes in *H. discus hannai*; while Takashima et al. (1978) suggested that there are nine stages of female germ cells with oogonia and eight stages of oocytes in *H. diversicolor diversicolor*. In more recent works using TEM to observe the relative abundance of various organelles, particularly ribosomes and the development of rough endoplasmic reticulum (RER) and Golgi bodies in the cells, Martin et al. (1983) classified female germ cells in *H. rufescens* into five stages: oogonium, presynthetic oocyte, synthetic oocyte, early postsynthetic oocyte and fully developed postsynthetic oocyte; while Young and DeMartini (1970) suggested that there were only four stages of female germ cells in this species. In view of these conflicting reports, together with the fact that there are still no detailed studies of the female germ cells in *Haliotis asinina*, an abundant abalone species found in the tropics including the coastal water of Thailand, we have attempted to classify the female germ cells of this species by using ultrastructural characteristics.

Materials and Methods

Collection of adult abalone

Adult abalone (older than 24 months) from a land-based culture system were provided by the Coastal Aquaculture Development Center, Department of Fisheries, Prachaubkirikhun Province, Southern Thailand. They were kept in concrete tanks housed in the shade and well flushed with mechanically circulated filtered seawater and an air delivery system to maintain a stable controlled environment. The optimum level of salinity was 22.5–32.5 ppt and the temperature was 22–26°C (Singhagraiwan and Doi, 1993). They were fed with macroalgae (usually *Gracilaria* spp. and *Laminaria* spp.), supplemented with artificial food.

Transmission electron microscopy (TEM)

For TEM studies, ovaries were cut into small pieces and fixed in a solution of 3% glutaraldehyde in 0.1 M sodium cacodylate buffer pH 7.8 at 4°C overnight. The specimens were post-fixed in 1% OsO_4 in 0.1 M sodium cacodylate buffer at 4°C for 2 h. They were dehydrated in the increasing concentrations of ethanol (50–100%) for 30 min each, cleared in two changes of propylene oxide, and embedded in Araldite 502 resin. Blocks of specimens were sectioned at 1-micron thickness by an MT-2 ultramicrotome and stained with methylene blue for light microscopic observations. Ultrathin sections were cut and stained with lead citrate-uranyl acetate and viewed under a Hitachi H-300 TEM at 75 kV.

Results

Female germ cells

Based on light and electron microscopic characteristics, there are six stages of female germ cells in the ovary of *H. asinina*, including oogonia and five stages of oocytes.

Oogonium (Og)

This is an oval or scallop-shaped cell whose size is 10–12 μm (Figs. 1A, 2A). Its nucleus is round and about 7 μm in diameter. It contains small blocks of heterochromatin attached to inner surface of the nuclear envelope, while the majority of chromatin appears as euchromatin, and the nucleolus is small. In

semi-thin sections the cytoplasm is basophilic and stained light blue by methylene blue, which reflects the presence of moderate numbers of ribosomes as observed in TEM. Other organelles have not yet been developed. Oogonia are concentrated in groups and attached to capsular side of the trabeculae (Fig. 1A). Each is surrounded by flat, squamous-shaped follicular cells.

Stage I oocyte (Oc_1)

This is a round cell that is closely adhered to the trabecula (Figs. 1A,B; 2B–F). It is 15–25 μm in size, with a round nucleus about 12 μm in diameter. Its nucleus exhibits numerous densely packed lampbrush chromosomes which consist of large fibers 100–120 nm in cross section, and small fibers 40–60 nm in diameter which are linked by thin zigzag filaments 7–12 nm in size (Fig. 2C). The nucleolus is enlarged and becomes quite prominent. In semi-thin sections, the cytoplasm is stained deep blue with methylene blue, which indicates its intense basophilic property due to the presence of numerous ribosomes as observed in TEM. In early Oc_1, other organelles consist of only a few mitochondria (Fig. 2B), while in late Oc_1 RER starts to develop (Fig. 2D,E). There are large aggregates of ribosome-liked particles close to the cytoplasmic side of the nuclear membrane. The dimension of each particle in the aggregates and its electron density are similar to those of ribosomes in the rest of the cytoplasm. Hence, these aggregates could be the newly formed ribosomes which are being translocated from the nucleus (Fig. 2E, F). There are still no secretory granules, and due to its enlarged size, each Oc_1 is surrounded by few follicular cells.

Stage II oocyte (Oc_2)

This cell still has a spherical or ovoid shape and is larger, with the cell size about 30×55 μm, and a nuclear size about 22 μm (Figs. 1B; 3A–G). It is still anchored to the connective tissue trabecula by a group of basal follicular cells, and each Oc_2 is surrounded by several peripheral follicular cells (Fig. 1A,B). The nucleus exhibits increasingly decondensed chromatin and a prominent nucleolus (Fig. 3A,B). Very few lampbrush chromosomes remain (Fig. 3A,B), while most of the chromatin assumes euchromatic form consisting mainly of chromatin fibers 40–60 nm and 7–12 nm in diameter (Fig. 3D). In tangential sections the nuclear membrane exhibits numerous nuclear pores arranged in close regular rows (Fig. 3C). The cytoplasm is stained light blue, similar to Og, and contains clusters of clear lipid droplets (Figs. 1B, 3A). In TEM the cytoplasm was observed to contain numerous well-developed Golgi bodies, RER (Fig. 3E,F) and abundant ribosomes bound to the fine microtrabecular network of the cytoplasm. There are two types of secretory granules: SG_1 and SG_2 both have diameters ranging from 350 to 450 nm, with an electron-dense and electron-lucent matrix, respectively (Fig. 3G). However, these granules are still comparatively few in number.

Stage III oocyte (Oc_3)

This cell becomes increasingly larger and assumes a pear shape, with the narrow side or base still attached to the connective tissue trabecula by a thin cytoplasmic process surrounded by a group of follicular cells (Fig. 1C,D). The cell size is 35×70 μm, and the nuclear size is 25 μm. The nucleus contains mostly euchromatin, as the lampbrush chromosomes become unraveled into smaller-sized fibers (Fig. 4A,D), and the nucleoplasm becomes fairly transparent. The nucleolus is enlarged due to uncoiling of the nucleolar chromatin, and few vacuoles are present (Fig. 4C). In addition to the increasing number of clear lipid droplets, the cytoplasm begins to show numerous small granules representing SG_1 and SG_2 which are concentrated around Golgi bodies (Fig. 4B,E,F), whilst only a few larger and more electron-dense yolk granules were observed. Remnants of ribosomal aggregates are still sporadically present (Fig. 4F).

Stage IV oocyte (Oc_4)

This cell is large and assumes a flask or polygonal shape that is still attached to the trabecula by a slender cytoplasmic process surrounded by a group of basal follicular cells (Fig. 1D). The cell size is about 60×80 μm, and the nuclear size about 35 μm. The nucleus contains only euchromatin consisting of 40–60 nm and 7–12 nm fibers, and the nucleoplasm is virtually transparent (Figs. 1D, 5A–C). The nucleolus becomes maximally enlarged due to the complete uncoiling of its chromatin. The cytoplasm is filled with electron-dense oval-shaped yolk granules each 1.5–2.5 μm in diameter, mixed with numerous lipid droplets each 1.5–3 μm in diameter (Fig. 5A,D,E). Small SG_1 and SG_2 granules are present in fewer numbers in the central area of cytoplasm, since most are located peripherally beneath the plasma membrane. A thin layer of homogenous jelly coat begins to form on the outer surface of the cell membrane which shows numerous short microvilli (Figs. 1D, 5F–H). The coat is in turn surrounded by the processes of follicular cells.

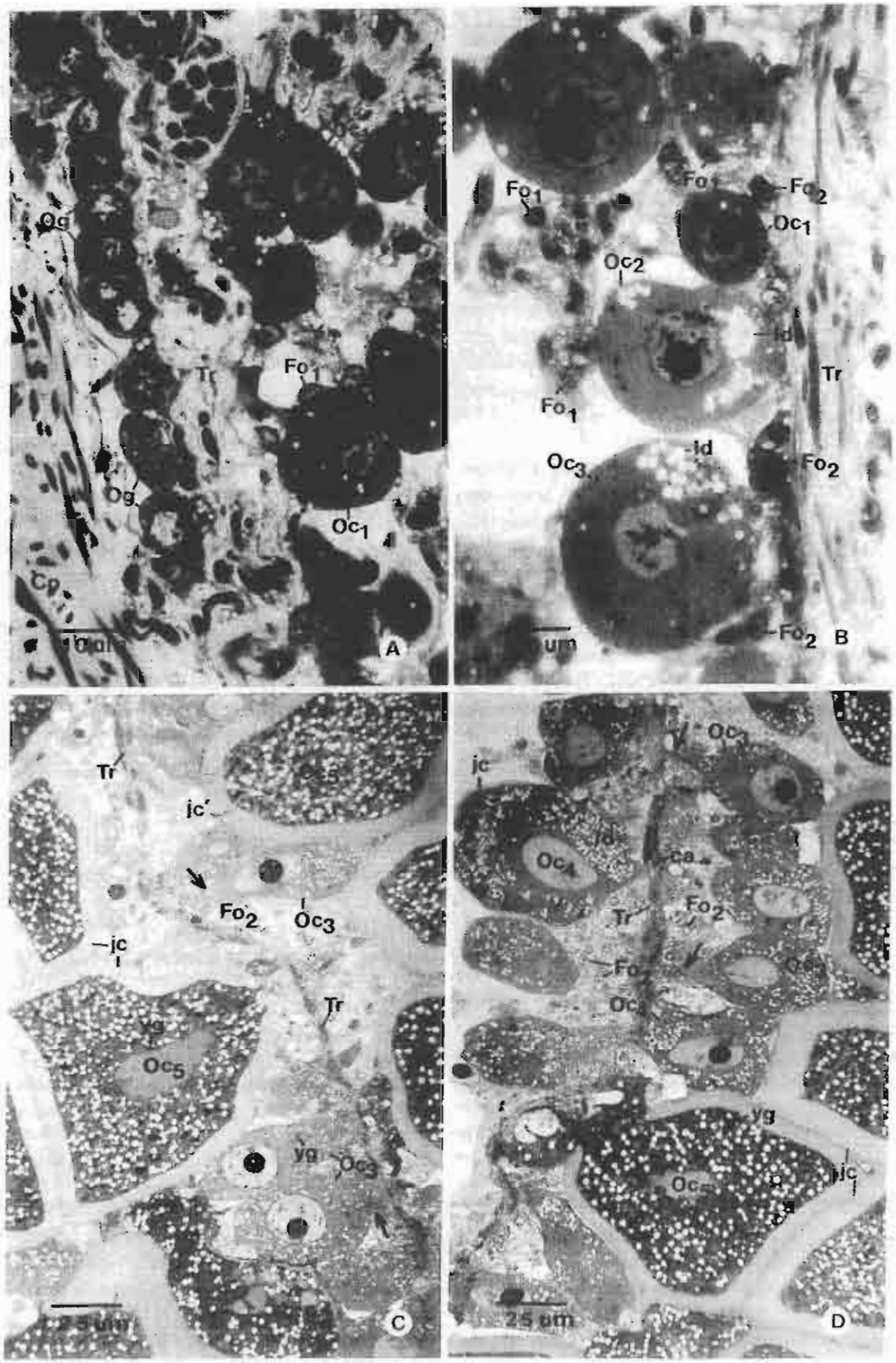
Og
Tr
Fo1
Og
Oc1
Cp
A
Fo1
Fo1
Fo2
Oc1
Oc2
id
Tr
Fo1
id
Oc3
Fo2
Fo2
B
Tr
jc
Oc5
jc
Fo2
Oc3
jc
Tr
vg
Oc5
vg
Oc3
C
Oc1
jc
id
Oc4
ca
Tr
Fo2
Fo2
Oc3
vg
Oc5
jc
25 µm
D

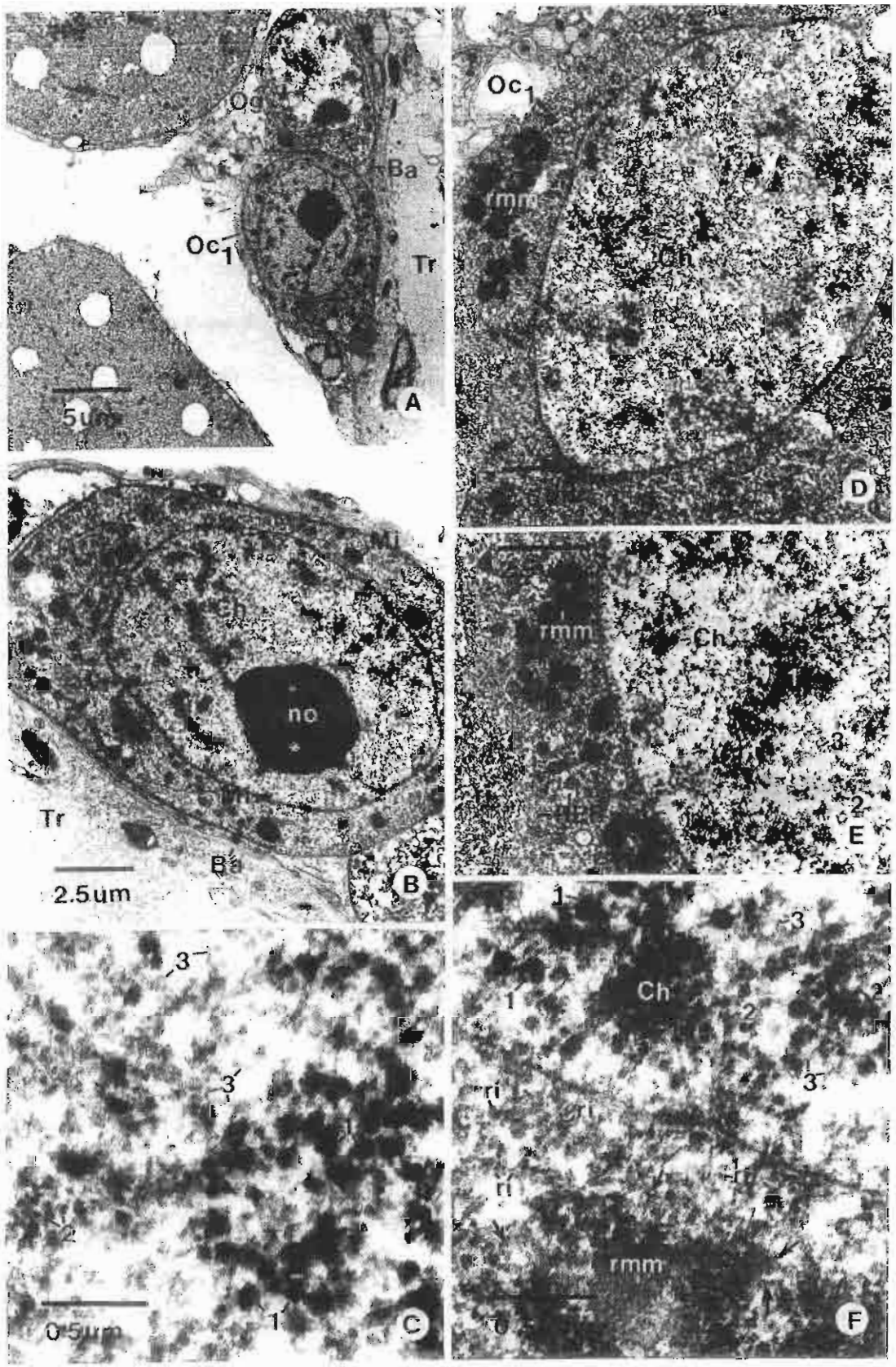
Og
Ba
Oc1
Tr
5um
A
Oc1
rmm
Ch
D
Mi
Ch
no
Mi
Tr
Ba
2.5um
B
rmm
Ch
E
3
0.5um
C
Ch
rmm
F

Stage V oocyte (Oc_5)

This is the largest cell with a polygonal or round shape, and the cell and nuclear sizes are 100×140 μm and 40 μm, respectively (Fig. 1C,D). Oc_5 exhibits similar nuclear and cytoplasmic ultrastructural characteristics as Oc_4, but the cell has more and evenly distributed yolk granules and lipid droplets (Fig. 1C,D). In addition, the jelly coat of Oc_5 is uniformly thick and composed of the network of dense and coarse fibers in comparison to the thin homogeneous jelly coat that contains evenly distributed fine filaments in Oc_4 (Figs. 5H, 6A). This coat may be partially formed by the contents of SG_1 which were seen apparently engaged in exocytosis at the oocyte's plasma membrane (Fig. 5F–H).

Follicular cells

Follicular cells could be divided into two groups: those that aggregate at the bases or around the cytoplasmic processes of oocytes and help to anchor them to the connective tissue of trabeculae (Figs. 1B, D; 6B,C), and those that surround the periphery of the oocytes (Figs. 1B,D, 6E,F). Cells in the first group have a columnar shape, and they adhere to the basal lamina lining the trabecular connective tissue proper on one side, while the other side is attached to the oocytes (Fig. 6B). The nucleus of each cell is characterized by a uniform thick rim of heterochromatin lining inner surface of the nuclear envelope. There are only one or two blocks of heterochromatin in the central area of the nucleus, whilst the remaining chromatin is in euchromatic form. The cytoplasm has numerous large mitochondria with tubular cristae, dilated RER and a few clear lipid droplets (Fig. 6B,C). Within the connective tissue proper of trabeculae, there are cells possessing similar nuclear characteristic but with only scanty cytoplasm (Fig. 6C). These cells could be the precursors of the basal follicular cells and, by traversing the basal lamina into the germ cell compartment, they could give rise to the latter. In contrast, the peripheral follicular cells that surround the oocytes exhibit ellipsoid shape and taper into thin

Fig. 1. A. Semi-thin sections of the ovarian tissue in *H. asinina*, showing a row of oogonia (Og) and a few Oc_1 attaching to a trabecula (Tr). Cp, ovarian capsule. B. Also anchoring to the trabeculae are stages I, II and III oocytes (Oc_1, Oc_2, Oc_3). The cytoplasm of Oc_1 is intensely basophilic, while Oc_2 and Oc_3 have decreased basophilia but increased lipid droplets (ld). All these cells are surrounded by peripheral follicular cells (Fo_1) and anchored to the trabeculae by basal follicular cells (Fo_2). C. Oc_3 remain attached to the trabeculae (Tr) by slender cytoplasmic processes (arrows) which are surrounded by basal follicular cells (Fo_2). Yolk granules (yg) start to appear. D. Oc_4 could be identified by a thin jelly coat on the surface (jc) and increasing number of lipid droplets (ld) and yolk granules (yg). Oc_5 (also shown in C) are surrounded by a uniformly thick jelly coat (jc), and contain numerous lipid droplets and yolk granules (yg) in the cytoplasm. Magnifications of all micrographs are indicated by micron bars (μm).

Fig. 2. A, B. TEM micrographs of an oogonia (Og) and an early oocyte I (Oc_1) which lie on the basal lamina (Ba) of a trabecula (Tr). Og has a rather clear nucleus and a small nucleolus, while Oc_1, also shown at higher magnification in B, has increasing number of lampbrush chromosomes (Ch) and a large nucleolus (no). The cytoplasm has abundant ribosomes and a few mitochondria (Mi). C. The lampbrush chromosomes of Oc_1 in B show three levels of chromatin fibers. The first two levels usually appear as dense granules in cross sections with diameters 100–120 nm (1), and 40–60 nm (2), while the third level appears as thin zigzag fibers 7–12 nm in thickness (3). D,E. Late oocyte I, showing highly decondensed lampbrush chromosomes (Ch) which exhibit increasing amount of level 2 and 3 fibers. The cytoplasm contains abundant ribosomes (ri) which are evenly distributed throughout. In addition, there are large aggregates of ribosome-liked particles (rmm) around the cytoplasmic side of the nuclear membrane, and only a little RER. F. A high magnification of the cell shown in D, showing the nucleus containing three-level chromatin fibers (1,2,3) and ribosomal aggregates (rmm) near the nuclear membrane. At the edge of the aggregates (arrows) strings of these particles are dispersed out to form individual ribosomes (ri) as appear in the rest of the cytoplasm.

Fig. 3. A. Oocyte II (Oc_2), showing a very large nucleolus (no) and highly decondensed chromatin in the nucleus (nu), and lipid droplets (ld) and ribosomal aggregates (rmm) in the cytoplasm. B. The nucleolus (no) in the nucleus of Oc_2, also shown in A, is enlarged and consisted of granular inner area surrounded by dense fibrous ring (arrow). C. A tangential section of the nuclear membrane exhibits numerous nuclear pores (np) arranged in regular rows. D. A high magnification of the nucleus of Oc_2 in A, showing chromatin which is highly decondensed to assume mostly level 2 and level 3 fibers. E. The cytoplasm of Oc_2 in A contains numerous newly formed Golgi bodies (Gc). F. There are abundant ribosomes (ri) anchored on the filamentous microtrabecular network of the cytoplasm (arrows). One fairly well developed Golgi complex (Gc) is also shown. G. There are still very few secretory granules in the cytoplasm of Oc_2, and those that are present comprise two types of spherical granules, one with dense matrix (SG_1) and the other with light matrix (SG_2) whose diameters range from 350 to 450 nm.

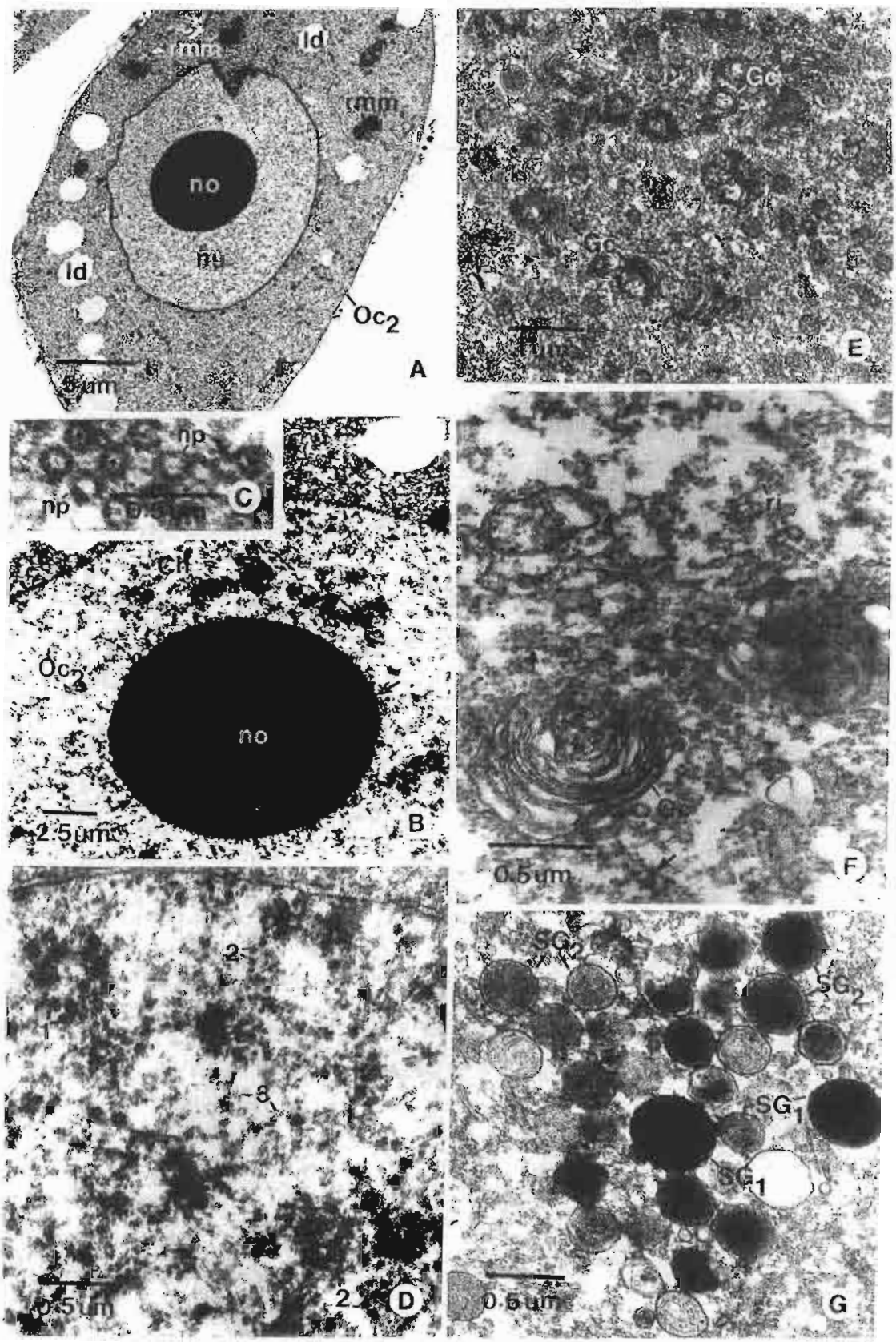
ld
no
nu
ld
Oc2
A
Gc
Gc
E
np
np
C
ch
Oc2
no
2.5 µm
B
0.5 µm
F
2
1
3
0.5 µm
2
D
SG2
SG2
SG1
SG1
0.5 µm
G

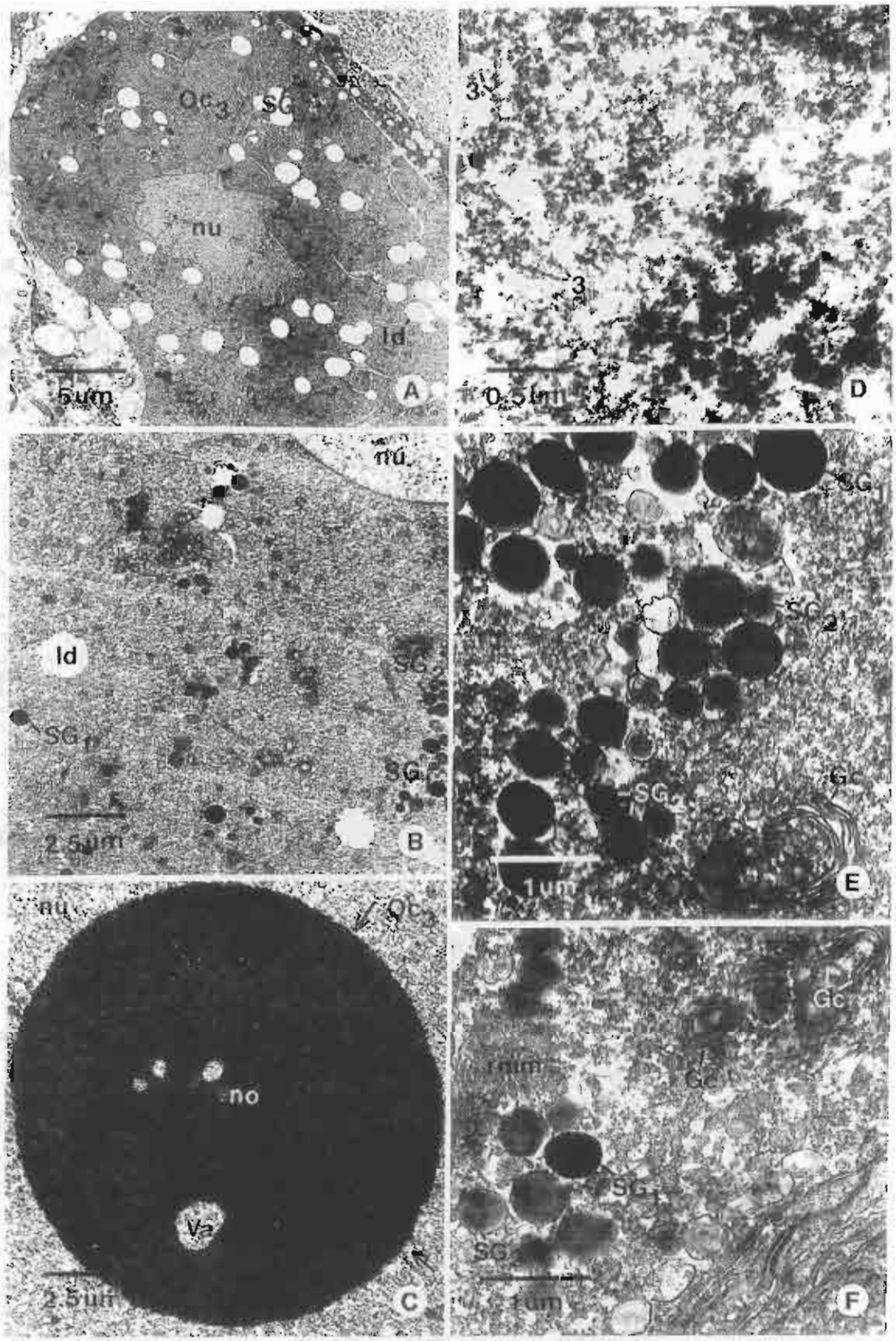
Oc
SG
nu
ld
5um
A
0.5um
D
nu
ld
SG
SG
SG
2.5um
B
SG
SG
SG
Gc
1um
E
nu
Oc
no
Va
2.5um
C
Gc
Gc
SG
SG
1um
F

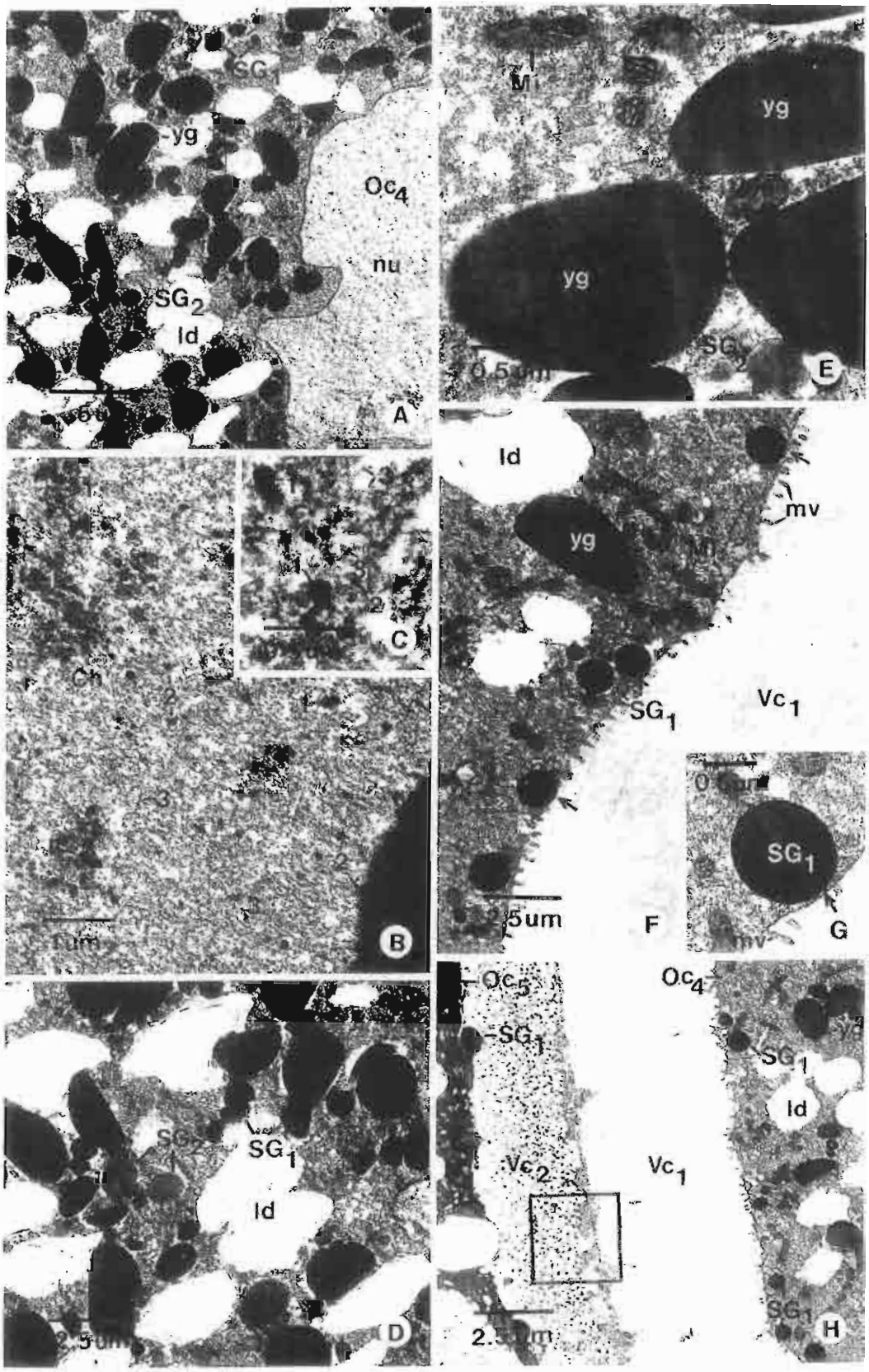
SG1
yg
Oc4
nu
SG2
Id
A
M1
yg
yg
SG2
0.5um
E
Id
yg
mv
M1
SG1
Vc1
2.5um
F
0.5um
SG1
mv
G
Ch
B
C
Oc5
SG1
Vc2
Vc1
Oc4
SG1
Id
SG1
H
SG2
SG1
Id
D

cytoplasmic sheets that form a complete covering of the remaining oocytes' surface. The nucleus of each cell exhibits large blocks of heterochromatin along the nuclear envelope and in the central area. The cytoplasm contains abundant dilated RER, a few secretory granules and lipid droplets (Figs. 1B, 6E,F). These cytoplasmic characteristics indicate that the cells may be quite active and not merely serving as a passive covering of the oocytes.

Discussion

In earlier studies, there are some disagreements on the classification of the stages of germ cells in the oogenetic processes (Tomita, 1967; Young and DeMartini, 1970; Takashima et al., 1978). In the present study we divide the cells according to changes in histological and ultrastructural characteristics which reflect the synthetic activities in various developmental stages. These characteristics include: (1) the appearance of the nucleus and nucleolus especially with regard to the uncoiling of chromatin; (2) the basophilia imparted to the cytoplasm of the cells by methylene blue stain, which reflects the abundance of ribosomes in the cytoplasm as observed in TEM; (3) the development of secretory organelles, particularly RER and Golgi bodies; (4) the occurrence of secretory products including cortical granules, yolk granules, and their relative abundance; (5) the presence of lipid droplets; and (6) the presence and nature of the jelly coat surrounding the oocytes. By using these rather stringent morphological criteria, we could identify six stages of female germ cells, starting from oogonia, which are the smallest cells closely attached to the connective tissue trabecula. These cells, particularly those that are clustered on the capsular side of the trabeculae, maintain a constant pool of early stem cells (Sobhon et al., 1999).

The most pronounced characteristics of the first stage oocytes (Oc_1) are the increasing basophilia of their cytoplasm, the prominence of nucleoli, and the presence of large aggregates of ribosome-liked particles around the nuclear membrane which could represent the nascent ribosomes that have just been transported from the nucleus to the cytoplasm. This process may be facilitated by the presence of numerous nuclear pores in the nuclear membrane in late Oc_1 and Oc_2 stages. The above characteristics suggest that this stage of oocyte is involved largely in the synthesis, assembly and transport of ribosomes from the nucleolus to the cytoplasm. Thus, we designate Oc_1 as a ribosomal phase which may correspond to the presynthetic oocytes as described in *H. rufescens* by Martin et al. (1983) when the cells are preparing themselves for the onset of synthetic activities.

Fig. 4. A, B. Oocyte III (Oc_3), showing the nucleus with completely decondensed chromatin (nu), and the cytoplasm which contains large amount of lipid droplets (ld) and secretory granules (SG_1, SG_2, in B). C. The nucleolus of Oc_3 becomes highly decondensed and contains a pale lace-like interior with few vacuoles (va) and a dense edge (arrows). D. Most of the chromatin in Oc_3 is decondensed to levels 2 and 3 with very few level 1 fibers remaining. E. Secretory granules (SG_1, SG_2) in Oc_3 are located close to the Golgi complex (Gc). F. There is small amount of ribosomal aggregates (rmm) remaining in the cytoplasm of Oc_3.

Fig. 5. A. Oocyte IV (Oc_4) showing the nucleus (nu) with completely decondensed chromatin and the light nucleoplasm, and the cytoplasm which contains numerous yolk granules (yg), lipid droplets (ld), and secretory granules (SG_1, SG_2). B, C. The chromatin of Oc_4 is almost completely decondensed to levels 2 and 3 fibers with only sporadic level 1 fibers remaining. D, E. Medium and higher magnifications of an Oc_4 cytoplasm showing the large ovoid-shaped yolk granules (yg), the small spherical secretory granules (SG_1, SG_2) interspersed with lipid droplets (ld) and mitochondria (Mi). F, G. The peripheral cytoplasm of Oc_4 showing SG_1 granules close to the plasma membrane (arrows) bearing short microvilli (mv). The vitelline-jelly coat (Vc_1) appears fairly homogeneous. H. In Oc_5 some SG_1 granules are exocytosed to form the jelly coat (Vc_2) which appears fibrous, while in Oc_4 most of SG_1 have not yet been exocytosed and the jelly coat appears homogeneous (Vc_1).

Fig. 6. A. Higher magnification of the boxed area from Fig. 5H, showing the homogeneous jelly coat surrounding Oc_4 (Vc_1) which could be partly derived from peripheral follicular cells and the fibrous jelly coat surrounding Oc_5 (Vc_2) which receives exocytosed material from SG_1. B,C. Basal follicular cells (Fo_1) anchor oocytes to the basal lamina (Ba) of a trabecula (Tr). The nucleus of this type of cell exhibits uniformly thick rim of heterochromatin on the nuclear envelope (arrows, in C), with only a few small blocks of dense chromatin (hc) in the central area. The cytoplasm has numerous mitochondria (Mi) and dilated vesicular RER and a few lipid droplets (ld). Mu, muscle cell. D. A cell (Fo'_1) within a trabecular compartment (Tr) exhibits the nucleus with similar characteristics as that of the basal follicular cell (Fo_1) shown in C but with scant cytoplasm. This cell may be the precursor of Fo_1 cells. Ba, basal lamina; Mu, muscle cell. E. Peripheral follicular cells (Fo_2) have a squamous shape, forming flat sheets covering the oocytes (Oc). F. A nucleus (nu) of the peripheral follicular cell (Fo_2) exhibits more heterochromatin than in the basal follicular cell, and the cytoplasm contains fewer mitochondria (Mi) but numerous flattened RER.

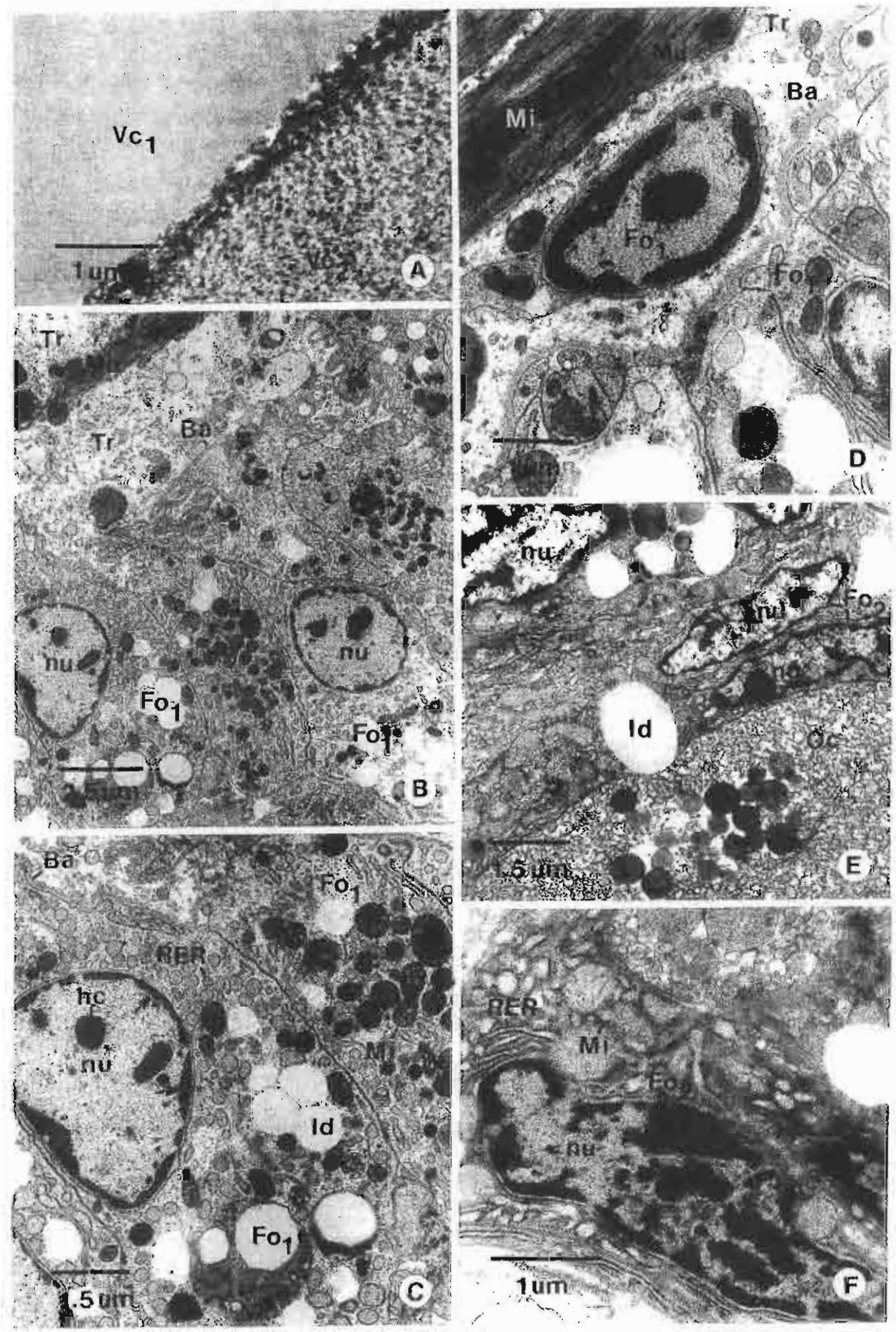
Vc1
1um
A
Tr
Ba
Mi
Fo1
D
Tr
Tr
Ba
nu
nu
Fo1
Fo1
B
nu
nu
Fo2
Id
Oc
.5um
E
Ba
Fo1
RER
hc
nu
Mi
Id
Fo1
.5um
C
RER
Mi
Fo2
nu
1um
F

The second stage oocyte (Oc_2) is characterized by a decondensation of most chromatin, an increased translucence of the nucleoplasm, the presence of numerous nuclear pores on the nuclear membrane, and a significantly enlarged nucleolus. All of these characteristics imply increased transcriptional activity. In the cytoplasm, the most distinctive feature is the proliferation of numerous Golgi bodies that are distributed throughout the cytoplasm. However, only a few SG_1 and SG_2 granules start to appear in this stage, and most of them cluster around the Golgi complexes. Thus, Oc_2 could represent the initial phase of synthetic activities in which the cell is preparing itself by developing secretory organelles, including Golgi bodies and RER; and the cell begins to synthesize a small number of secretory granules. From these unique ultrastructural characteristics, we designated Oc_2 as the RER–Golgi phase.

The third stage oocyte (Oc_3) is the cell in which SG_1 and SG_2 appear in large numbers and are concentrated around the Golgi bodies, while yolk granules begin to appear, but are still very few in number. The chromatin becomes completely euchromatic and the nucleolus is enlarged to the maximum size which implies the active transcriptional activities in the nucleus as well as translational activities in the cytoplasm. Oc_3 is therefore designated the synthetic phase.

The fourth stage oocyte (Oc_4) is the stage at which a thin jelly coat is first observed between the oocyte's plasma membrane and the surrounding follicular cells. Initially this coat appears homogeneous and could be partly derived from the secretion of peripheral follicular cells. The chromatin of Oc_4 is completely in the euchromatic state, and the nucleolus is fully enlarged. These imply that there are still high levels of both nuclear and nucleolar transcriptional activities. The cytoplasm of Oc_4 is filled with SG_1, SG_2 and yolk granules, which reflect the near saturation of synthetic activities. Oc_4 is therefore equipped with most essential cellular structures with the exception of a mature jelly coat; hence, it is designated the premature phase.

The fifth stage oocyte (Oc_5) has a jelly coat that is uniformly thick and deprived of the surrounding layer of follicular cells. Most SG_1 granules were seen exocytosed at the plasma membrane to contribute material to the formation of the jelly coat, whilst SG_2, which could be the cortical granules, remain in the peripheral cytoplasm. As a result, the jelly coat is transformed from a homogeneous to a fibrous organization. There is no division of this coat into the jelly and vitelline layers as reported in other species (Monzingo et al., 1995). Thus, Oc_5 appears to be the completely mature cell, and could correspond to the late postsynthetic stage as defined by Martin et al. (1983). The absence of basal follicular cells might allow the detachment of Oc_5 from the trabeculae, as they are ready to be released from the ovary.

Acknowledgement

This investigation was supported by the Thailand Research Fund (Contract BRG4080004) and Senior Research Scholar Fellowship to Prasert Sobhon.

References

Apisawetakan, S., Thongkukiatkul, A., Wanichanon, C., Linthong, V., Kruatrachue, M., Upatham, E.S., Pumthong, T. and Sobhon, P., The gametogenic processes in a tropical abalone, *Haliotis asinina* Linnaeus. J. Sci. Soc. Thailand, 23 (1997) 225–240.

Apisawetakan, S., Chanpoo, M., Wanichanon, C., Linthong, V., Kruatrachue, M., Upatham, E.S., Pumthong, T. and Sobhon, P., Characterization of trabecular cells in the gonad of *Haliotis asinina* Linnaeus. J. Shellfish Res., in press.

Brickey, B.E., The histological and cytological aspects of oogenesis in the California abalone. MS Thesis, Long Beach, California State University, 1979.

Bussarawit, S., Kawintertwathana, P. and Nateewathana, A., Preliminary study on reproductive biology of the abalone (*Haliotis varia*) at Phuket, Andaman Sea Coast of Thailand. Kasetsart. J. (Nat. Sci.), 24 (1990) 529–539.

Croft, D.R., *Haliotis*. L.M.B.C. mem, Liverpool University Press, Vol. 29, 1929.

Giorgi, A.E. and DeMartini, J.D., A study of the reproductive biology of the red abalone, *Haliotis rufescens* Swainson, near Mendocino, California. Calif. Fish and Game, 63 (1977) 80–94.

Hahn, K.O., Gonad reproductive cycle. In: Handbook of Culture of Abalone and Other Marine Gastropods, K.O., Hahn (ed.), CRC Press, Boca Raton, 1989, pp. 13–39.

Jarayabhand, P., Jew, N., Menasveta, P. and Choonhabandit, S., Gametogenic cycle of abalone *Haliotis ovina* Gmelin 1791 at Khangkao Island, Chon-buri province. Thai J. Aqua. Sci., 1 (1994) 34–42.

Martin, G.G., Romero, K. and Miller-Walker, C., Fine structure of the ovary in the red abalone *Haliotis rufescens* (Mollusca: Gastropoda). Zoomorphology, 103 (1983) 89–102.

Minh, L.D., Reproductive cycle of *Haliotis ovina* Gmelin, 1791 in Nha Trang Bay, south central Vietnam. Phuket Mar. Biol. Cent. Spec. Publ., 18 (1998) 99–102.

Monzingo, N.M., Vacquier, V.D. and Chandler, D.E., Structural features of the abalone egg extracellular matrix and its role in gamete interaction during fertilization. Mol. Reprod. Dev., 41 (1995) 493–502.